Computational Analysis of the Neurophysiological Effects of Spinal Cord Stimulation

by

Evan R. Rogers

A dissertation submitted in partial fulfillment
of the requirements for the degree of
Doctor of Philosophy
(Biomedical Engineering)
in the University of Michigan
2023

Doctoral Committee:

Associate Professor Scott F. Lempka, Chair
Associate Professor Tim M. Bruns
Assistant Professor Bo Duan
Associate Professor Parag G. Patil

Evan R. Rogers

evrogers@umich.edu

ORCID iD: 0000-0002-7112-2289

Dedication

I dedicate this work to my parents: George and Donna Rogers.

Acknowledgements

I would like to acknowledge the many people who have contributed to my wonderful experience at the University of Michigan.

First and foremost, I am incredibly thankful to Dr. Scott Lempka for serving as my advisor. Scott has allowed me the independence to pursue my interests while always being available to provide feedback and sharpen my thinking. I am grateful for his unwavering encouragement and patience, as well as the many times he has gone out of his way to support my personal and professional development. Scott is an excellent scientist and mentor, and I look forward to many more years of friendship and scientific collaboration.

Next, I am incredibly grateful to my committee: Drs. Tim Bruns, Bo Duan, and Parag Patil. For as long as I've been at Michigan, each has been incredibly generous with their time and provided thoughtful and helpful feedback. I can't believe how lucky I am to have had a team of such brilliant and kind scientists support my dissertation research and career development.

Many people have come through the Neuromodulation Lab throughout my time here, and I'd like to thank them all for their many, many positive contributions to my time here. With that said, I want to thank the early lab members (Vish Sankarasubramanian, Ehsan Mirzakhalili, Hans Zander, Bobby Graham, and Carlos Anaya) who taught me so much about spinal cord stimulation, quantitative sensory testing, chronic pain, neuroscience, neural engineering, computers, research, and anything else I needed to know. Additionally, I am incredibly grateful to Jessica Loechli for all of her hard work and infectiously positive attitude towards the clinical research projects. Speaking of the clinical research, although it is not discussed in depth in this dissertation, I am

grateful beyond belief to our clinical trial participants who so generously offered their time to try and help improve SCS systems for future chronic patients. I learned so much from them about how these devices work in the real world that you could never learn from a textbook or journal article. They are all kind and wonderful people, and I (and the neurostimulation research community and future chronic pain patients) am forever indebted to them.

I have been fortunate to work on several collaborative projects during graduate school. Each has been an enriching and enjoyable experience, and I'd like to thank our collaborators at Presidio Medical, Kings College London, Pitt, CCNY, and throughout the University of Michigan (Michigan Medicine, Chronic Pain & Fatigue Research Center, Michigan Math Departments) for making each project so rewarding and teaching me new things.

I would like to thank my family (Mom, Dad, Curtis, and Martin) for being my best friends and always supporting me. I hope they know how much I love and appreciate them.

Finally, Nicole Friend has been by my side for my entire time at Michigan, and I couldn't have made it this far without her endless support and encouragement. Nicole has the uncanny ability to instantly raise my spirits, even on the most stressful of days. I have no doubt my fondest graduate school memories will be the countless laughs and adventures we've shared along the way. I am inspired by your passion and talent for science and can't wait to see the amazing things you will accomplish. Thank you for brightening my life every day!

Table of Contents

List of Tables

List of Figures

Abstract

Chronic pain is a major public health burden and cause of global human suffering. Spinal cord stimulation (SCS) is a common neurostimulation treatment option for patients with refractory chronic pain. Unfortunately, despite decades of clinical experience, only about 60% of patients successfully respond to the therapy (typically defined as a reduction of pain by at least 50%), and many patients report loss of efficacy over time. This inadequate success rate is largely because very little is known about the neurophysiological effects of SCS and its analgesic mechanisms of action. This dissertation describes a computational modeling approach to investigate the effects of SCS on the nervous system.

The first study analyzes the most fundamental question: which neurons are directly driven to fire action potentials by various available SCS waveforms including conventional, burst, and 10-kHz SCS? We used a finite element model of the lower thoracic spinal cord to assess the spatial electric potential generated by clinical SCS systems, which was then paired with biophysical multi-compartment models of the relevant neural populations. This study provides insights into the neural recruitment order during clinically relevant SCS, as well as the effects of various factors such as axonal collateralization on activation thresholds. One important finding is that all waveforms produced the same neural order of activation, albeit at different amplitudes.

Study two expands this analysis to evaluate recently proposed mechanisms for novel SCS modalities beyond simple activation of large diameter myelinated axons. Specifically, we evaluated potential alterations in spike timing in afferent fibers, altered dorsal horn neuron excitability due to membrane polarization, and selective activation of unmyelinated C fibers. We

also evaluated the effects of including stochastic ion channel properties on the dorsal column fiber response to stimulation. Overall, our results refute several proposed mechanisms of action and highlight the value of including stochastic ion channels in models of extracellular stimulation to produce realistic variability in firing responses.

Finally, the third study comprehensively evaluated the effects of stimulation frequency on the neural response to SCS, including effects on dorsal column fiber activation thresholds, synaptic transmission in the brainstem, action potential fidelity in primary afferent collateral arbors, and the output of the dorsal horn pain processing network. We found that high frequency stimulation of at least 100 Hz reduced activation thresholds (mirroring clinical paresthesia perception thresholds), produced asynchronous firing in the brainstem, and promoted branch point failure within the branching collateral arbors of the dorsal horn.

Overall, this dissertation contributes to our understanding of the neural response to clinically relevant SCS. The results presented in this study clarify which neurons are most likely to be activated during SCS as well as higher order properties such as firing properties during suprathreshold stimulation and synaptic processing. Ultimately, these insights will help guide developing future SCS systems to optimize pain relief while minimizing power consumption.

Chapter 1 - Introduction

Electrical stimulation of the nervous system (i.e., "neurostimulation") is the basis for many existing and proposed medical devices. Spinal cord stimulation (SCS) is a common neurostimulation therapy to provide pain relief in subjects with chronic pain refractory to conventional medical management.[1] In this procedure, electrodes are implanted into the epidural space behind the spinal cord and short pulses of mild electrical current are applied to the dorsal spinal cord, the initial site for pain processing in the nervous system.[2] SCS was introduced in 1967 by Shealy and colleagues, who produced total pain relief in a subject with diffuse pain of the chest and abdomen via stimulation of the thoracic spinal cord.[3] In the decades following this proof-of-concept study, SCS has become a common treatment option for refractory chronic pain. SCS systems have received FDA approval for various painful conditions, and tens of thousands of units are implanted annually in what constitutes a growing multi-billion dollar market.[4] However, despite the clinical prevalence of SCS, its precise analgesic mechanisms of action are poorly understood.[5] Unfortunately, this scientific uncertainty begets suboptimal clinical outcomes, and the clinical success rate (defined as at least 50% reduction in self-reported pain score) for SCS is only about 60%.[6] Thus, there is a substantial clinical need to better understand the neural response to SCS.

1.1 Chronic Pain

The international Association for the Study of Pain (IASP) recently defined pain as "an unpleasant sensory and emotional experience associated with, or resembling that associated with, actual or potential tissue damage.[7]" Acute pain is protective and warns us to minimize contact with

noxious stimuli and encourages behavior that promotes tissue healing.[8] Relatedly, people with congenital pain insensitivity are often prone to injuries, such as burns, and develop orthopedic issues arising from untreated fractures.[9] When pain lasts beyond normal healing time, it is referred to as "chronic pain" (usually defined as pain lasting at least three months).[10,11] In contrast to acute pain, chronic pain represents maladaptive plasticity, serves no protective function, and is a major cause of global human suffering.

1.1.1 Personal and societal burden of chronic pain

Chronic pain is one of the most common reasons people seek medical care and is a leading cause of disability.[12] Approximately 20% of Americans suffer from chronic pain, and 8% from high impact chronic pain that interferes with work or life on most or every day.[13] Chronic pain is estimated to cost the United States between 560 and 635 billion dollars annually in medical costs and lost productivity, which is greater than the cost for heart disease, cancer, and diabetes.[14] Remarkably, this value is necessarily an underestimate, as it does not include care for military personnel, children, and institutionalized individuals, or the cost of caregiving.[12,14]

1.1.2 Pharmacological management of chronic pain

Chronic pain is an all-encompassing oversimplification that belies the highly heterogeneous and personalized experiences of patients.[15] The current understanding of chronic pain is the "biopsychosocial approach," which describes pain as the dynamic interaction of biological, psychological, and social factors.[16] Due to its complex nature, chronic pain is notoriously difficult to treat.[17]

Oral analgesics are ubiquitous in the treatment of chronic pain.[17,18] The pharmacological approach to treating chronic pain is often guided by the underlying pain condition. Chronic pain

is typically categorized as nociceptive (due to noxious stimulus), neuropathic (due to neural tissue damage), or nociplastic (due to nervous system dysfunction without observed tissue damage or pathology), although an individual may be simultaneously experiencing mixed pain best described by more than one of these categories.[12] These disparate pain phenotypes respond differently to the various available medications.[19,20] For instance, neuropathic pain is generally resistant to nonsteroidal anti-inflammatory drugs (NSAIDS) and opioids, and instead tricyclic antidepressants, serotonin-noradrenaline uptake inhibitors, and gabapentinoids are more effective.[20–22]

Despite these considerations, chronic pain is often inefficiently treated as prolonged acute pain rather than its own entity.[19] For instance, there is scant evidence supporting the efficacy of long-term opioid use for chronic pain, yet 8 to 30% of chronic non-cancer pain patients receive opioids.[23,24] Unfortunately, overprescription of opioids exacerbates the ongoing opioid epidemic in America, as more than a third of drug-overdose deaths are attributable to pharmaceutical opioids, the major source of which is diversion of prescription drugs.[25] Likewise, NSAIDs are highly prevalent, as illustrated by a recent European survey finding them to be the most common medication class for chronic pain patients (both prescription and over-the-counter).[26] Be that as it may, limited evidence supports long-term NSAID use in managing chronic pain, and they carry the risk for serious side effects, such as life-threatening gastrointestinal bleeding and ulcers. Over 100,000 hospitalizations and 16,500 deaths in the United States annually are attributable to the side-effects of long-term NSAID use.[27]

Unfortunately, even using the best evidence-based approaches and individualized treatment plans, chronic pain treatments are generally only partially beneficial for a subset of patients.[28] Beyond pharmaceuticals, various surgical and non-surgical options are available (depending on the nature of the painful condition), such as radiofrequency ablation, steroid

injections, and spinal fusions, as well as neurostimulation options including SCS or less common options such as dorsal root ganglion stimulation, peripheral nerve stimulation, or motor cortex stimulation. Unfortunately, results for these different options are heterogeneous between patients and often only temporary for responders.[12] Chronic pain is often comorbid with psychological distress, and ineffective treatment can exacerbate these issues by promoting a sense of hopelessness and frustration.[29,30]

1.2 Pain processing in the spinal cord

The spinal cord is a crucial component of the central nervous system (CNS) and is the first relay point for nociceptive signals as they are transmitted from the periphery to the brain.

1.2.1 Primary afferent input

Nociceptive signals originate in the peripheral axon terminals of primary afferent neurons, which are tuned to detect noxious thermal, mechanical, and/or chemical signals.[31] Classically, nociception is associated with slowly conducting unmyelinated C fibers and thinly myelinated Aδ fibers, although this is an oversimplification as a subset of Aβ fibers may transmit noxious information and not all C and Aδ fibers are nociceptors.[32,33] The cell bodies of these neurons are located in the dorsal root and trigeminal ganglia of the spinal cord and brainstem, respectively.[34] These pseudounipolar neurons produce a bifurcating axon that transduces noxious stimuli in the periphery and relays this information to postsynaptic targets in the CNS gray matter (**Fig. 1.1)**. In parallel, rapidly conducting, large diameter, and thickly myelinated Aα and Aβ fibers transduce proprioceptive and innocuous mechanoreceptive (e.g., light touch, vibration) information. Centrally, these fibers enter the dorsal column white matter pathway in the spinal cord, producing

small diameter collaterals that descend into the spinal gray matter and form synapses on local interneurons and projection neurons.[32]

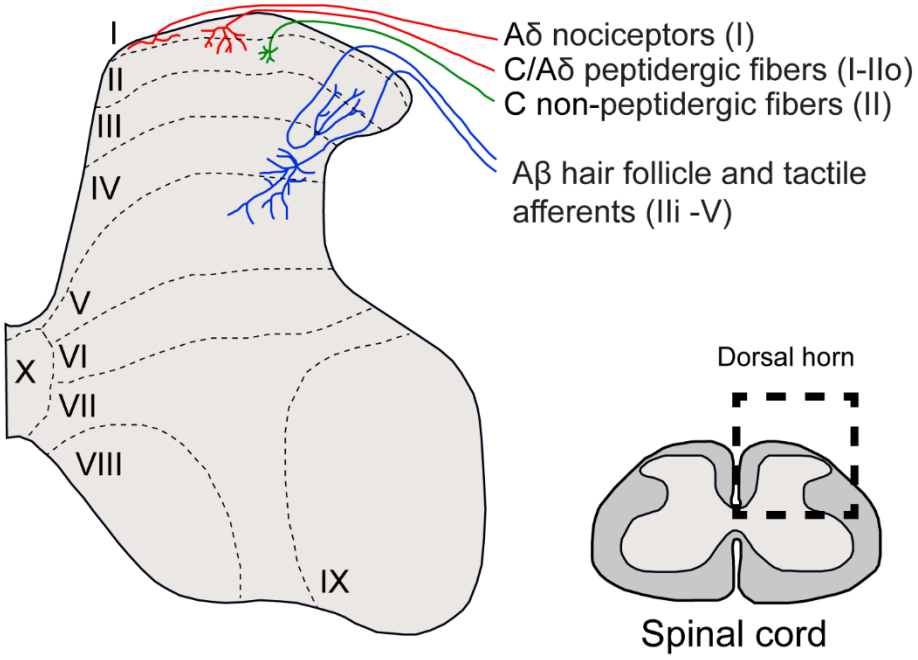

Figure 1.1: Peripheral input to the dorsal horn. Peripheral fibers carrying somatosensory information produce lamina-specific terminations within the dorsal horn. Figure is adapted from Todd, 2010.[35]

1.2.2 Dorsal horn

The dorsal horn gray matter contains the local second-order neurons that receive nociceptive information from the periphery, process this input, and transmit it supraspinally. The dorsal horn is discretized dorsoventrally into distinct laminae that vary in both their resident cell types as well as the primary afferent fibers from which they receive input.[36] Many different neuronal populations have been defined in the dorsal horn based upon cellular morphology, electrophysiological properties, and/or neurochemical expression.[37–41] The tireless research effort to catalog the dorsal horn neural populations has provided a wealth of information about the relevant neurons, but much remains to be learned about the various cell types, including their

interconnections and their functional roles in pain processing and the development of chronic pain.[35]

One simple classification scheme is to divide the projection neurons (i.e., those that project supraspinally) and interneurons within the dorsal horn.[37] Nociceptive-signaling projection neurons reside in lamina I as well as the deeper dorsal horn laminae (e.g., laminae III and deeper).[42,43] However, the vast majority of neurons (>99%) in the dorsal horn are interneurons with their axons restricted to the spinal cord.[32] The interneurons are typically further subdivided into those that are excitatory (i.e., releasing glutamate) or inhibitory (i.e., releasing GABA and/or glycine). These inhibitory interneurons are considered vital in regulating painful information flow in the dorsal horn, and dorsal horn disinhibition (e.g., via shift of the transmembrane chloride concentration gradient) is sufficient to generate neuropathic pain related behavior in rats.[44–46] Importantly, a shift in the chloride ion gradient that transforms the effect of GABA from hyperpolarizing to depolarizing has been observed following various neuronal injuries.[47]

1.3 Spinal cord stimulation

SCS is a common neurostimulation option (approximately 50,000 units implanted annually[1]) for chronic pain that is refractory to conventional medical management. Modern SCS systems utilize various electrode designs and temporal stimulation patterns to produce pain relief.[48] The different types of stimulation, as well as their scientific rationale, are described in detail in the following sections.

1.3.1 Gate control theory

SCS-induced analgesia was first successfully demonstrated in 1967 by Shealy and colleagues.[3] This approach was motivated by the highly influential "Gate Control Theory of Pain,"

introduced by Melzack and Wall in 1965, which suggested that large diameter mechanoreceptors ascending in the dorsal column white matter pathway can block the transmission of nociceptive signals carried via small-diameter, slowly conducting afferent fibers (**Fig. 1.2)**.[49]

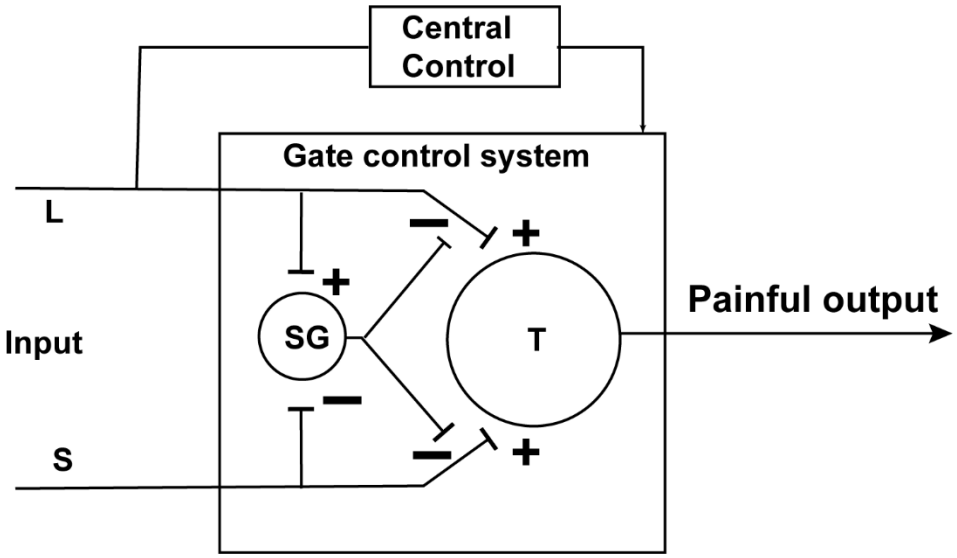

Figure 1.2: Gate control theory. Gate control theory describes a theoretical network for modulating pain processing in the dorsal horn. Gate control suggests that large (L) myelinated fibers carrying innocuous mechanoreceptive information will inhibit (-) painful transmission introduced into the spinal cord by small-diameter (S) nociceptive fibers. This is theoretically done by exciting (+) inhibitory interneurons in the substantia gelatinosa (SG), which will then inhibit supraspinal signaling of painful information by the output transmission (T) neuron. Figure is adapted from Melzack and Wall, 1965.[49]

Specifically, Melzack and Wall proposed a simple four-component dorsal horn network that regulated painful signaling: (1) large-diameter afferent fibers ("L fibers"), (2) small-diameter nociceptive-signaling fibers ("S fibers"), (3) local substantia gelatinosa cells ("SG cells"), and (4) the transmission cells whose firing rate is the network output ("T cells").[49] In this model, both L and S afferent fibers produce excitatory connections with the T cell. However, SG cell activity presynaptically inhibits these connections between these afferent fibers and the output T cell. Thus, SG cell activation reduces T cell activity. Finally, the two afferent fiber classes both synapse on the SG cell, but with opposite effects. The L fibers excite the SG cell and increase its activity, whereas the S fibers inhibit the SG cell. Taken together, the gate control theory suggests that activating the L fibers will increase SG cell activity, which will in turn inhibit excitatory drive of

the T cell, and thus reduce T cell activity and pain perception. This proposition is the theoretical mechanistic basis for several analgesic neurostimulation treatments, including SCS.

Unsurprisingly, this simple model does not completely describe dorsal horn pain processing or the effects of SCS. For instance, the model does not incorporate descending antinociceptive signals originating in supraspinal centers or direct postsynaptic inhibition.[50,51] Moreover, clinical observations of SCS patients require mechanistic explanations beyond that of gate control, such as the fact that stimulation-induced analgesia can persist beyond the cessation of stimulation and that SCS does not relieve nociceptive pain.[52] However, the existence of an interneuron population, driven by Aβ activity, that inhibits noxious mechanical pain signaling has been demonstrated, and electrical stimulation of Aβ fibers reduces nociceptive C fiber-evoked response and spinal hyperexcitability.[53–55]

1.3.2 Conventional spinal cord stimulation

SCS was developed to exploit the gate control theory of pain. Thus, SCS systems traditionally have been designed to activate Aβ mechanoreceptive fibers in the dorsal columns, which produces both orthodromic and antidromic action potentials.[56] The orthodromic action potentials in these mechanoreceptive fibers produce paresthesias, which is often described as a buzzing or tingling sensation.[57] Importantly, overlap between the induced paresthesia and the painful area(s) predicts successful pain relief, and thus maximizing paresthesia coverage of the painful sites is the main clinical and engineering consideration.[56,58] Serendipitously, preclinical evidences suggests that this orthodromic activation also produces analgesia by activating descending pain inhibition pathways, as stimulating with electrodes rostral to bilateral lesions of the dorsal columns reduces nociceptive transmission in the dorsal horn and pain-related behavior.[59–62]

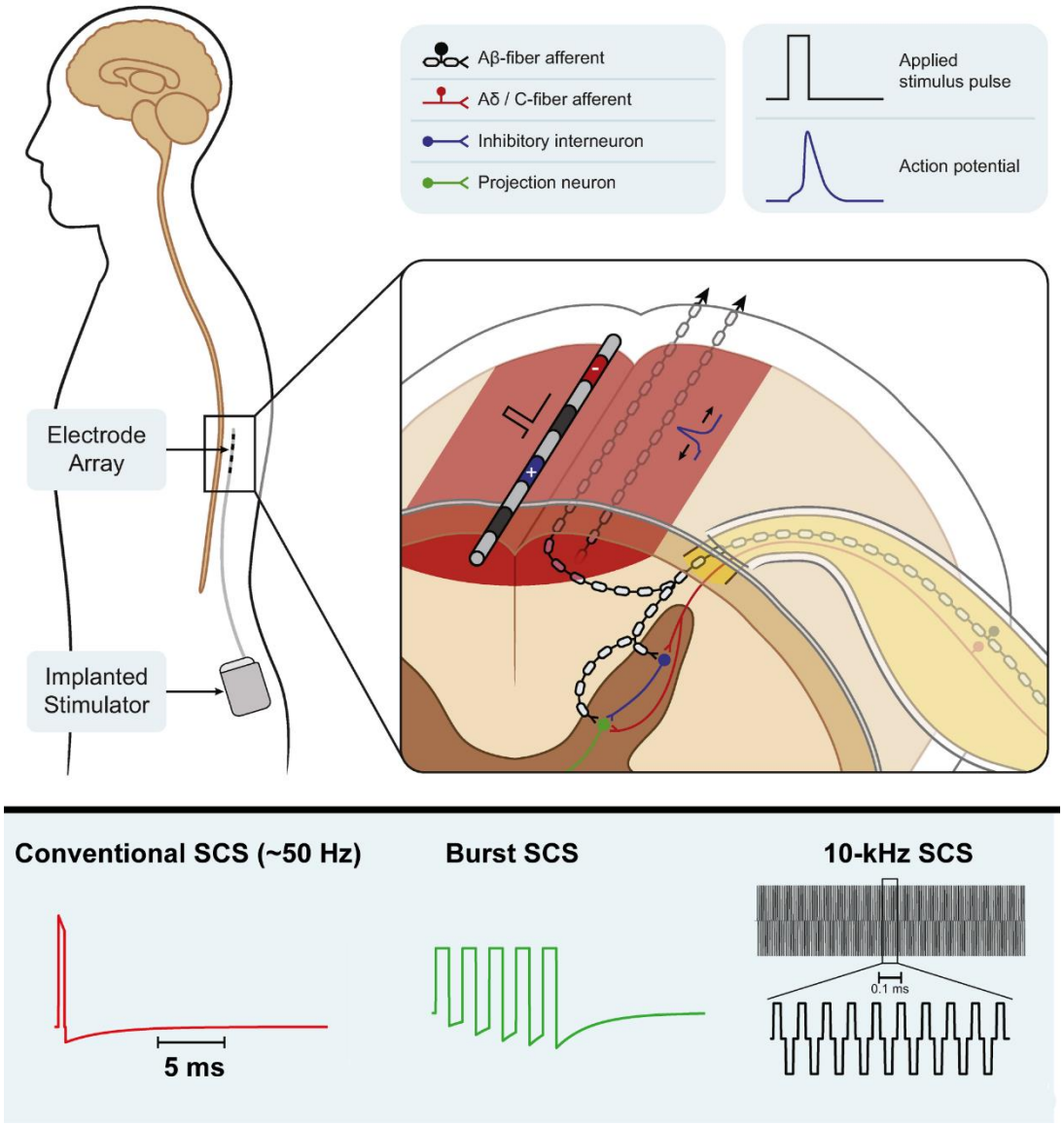

Figure 1.3: Spinal cord stimulation. **(**Top) In spinal cord stimulation (SCS), an electrode is implanted into the epidural space and short pulses of electric current are applied to the dorsal spinal cord. Conventional SCS aims to activate large, myelinated Aβ mechanoreceptors to drive inhibitory interneuron activity in the dorsal horn. (Bottom) Different SCS modalities apply different temporal stimulation waveforms. Conventional SCS is applied at ~50 Hz and generates a perceivable paresthesia. Novel burst and 10-kHz SCS are applied at subparesthetic amplitudes. Figure is adapted from Lempka and Patil, 2018.[48]

These systems typically employ frequencies on the order of 50 Hz and pulse widths from ~100 to 500 μs, which allow for paresthetic overlap of the painful areas in an energetically efficient fashion that maximizes device battery life.[5,56,63,64] Stimulation configurations utilizing this standard approach are often referred to as "conventional" or "tonic" SCS systems **(Fig. 1.3)**.

Unfortunately, these conventional SCS systems possess shortcomings. For one, achieving sufficient pain-paresthesia overlap while avoiding off-target stimulation is not trivial, and some common painful regions, such as the lower back, are particularly difficult to target.[65,66] Additionally, many patients find the paresthesia uncomfortable or unpleasant, and are frustrated the by frequent changes in paresthesia intensity that accompany changes in posture.[67,68]

1.3.3 Novel stimulation paradigms

Given the limitations inherent to conventional SCS, novel stimulation paradigms are an active area of recent innovation. Examples of these novel stimulation techniques include burst SCS, kilohertz-frequency SCS, ultra-low frequency SCS, closed-loop SCS, and differential target multiplexed SCS.[69–74] Notably, some of these recently developed modalities produce analgesia without concomitant paresthesia and are suggested to engage pain-relieving mechanisms other than the gate control theory.[5,48] Of these paresthesia-free varieties, kilohertz-frequency and burst SCS are particularly relevant due to their widespread clinical prevalence.

Kilohertz-frequency SCS is defined by stimulation frequencies of at least 1,000 pulses per second, which is substantially higher than the approximately 50 Hz stimulation utilized in conventional SCS. Several clinical studies demonstrate the analgesic effectiveness of 1-kHz stimulation, and 1-kHz SCS can reduce mechanical hypersensitivity in nerve-injured rodents and reduce spinal activity following noxious stimulation.[74–78] Differences in preclinical and clinical observations between these high frequency paradigms and conventional SCS suggest underlying mechanistic differences. For instance, in addition to delivering stimulation without paresthesia, kilohertz-frequency SCS often requires a substantial wash-in time (hours or days) before pain relief occurs.[78] Additionally, in rodent models of neuropathic pain, both conventional and kilohertz-frequency SCS are effective in reducing mechanical hypersensitivity, but only conventional SCS

effectively attenuates windup in wide-dynamic range spinal neurons.[75] Many hypotheses have been proposed to explain the analgesic effects of kilohertz-frequency SCS including (but not limited to) asynchronous axonal activation, desynchronization of nociceptive signals, membrane temporal summation, and glial effects.[5,79,80] However, these theories remain largely untested, and work is needed to better understand the neural effects and analgesic mechanisms of high-frequency SCS.

One popular high-frequency implementation is 10-kHz SCS, which applies symmetric rectangular pulses with a pulse width of 30 μs at a rate of 10,000 pulses per second.[81] A system delivering 10-kHz SCS received US Food and Drug Administration (FDA) regulatory approval following the pivotal SENZA randomized control trial, in which more than 80% of subjects were responders (defined as at least 50% pain reduction) for both leg and back pain, which was superior to conventional SCS.[72] Unfortunately, little is known about the neural mechanisms underlying these analgesic effects. Originally, 10-kHz SCS was hypothesized to produce analgesia by blocking axonal conduction, but both preclinical evidence and computational modeling suggest the threshold for conduction block is above the clinical range.[82,83] Recent preclinical evidence suggests 10-kHz SCS can selectively activate inhibitory interneurons in the dorsal horn, thus reducing painful transmission while avoiding paresthesia-inducing axonal activation.[84] While this is an appealing theory, to-date no biophysical mechanism has been proposed that would explain this phenomenon, and anatomical, technical, and physiological differences between the preclinical rodent model (e.g., fiber diameter, CSF thickness, and gray matter dimensions) and clinical SCS settings, preclude direct translation of these results.[6] Interestingly, a recent small double-blinded study demonstrated pain reduction following 10-kHz peripheral nerve stimulation, which supports a potential axonal mechanism of action.[6,85]

Burst SCS is another recently developed modality that can produce impressive analgesia without generating concomitant paresthesia. This waveform applies bursts of five closely spaced pulses (1 ms pulses; 500 Hz intra-burst frequency; 40 bursts per second) and allows for an asymmetric passive recharge phase.[5] Burst stimulation was designed to mimic natural burst firing patterns within the nervous system, which may produce different postsynaptic effects than tonic firing modes.[71] In the pivotal SUNBURST trial, burst SCS demonstrated superior pain relief compared to conventional SCS and a majority of patients (~70%) reported preferring burst SCS to conventional stimulation, leading to U.S. FDA regulatory approval in 2016.[86] Despite impressive clinical outcomes, little is known about the mechanisms of burst stimulation. However, the available evidence suggests alternate mechanisms compared to conventional stimulation. Early experimental evidence in a rodent neuropathic pain model showed that both burst and conventional SCS reduced tactile allodynia and spinal neuron firing rates in response to nociceptive stimuli.[87] However, only the effects of conventional SCS were blocked by application of the $GABA_B$ receptor antagonist CGP35348, and conventional SCS (but not burst stimulation) partially restored injury-induced reductions in serum GABA levels, suggesting differing involvements of the GABAergic system (although conflicting results have been reported by Meuwissen and colleagues[88]). Additionally, burst stimulation is proposed to modulate the medial pain pathway more strongly than conventional SCS, thereby reducing the affective component of pain in addition to pain intensity.[89] This proposition is supported by several neuroimaging studies in both humans and rodents.[90–94] However, these studies employ small sample sizes, and no clear biophysical mechanism linking the neural effects of burst SCS to enhanced medial pathway modulation has been demonstrated.

1.4 Computational modeling of spinal cord stimulation

Measuring the effects of neurostimulation therapies on the human nervous system is difficult due to the experimental inaccessibility of the relevant neural populations. As a result, human studies often rely on indirect measurements to infer biophysical effects, such as self-reported measures, neuroimaging (e.g., EEG, fMRI), and quantitative sensory testing (QST).[95] Preclinical models offer greater experimental access to directly measuring effects at the level of single cells, and have been the basis for most of our understanding of the biophysical effects of these neurostimulation systems.[96] However, these preclinical models possess several inherent drawbacks that complicate translation, including (but not limited to) their anatomical and neurophysiological differences from humans.[6,96] In one interesting recent example, Formento and colleagues demonstrated that epidural SCS more strongly interferes with proprioception in humans compared to preclinical rat models due to the longer traveling time in human fibers.[97] On the other hand, computational modeling offers a cost- and time-efficient method to evaluate the biophysical effects of neurostimulation therapies at human-scale, and has greatly contributed to both the scientific understanding and clinical implementation of SCS.[98]

Current computational modeling approaches typically employ two paired subcomponents (**Fig. 1.4)**. First, a volume conductor model is used to evaluate the electric fields generated within the spinal tissue, which is then paired with models of the relevant cells to assess their response to the stimulation.[99,100] Both of these elements will affect predictions of the neural response to stimulation, with greater complexity models tending to produce more accurate results at the expense of longer development and runtime.[99,101] Thus, model parameter selection involves a tradeoff between scientific accuracy and efficiency, and appropriate model selection depends on the unique needs and available resources of an individual project.

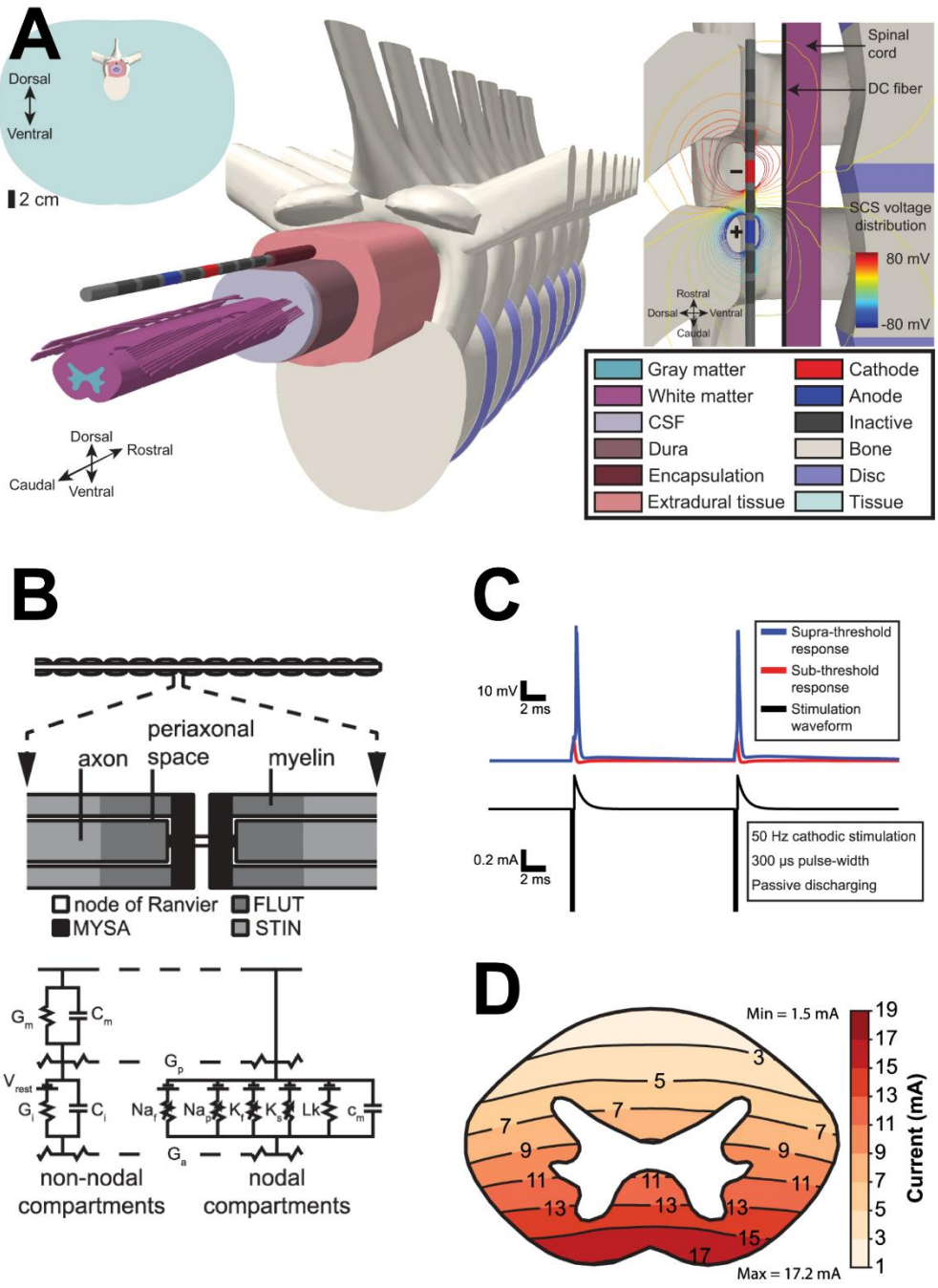

Figure 1.4: Overview of SCS computer modeling. (A) A volume conductor model is developed to evaluate electric potentials within the spinal cord. (B) Neurons are modeled using multi-compartment models utilizing electric circuit elements. (C) The neural response to extracellular stimulation is recorded. (D) The model output of interest, such as activation thresholds for dorsal column fibers, is evaluated. Figure was adapted from McIntyre et al., 2002,[102] and Zander et al., 2020.[103]

The volume conductor component of a biophysical model assesses the spatial electric field distribution generated within the tissue. To do this, a model of the spine and surrounding anatomy

is meshed into discrete units, each of which is assigned appropriate tissue-specific parameters, and a numerical method is used to solve the Laplace equation to evaluate the spatial electric potentials (most commonly the finite element method).[98] Typically, the quasi-static assumption is employed, which assumes that the tissue behaves purely resistive.[104] This has been shown to be a reasonable assumption even for 10-kHz stimulation (the highest frequency stimulation employed clinically), with differences in predicted axonal activation thresholds versus a frequency-dependent model being <10%, which is small compared to the effects of varying other relevant parameters (e.g., tissue conductivity) within a reasonable range.[103] The most advanced volume conductor models are patient-specific and incorporate a subject's medical imaging (e.g., magnetic resonance imaging and computed tomography) to localize their implanted electrode and account for variations in anatomy. Patient-specific models have demonstrated the ability to better predict correlates of neural activation (e.g., sensory threshold) than canonical models based on atlases or average measurements, but are labor-intensive and complex to develop.[105]

The neural response to extracellular stimulation is complex and can be modeled in various ways. The simplest approaches estimate a region of activation based on thresholds for the electric potential (or the first or second derivative thereof).[99] Biophysical models, which incorporate experimental measurements into physics-based models of the underlying cells, produce more accurate solutions at a greater computational cost. Specifically, neurons can be spatially discretized into distinct subsections and their electrical behavior modeled using standard electric circuit components (e.g., resistors and capacitors), the values of which are derived experimentally. Additionally, active properties (e.g., voltage-gated ion channels) can be represented as time-varying conductances whose conductance at a given time is dependent on factors such as membrane voltage or ligand binding. This approach was pioneered by Hodgkin and Huxley who

developed this technique to study membrane behavior in the squid giant axon with remarkable accuracy.[106] Today, this approach is termed the "Hodgkin-Huxley" formalism and they were appropriately awarded the 1963 Nobel Prize in Physiology or Medicine for this work.[107] From here, the response of the neuron to an applied intracellular or extracellular stimulus can be modeled using standard approaches to evaluating electric circuits.[108]

Overall, computational modeling has greatly influenced the scientific understanding and clinical implantation of SCS. For instance, many modeling studies have evaluated various electrode designs and active contact configurations which are now common clinically, often targeting maximal dorsal column fiber activation while avoiding dorsal rootlet fibers.[98] Additionally, computational models have provided insights into the biophysical response to clinical stimulation which have been later confirmed experimentally, such as the fact that 10-kHz stimulation is not blocking axonal conduction at therapeutic amplitudes.[82,83] Excitingly, commercial systems implementing model-based approaches have demonstrated superior results over traditional programming methods.[109]

1.5 Summary of dissertation

Currently, the analgesic mechanisms of action of SCS remain largely unknown, leading to suboptimal clinical outcomes. Thus, the goal of this work was to use computational modeling to characterize the neural response to clinically relevant SCS.

In Aim 1, I evaluated neural recruitment during three clinically relevant forms of SCS: conventional, burst, and 10-kHz SCS. Specifically, I determined activation thresholds for dorsal column fibers, dorsal rootlet fibers, and local interneurons and projection neurons in the dorsal horn. Additionally, I evaluated how collateralization affected activation thresholds of both dorsal

column and dorsal rootlet fibers, considering collateral termination patterns, the interspacing of collaterals, and the positioning of the parent afferent fibers within the white matter.

Aim 2 expands upon this work to develop a more complete understanding of the neural effects of clinically relevant SCS (conventional, burst, 1-kHz, and 10-kHz). Specifically, I computationally evaluated various proposed subthreshold mechanisms of action, including quantifying the effects of stimulation on spike timing and evaluating polarization throughout the axonal and somatodendritic arbors of local dorsal horn neurons. Additionally, I investigated the effects of incorporating stochastic ion channel properties on both action potential thresholds and firing properties of dorsal column axons in response to clinically relevant stimulation.

Finally, Aim 3 describes the effects of stimulation frequency on the neural response to SCS. This work includes characterization of the firing response of dorsal column fibers, synaptic processing in the dorsal column nuclei, and action potential fidelity within the dorsal horn. Additionally, I compared model predictions with paresthesia thresholds collected from 16 SCS patients to associate the neural response with clinical observations.

Chapter 2 - Neural Recruitment During Conventional, Burst, and 10-kHz Spinal Cord Stimulation for Pain

The work described in this chapter is adapted from the following published article:

Rogers, Evan R., Hans J. Zander, and Scott F. Lempka. "Neural recruitment during conventional, burst, and 10-khz spinal cord stimulation for pain." *The Journal of Pain* 23.3 (2022): 434-449.[110]

2.1 Abstract

Spinal cord stimulation (SCS) is a popular neurostimulation therapy for severe chronic pain. To improve stimulation efficacy, multiple modes are now used in the clinic, including conventional, burst, and 10-kHz SCS. Clinical observations have produced speculation that these modes target different neural elements and/or work via distinct mechanisms of action. However, in humans, these hypotheses cannot be conclusively answered via experimental methods. Therefore, we utilized computational modeling to assess the response of primary afferents, interneurons, and projection neurons to conventional, burst, and 10-kHz SCS. Contrary to previous reports, axon collateralization produced complex changes in activation thresholds of primary afferents. Furthermore, local cell thresholds were always higher than afferent thresholds, arguing against direct recruitment of these local cells. Finally, although we observed relative threshold differences between conventional, burst, and 10-kHz SCS, the recruitment order was the same. These results motivate future work to contextualize clinical observations across SCS paradigms.

2.2 Introduction

Spinal cord stimulation (SCS) is a neurostimulation approach for managing chronic pain refractory to conventional medical management. Inspired by the gate control theory of pain, SCS

was introduced in 1967 and its demand has dramatically increased with 50,000 units now implanted annually.[1,111] Utilizing electrodes implanted in the epidural space, conventional SCS applies short-duration electrical pulses (typically at a rate around 50 Hz) to activate primary afferent Aβ fibers carrying innocuous touch information in the dorsal columns. These Aβ fibers produce collaterals that project into the dorsal horn and synapse on inhibitory interneurons whose post-synaptic activation can "close the gate" on nociceptive transmission.[3,49] It is important to note that conventional SCS generates paresthesias that result from repetitive stimulation of these Aβ fibers. Although it can have impressive analgesic effects, conventional SCS is not a panacea and only around 58% of patients achieve clinical success.[112,113]

In an attempt to address the shortcomings of conventional SCS, recent work has produced novel waveform paradigms. Two innovative waveforms of note are burst SCS and 10-kHz SCS. Following successful pivotal clinical trials, these SCS modalities have received marketing approval from the United States Food and Drug Administration.[72,86] One widely used form of burst SCS applies rapid bursts of pulses (~five pulses at 500 Hz, delivered 40 times per second) that is believed to mimic burst firing in the human nervous system.[71] 10-kHz SCS applies balanced rectangular pulses at a frequency of 10 kHz.[114] Contrary to conventional SCS, at clinical stimulation amplitudes, these modalities do not produce paresthesias.[1,5,115] This clinical pearl has been interpreted as possible mechanistic differences between conventional, burst, and 10-kHz SCS.[1,5,115]

A major barrier to understanding the analgesic mechanisms of different SCS paradigms is that we still do not know which neurons are being directly activated by the stimulation.[1,5,116] Without this fundamental knowledge, it is impossible to infer causal relationships linking therapeutic stimulation parameters to physiological effects, develop optimized stimulation

protocols, or understand higher-order effects, such as alterations in the activity of spinal and supraspinal networks. In humans, it is infeasible to record the direct response of different neuronal populations to SCS, so computational modeling has emerged as a useful tool to study the neuromodulatory effects of SCS.[98,117–123] Therefore, in this study, we used a comprehensive modeling approach to evaluate which neurons are likely to be directly activated by conventional, burst, and 10-Hz SCS. Our workflow utilized a finite element model of the lower thoracic spinal cord and surrounding tissues along with multi-compartment models of dorsal column fibers, dorsal root fibers, interneurons, and projection neurons. We used this approach to systematically investigate how various physiological and technical factors affected the neural response to SCS.

Our results suggest that all three SCS paradigms have the same relative recruitment order. Furthermore, local cell thresholds were always higher than afferent thresholds, refuting direct recruitment of these local cells. These results argue against distinct neural recruitment profiles that would produce divergent analgesic mechanisms between the three SCS paradigms and highlight the need for additional work to interpret clinical experiences with these SCS technologies.

2.3 Methods

We used computational modeling to study the direct effects (i.e., which neurons are activated in response to the SCS-induced potential field) of conventional, burst, and 10-kHz SCS. Our approach was divided into two stages. In the first step, we solved a high-resolution finite element method (FEM) model of the lower thoracic spinal cord to evaluate the potential field generated by a percutaneous electrode during bipolar SCS (**Fig. 2.1A**-**B**). In the second step, we applied these voltages to multi-compartment neuron models and we used a bisection algorithm (error < 0.02 mA) to find the individual activation thresholds. For each SCS waveforms considered

in this study, activation threshold was defined to be the minimum amplitude necessary to generate at least one action potential (**Fig. 2.1C**).

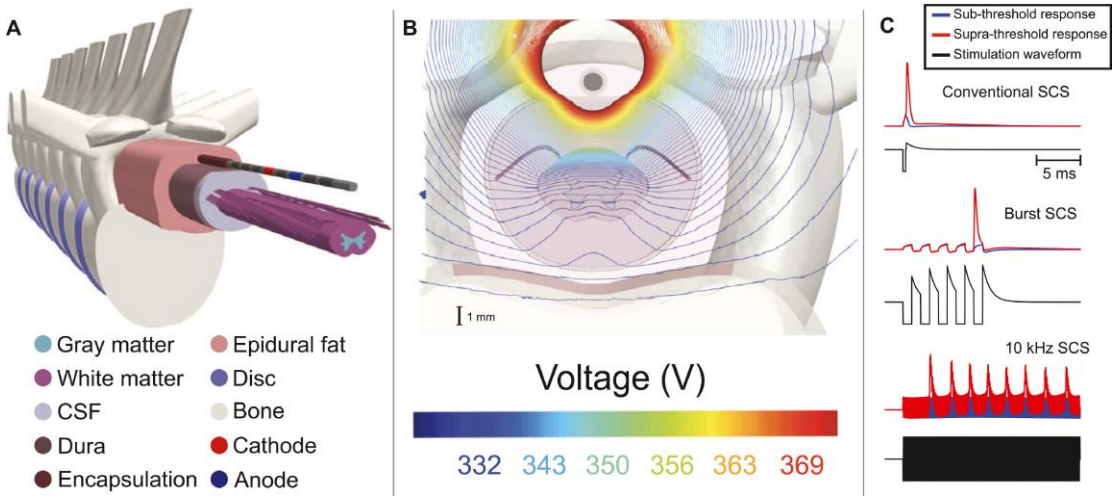

Figure 2.1: Overview of computational modeling approach. (A) Three-dimensional anatomy used in the finite element method model. (B) Representative example of the isopotential lines generated throughout the spinal cord and surrounding tissues due to a unit current (1 A) applied by SCS. (C) Examples of suprathreshold and subthreshold responses to conventional, burst, and 10-kHz SCS.

For conventional SCS, we utilized a 300 μs cathodic pulse followed by passive discharging (**Fig. 2.2A**). The burst SCS waveform consisted of five pulses (intra-burst frequency of 500 Hz) with a 1 ms cathodic pulse width, 1 ms interpulse interval, and passive discharging (**Fig. 2.2B**). This form of burst stimulation corresponds to the widely used waveform pattern described by de Ridder et al., in which passive discharging occurs between each stimulus pulse and at the end of the five pulses.[71] Another form of burst stimulation applies active discharging after each stimulus pulse, but was not considered in this study.[124] We determined the conventional and burst waveforms, which both contain passive discharging, by solving a circuit model of bipolar neural stimulation.[103,125] The 10-kHz waveform consisted of symmetric biphasic pulses with 30 μs pulse widths, 20 μs interphase delay, and active discharging (**Fig. 2.2C**). We applied the 10-kHz SCS waveform for 30 ms. We performed all neuronal modeling in the NEURON programming environment through a Python interface.[108,126]

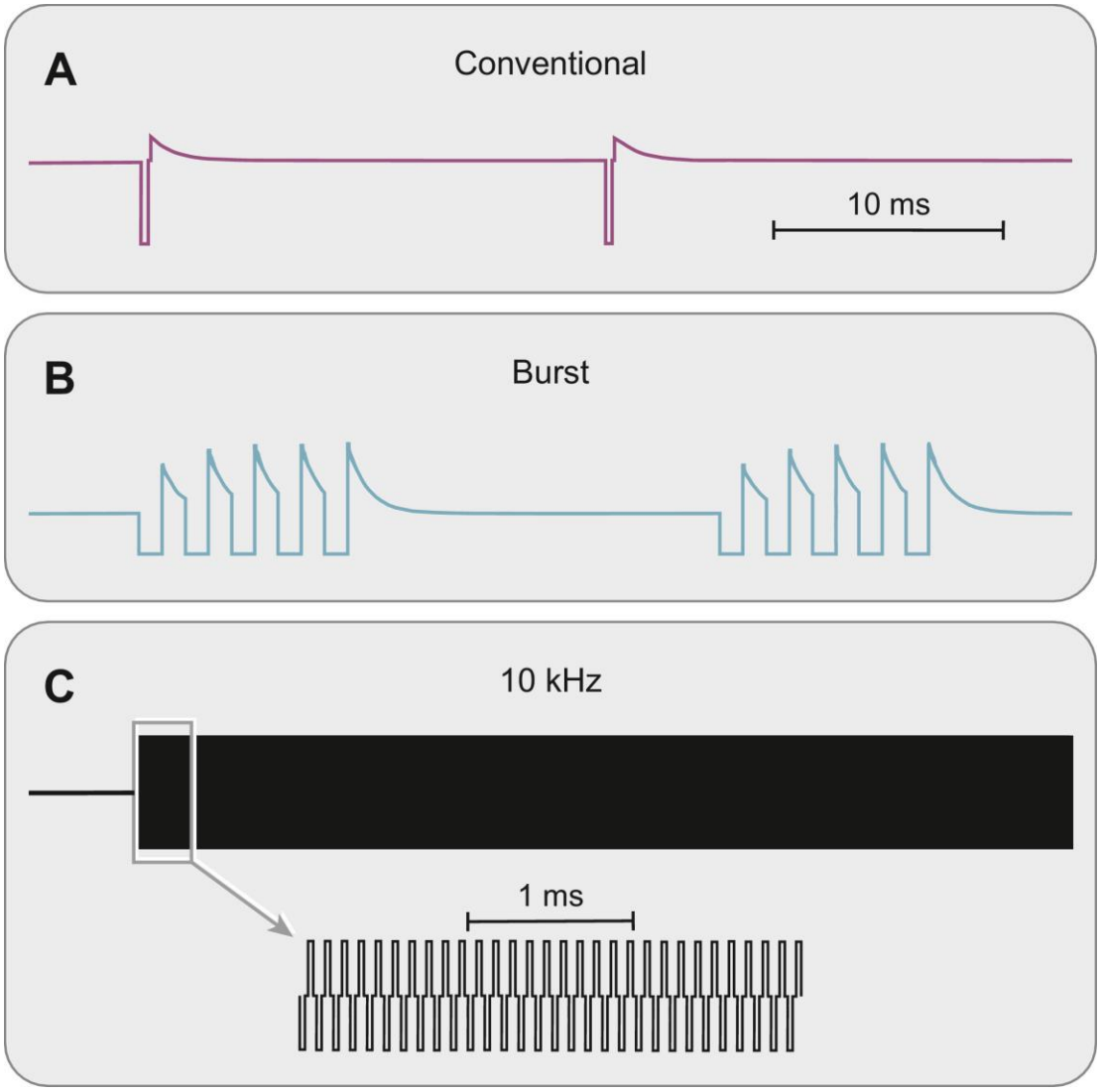

Figure 2.2: Clinical spinal cord stimulation (SCS) waveform paradigms considered in this study. (A) Conventional SCS applies short-duration pulses typically within a frequency range of 40 to 60 Hz. (B) Burst SCS applies intermittent bursts of electrical pulses at a burst rate of 40 Hz, intra-burst frequency of 500 Hz, and 5 pulses per burst. Each pulse has a pulse width of 1 ms and an inter-pulse interval of 1 ms. (C) 10-kHz SCS applies 30 μs rectangular pulses at a rate of 10 kHz.

2.3.1 Finite element analysis

In this study, we utilized a lower thoracic spinal cord FEM model which has been described in detail in a previous study (**Fig. 2.1**).[127] The volume conductor model domains were gray matter, white matter (with attached dorsal rootlets), cerebrospinal fluid (CSF), dura mater, epidural fat, vertebral bone, intervertebral discs, electrode encapsulation, and general thorax (**Fig. 2.1A**). The

electrical conductivities for each region are given in **Table 2.1**.[83,127–131] The white matter had an anisotropic conductivity, which is known to affect thresholds in neurostimulation models.[132] We defined the gray and white matter boundaries and dimensions from previously published transverse cross sections of a cadaveric T11 spinal cord.[133] We attached five 0.25 mm diameter dorsal rootlets at each spinal level.[134] The dorsal CSF layer separating the spinal cord and dura was 3.2 mm thick.[135] The dura mater was 300 μm thick with the dorsal surface flattened for computational simplicity.[83,136] We aligned nine identical vertebrae in the rostrocaudal direction that were separated by intervertebral discs.[137] The SCS lead was surrounded by a 300 μm thick encapsulation layer.[129] The SCS lead was a cylindrical percutaneous electrode array with eight contacts and a diameter of 1.3 mm. The electrode contacts were 3 mm long separated by 1 mm of insulation in between each contact. We generated a volume mesh using 3-matic (Materialize, Belgium), with a higher mesh density in the regions surrounding the electrode contacts.

Table 2.1: Tissue conductivities in finite element model

FEM Model Domain	Conductivity (S/m)	Reference
Gray matter	0.23	[128]
White matter (longitudinal)	0.60	[128]
White matter (transverse)	0.083	[128]
CSF	1.70	[128]
Dura	0.60	[83]
Electrode encapsulation	0.11	[127,129]
Epidural fat	0.25	[131]
Vertebrae	0.02	[130]
Intervertebral disc	0.65	[131]
Outer thorax	0.25	[128]

We imported the volume mesh into COMSOL Multiphysics (COMSOL, Inc., MA, USA). In COMSOL, we solved the Laplace equation $\nabla \cdot \sigma \nabla V = 0$ (σ = electrical conductivity, V = electric voltage) to evaluate the spatial potential distributions generated during stimulation. We applied unit current sources of +1 mA and -1 mA to the anode and cathode, respectively. The anode and cathode were separated by one inactive electrode, which corresponded to a total separation of 8 mm center-to-center. We grounded the outer surfaces of our model domain to 0 V. We modeled the electrode shaft as a perfect insulator and inactive contacts as floating equipotential surfaces with no net current across their surface. To calculate the spatiotemporal potential fields generated by a given stimulation amplitude and SCS paradigm, we calculated electrostatic solutions and scaled the resultant spatial potential field by the appropriate time-dependent waveform and stimulus amplitude.[103] To assess the neural response to SCS, we then applied these time- and space-dependent extracellular voltages to the neuron models described below. It is important to note that these electrostatic solutions ignore frequency-dependent and propagation effects that may affect the calculated extracellular potentials and the corresponding neural response, especially for higher stimulation frequencies (e.g., 10-kHz SCS).[104] However, recent work has shown that electrostatic solutions were able to predict activation thresholds during 10-kHz SCS that were in good agreement with the activation thresholds predicted using a frequency-dependent approach.[103]

2.3.2 Primary afferent models

In this study, we modeled two classes of afferent fibers: dorsal column (DC) fibers and dorsal rootlet (DR) fibers. The DC fibers were oriented rostro-caudally within the dorsal columns. We placed these DC fibers at 103 positions within the dorsal columns (**Fig. 2.3A**). We considered models both with and without small diameter collaterals that were produced at nodes of Ranvier and then traveled to terminate in the dorsal horn. We examined the effects of spacing between

these collaterals (**Fig. 2.3B**) as well as their termination patterns within the dorsal horn (**Fig. 2.3C-E**), and they are described in detail in the section "Primary afferent collateralization". The DR fibers ascended through a dorsal rootlet and then entered the spinal cord white matter (**Fig. 2.4A-B**). From here, they traversed medially and ventrally, while continuing to ascend rostrally a short distance, until reaching a branch point within the white matter, where they bifurcated into ascending and descending branches in the dorsal columns (**Fig. 2.4C**). We restricted these DR bifurcation points to the 33 most lateral dorsal column positions shown in **Fig. 2.3A**. We also tested these model fibers with and without collateralization. We modeled all primary afferents by adapting a previously published axon model.[102] This axon model has a double-cable structure with finite myelin impedance and periaxonal conductivity between the axonal membrane and the myelin. Nodal compartments contain fast sodium channels, persistent sodium channels, slow potassium channels, as well as passive leak channels and membrane capacitance. Nodes of Ranvier are separated by myelinated internodes, which are subdivided into the myelin sheath attachment area, the main paranodal segment, and general internode. This model is known to demonstrate excellent agreement with experimental results in predicting the axonal response to extracellular stimulation.[138] We generated DC fibers for the discrete fiber diameters of 5.7, 7.3, 8.7, 10.0, and 11.5 μm. DR fibers consisted of a "parent" fiber ascending the dorsal rootlet then bifurcating into a "child" fiber of smaller diameter that ascended and descended in the dorsal columns.[103,136] The parent/child fiber diameter pairings were as follows: 7.3/5.7, 8.7/7.3, 10.0/8.7, 11.5/10.0, and 12.8/11.5 μm.[103]

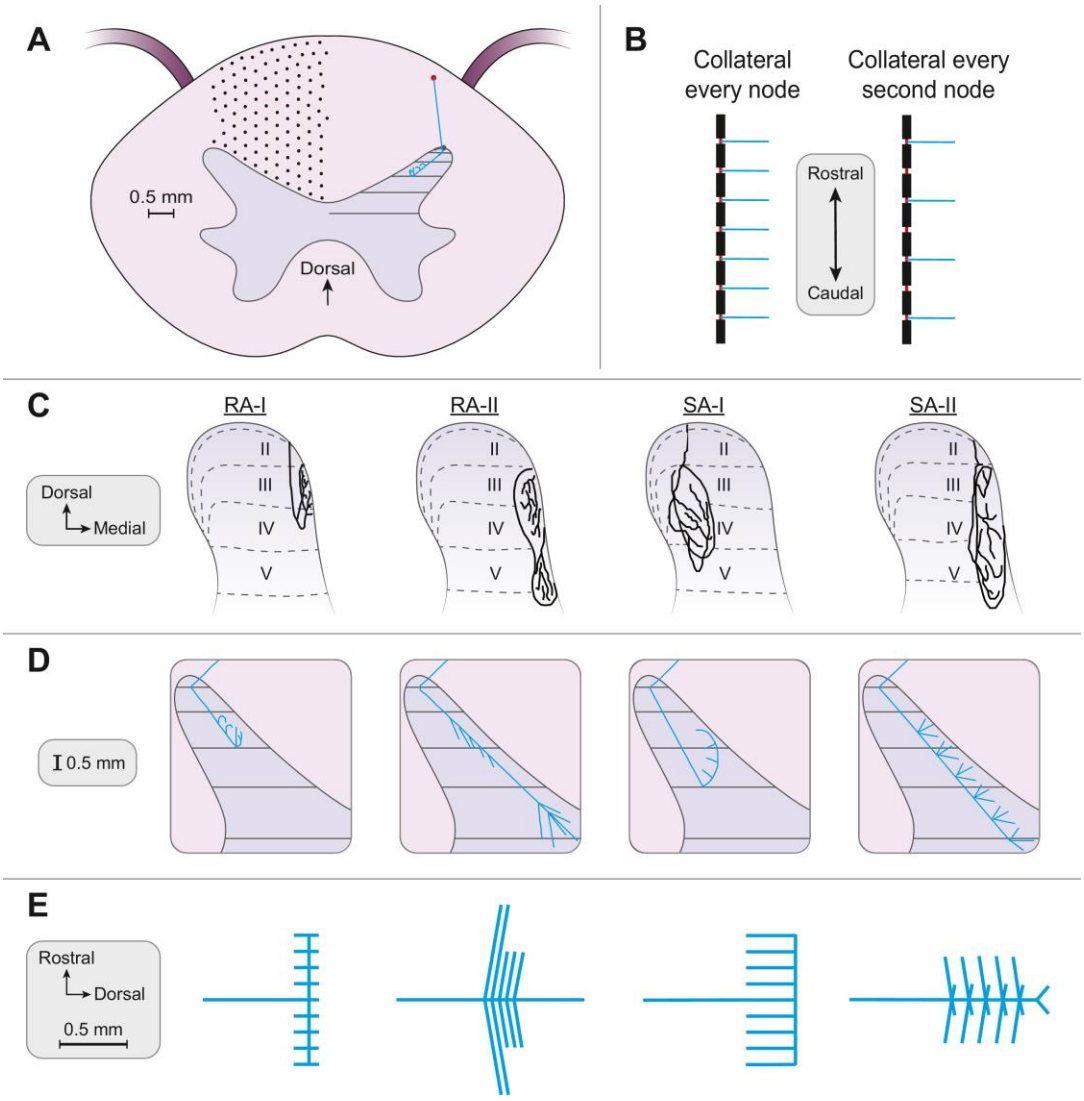

Figure 2.3: Dorsal column (DC) fibers and collateral termination patterns. (A) Axial spinal cord cross section along with black dots representing the positions of DC fibers (running in and out of the page) within our model. The right side shows a mirror-image example of a DC fiber and a collateral. The red dot is the position of the rostro-caudally oriented parent fiber. The blue line is a collateral taking a straight path to the superficial dorsal horn and producing a characteristic termination pattern within the gray matter. (B) Depiction of 2 different collateral spacing patterns that we examined in conventional spinal cord stimulation. On the left, a fiber produces a collateral at every node. On the right, collateral arises from every second node. (C) Tracing of textbook reproductions of collateral terminations for 4 different afferent subtypes: rapidly adapting type I (RA-I), rapidly adapting type II (RA-II) (alternatively referred to as Pacinian corpuscle or "PC"), slowly adapting type I (SA-1), and slowly adapting type II (SA-II). Reconstructions are from (Brown, 1981).[139] Transverse view of model collaterals terminating within the dorsal horn. (E) Sagittal view of model collaterals

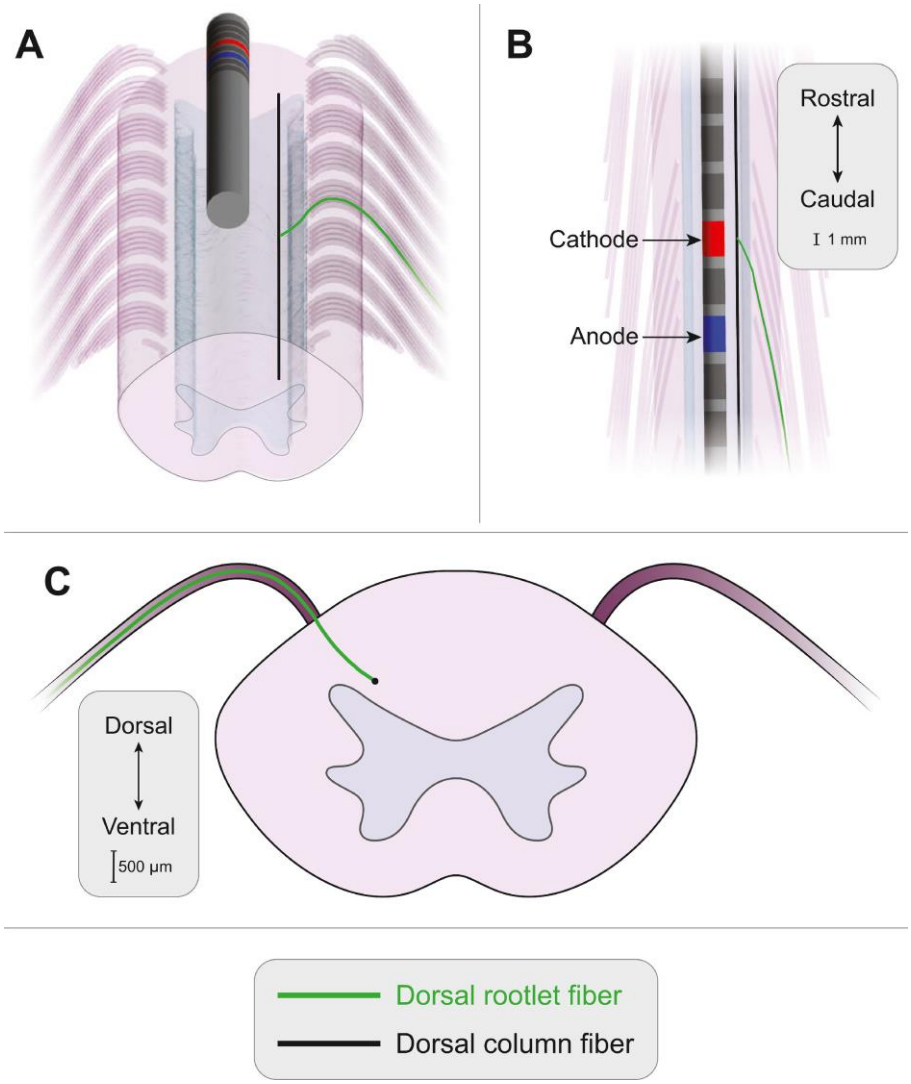

Figure 2.4: Dorsal rootlet (DR) fiber models. (A) The DR fibers ascend through a dorsal rootlet and then enter the white matter. The DR fibers then bifurcate into smaller diameter fibers that ascend and descend within the dorsal columns. (B) Top-down view of a DR fiber next to the SCS electrode array. (C) Transverse view of a DR fiber reaching its final position within the dorsal column before bifurcating.

2.3.3 Primary afferent collateralization

It is well known that primary afferent fibers in the dorsal columns produce small diameter collaterals that terminate in the dorsal horn and synapse on local neurons.[139] The effects of these collaterals have previously been studied *in silico*, and it is generally believed that they decrease SCS activation thresholds.[118,140,141] However, a recent modeling study of 10-kHz SCS found more complex effects of collateralization and, in some cases, increases in threshold during 10 kHz

SCS.[83] Typically, these collateral models have been implemented as straight axons traveling ventrally from axons located at a few positions within the dorsal columns. This approach is an oversimplification, as it is known that these collaterals project to the dorsal horn where they produce complex three-dimensional (3D) termination patterns that vary across different receptor classes.[32,139] In this study, we sought to perform comprehensive modeling of how collateralization affects the activation thresholds of primary afferent fibers. To achieve this goal, we developed four different 3D models of low-threshold mechanoreceptor collateral termination patterns, based upon previously published reconstructions and descriptions (**Fig. 2.3C-E**).[139,142–144] These termination patterns represented the following four receptor classes: rapidly adapting type I (RA-I), rapidly adapting type II (RA-II; Pacinian corpuscle; PC), slowly adapting type I (SA-I), and slowly adapting type II (SA-II). The collateral diameters were 2.0 μm. For all cases, the collaterals arising from the DC fibers took a straight path from the parent fiber in the dorsal columns to enter the gray matter at the same fixed point in the superficial dorsal horn. From this location, the collaterals differentiated into their characteristic termination pattern within the dorsal horn.

For conventional SCS, we tested three different conditions for each specific collateral type, all of which we compared to the basic DC fiber model with no collaterals. The first condition was to introduce one collateral at the central node of the axon, at the rostrocaudal level of the cathode's center. In the second motif, we added 11 collaterals, with a collateral coming off each of the five nodes rostral and caudal to the central node of Ranvier. In the third motif, we once again added 11 collaterals, but instead with a collateral coming off every other node of Ranvier (**Fig. 2.3B**).

For burst and 10-kHz SCS, we compared baseline (no collateral) models to a model with collaterals separated by one internode (i.e., arising from every adjacent node), starting with a node several millimeters caudal to the anode, all the way to a node several millimeters rostral to the

cathode. We chose to implement this approach for burst and 10-kHz SCS because the large-amplitude anodic phases during these newer stimulus waveforms are comparable to the amplitude of the cathodic phases, unlike the relatively low-amplitude and long-duration anodic phase in conventional SCS (**Fig. 2.2**). During the anodic portion of the biphasic waveform, the electrodes originally acting as the anode and cathode have reversed polarities. Therefore, activation can be triggered at a node near the contact that was originally designated the "anode," which is now being driven to a negative potential. For this reason, to study the effects of axon collaterals on activation thresholds, we increased the number of collaterals to extend past both active electrodes, which could both act as initiation points for activation in burst and 10-kHz SCS.

We also examined the effects of collateralization on DR fibers. In all cases, DR fiber collaterals were spaced by one internode. For conventional SCS, eleven total collaterals were produced surrounding the cathode, whereas for burst and 10-kHz SCS collaterals extended several millimeters rostral to the cathode and several millimeters caudal to the anode.

2.3.4 Local cell models

Activation of local neurons, specifically inhibitory interneurons in the dorsal horn, has been speculated as a mechanism of action in both conventional and novel forms of SCS.[84,116] Therefore, we investigated if there is direct activation of local neurons in the superficial dorsal horn by conventional, burst, and 10-kHz SCS. It is known that 3D cell morphology and orientation are important in determining the neuronal response to extracellular stimulation.[145,146] To incorporate realistic superficial dorsal horn cell morphologies, we utilized previously published digital reconstructions of a rat superficial dorsal horn interneuron (NeuroMorpho ID: NMO_34018) and projection neuron (NeuroMorpho ID: NMO_34017) (**Fig. 2.5A-B**).[147,148] The interneuron's soma was 25.4 μm in diameter, while the projection neuron's soma was 31.3 μm in diameter. We

positioned these local neuron models within five equally spaced cross-sectional slices (separated rostro-caudally by 2 mm) that ranged from the center of the anode to the center of the cathode. Within each slice, we placed the neurons at six locations in the superficial dorsal horn, separated by 150 μm mediolaterally and 200 μm dorsoventrally (**Fig. 2.5C**).

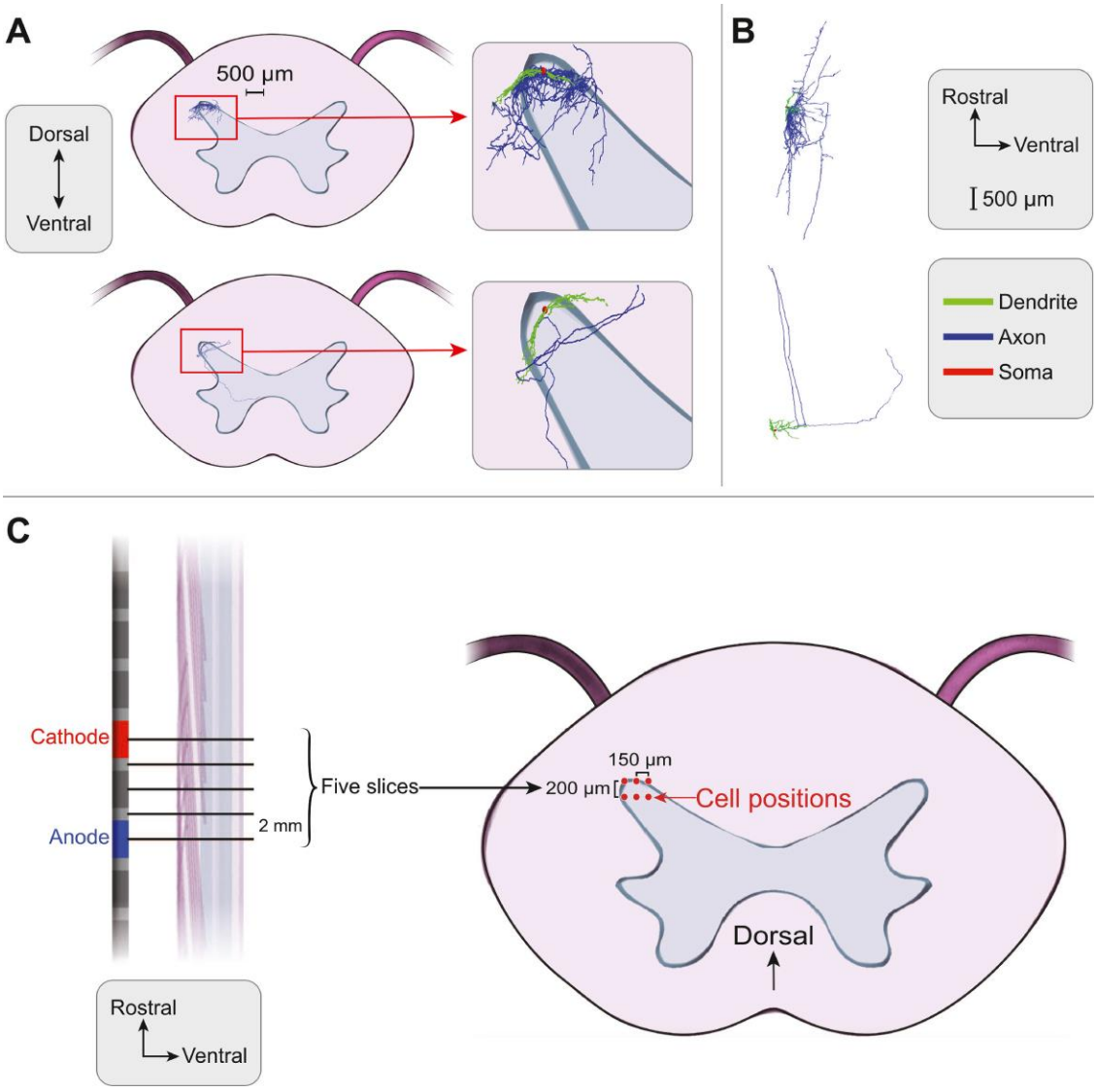

Figure 2.5: Local neuron models. (A) Transverse view showing an interneuron (top) and projection neuron (bottom) within the dorsal horn. (B) Sagittal view of the interneuron and projection neuron. (C) We placed interneuron and projection neurons at 30 positions within the dorsal horn. We took 5 transverse cross-sections separated by 2 mm each ranging from the center of the anode to the center of the cathode. Within each transverse slice, we placed the interneuron and projection neurons at 6 points within a 2-dimensional grid in the superficial dorsal horn. The positions were separated by 150 μm in the mediolateral direction and by 200 μm in the dorsoventral direction.

Both neurons had identical biophysical properties and thus differed only by morphology. We adapted the method described by Aberra et al. to myelinate the cell axons.[149] We introduced 1 μm long nodes of Ranvier at all bifurcations in the axonal arbor, separated by myelinated sections with intermittent nodes of Ranvier. We determined the internodal spacing by the ratio L/D = 100 (L = internodal spacing, D = fiber diameter) using the original compartments' diameters.[149–151] We scaled myelinated compartments assuming a g-ratio (ratio of inner axonal diameter to outer myelinated fiber diameter) of 0.8.[152] Axonal branches shorter than 20 μm or less than 0.2 μm in diameter were unmyelinated.[149] Myelinated sections had a membrane capacitance of 0.02 $\mu F/cm^2$ and a membrane resistance of 1.25 $M\Omega \cdot cm^2$. [149,153]

We derived the electrical biophysics of the nodes of Ranvier, soma, dendrites, and unmyelinated axons from previous experimental and computational modeling studies. We modeled the axonal terminations as biophysically equivalent to nodes of Ranvier.[149] We restricted active ion conductances to sodium and delayed rectifier potassium, which are sufficient in recapitulating the electrical behavior of tonic firing substantia gelatinosa neurons.[154] We used the ion channel dynamics for the sodium and potassium channels described by Melnick et al.[154] Unmyelinated axonal compartments had a maximum sodium conductance of 1.8 S/cm^2, whereas the axon initial segment and nodes of Ranvier had a maximum sodium conductance of 3.45 S/cm^2.[154,155] The soma had a maximum sodium conductance of 0.008 S/cm^2, while dendrites had no sodium conductance.[154] Non-myelinated compartments had a cell membrane specific capacitance of 0.85 $\mu F/cm^2$.[156] Maximum potassium conductances in the dendrites, soma, and active axonal compartments were 0.034, 0.0043, and 0.076 S/cm^2, respectively.[154,157] Non-myelinated compartments had a specific membrane resistivity of 91 $k\Omega \cdot cm^2$.[154] The reversal potentials were -70 mV for the leak channels, +60 mV for the sodium channels, and -84 mV for

the potassium channels. [154] The cytoplasmic axial resistivity was 200 Ω·cm. [147] Finally, to avoid self-activation for high sodium channel densities, we set the sodium channel steady state activation variable (m_∞) to 0 for membrane potentials more negative than -65 mV. [147] We validated the local cell models by comparing their response to both intracellular and extracellular stimulation to electrophysiological data reported in previous studies. First, we compared the model firing rates to current clamp data for tonically firing lamina I spinal neurons.[158] We also compared the model activation thresholds in response to extracellular microstimulation to previously published experimental and modeling data.[159]

2.4 Results

To predict neural recruitment during SCS, we used the FEM to calculate the electric potentials generated throughout the spinal cord by a clinical SCS electrode array implanted at the lower thoracic spinal levels (**Fig. 2.1A-B**). To model the neural response to SCS, we interpolated the electric potentials onto multi-compartment neuron models to find the minimum stimulation amplitudes necessary to produce a suprathreshold action potential response (**Fig. 2.1C**).[108,126] We determined activation thresholds for DC fibers, DR fibers, local interneurons, and local projection neurons. We performed this analysis for conventional, burst, and 10-kHz SCS (**Fig. 2.2**).

2.4.1 Primary afferent activation thresholds

We modeled the recruitment profiles of two primary afferent fiber classes which have been previously implicated in SCS: DC fibers ascending from more caudal dermatomes and DR fibers entering the spinal cord at approximately the same level as the active cathode.[119] These fibers produce small-diameter collaterals that terminate in the local gray matter, with different termination patterns depending on the fiber's physiological class. [32,139,142–144] It is known that DC

fiber collateralization can affect the stimulation amplitudes required to generate action potentials in target neurons during SCS, and there are numerous collateralization-related parameters that could individually affect these activation thresholds.[118] In this study, we considered the spacing between collaterals (i.e., number of nodes between adjacent collaterals), physiologic-specific termination pattern in the dorsal horn, and mediolateral electrode shift.

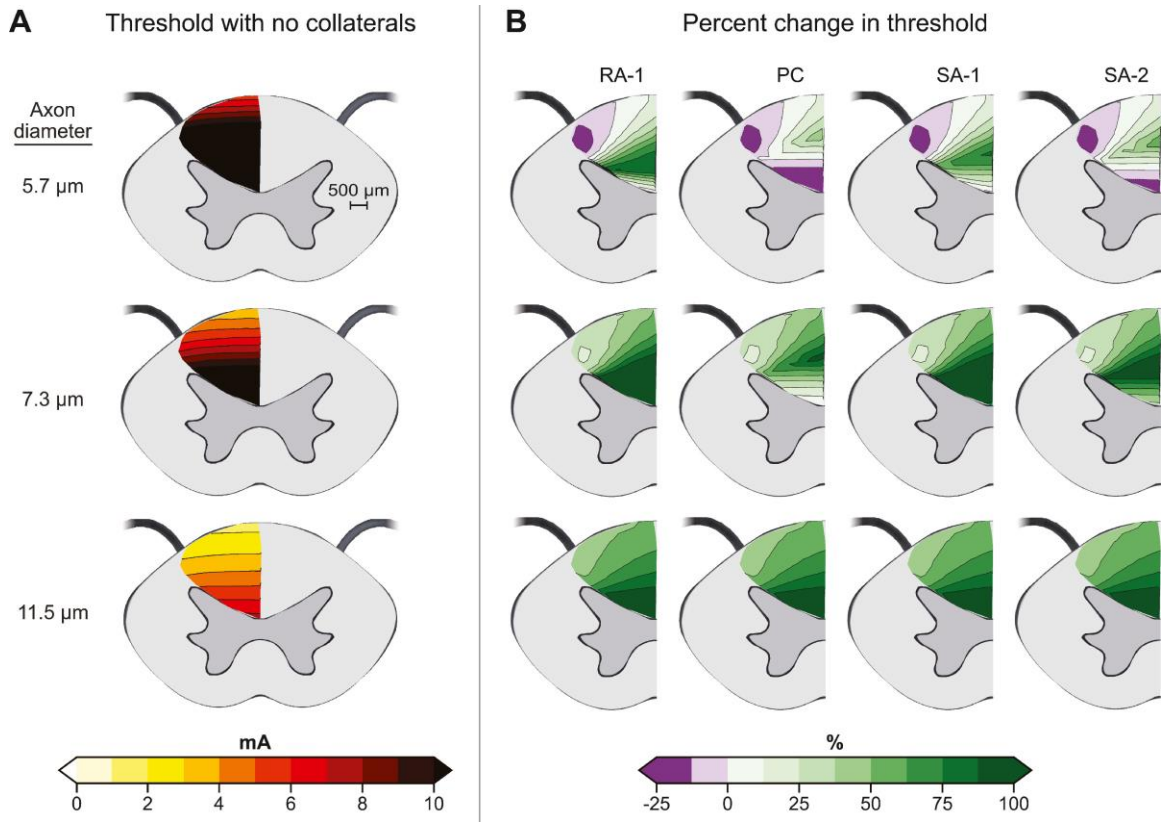

Figure 2.6: Effect of collateral termination patterns on activation thresholds for conventional spinal cord stimulation. (A) Activation thresholds for axons with no collaterals. (B) Percent change in the activation thresholds for 4 different collateral terminations patterns (rapidly adapting type I (RA-I), Pacinian corpuscle (PC), slowly adapting type I (SA-1), and slowly adapting type II (SA-II)) relative to the same axons without collaterals. We included collaterals at 11 nodes of Ranvier near the active electrodes. In (A) and (B), the results for 5.7, 7.3, and 11.5 µm axons are shown in the top, middle, and bottom rows, respectively.

We developed models of four different collateral termination patterns (all collaterals were 2.0 µm in diameter) based upon previously published reconstructions: rapidly adapting type I, rapidly adapting type II (also referred to as "Pacinian corpuscle"; PC), slowly adapting type I, and slowly adapting type II (**Fig. 2.3C-E**). For the fibers without collaterals, we observed that

activation thresholds decreased monotonically as fiber diameter increased (**Fig. 2.6A**; **Supp. Fig. 2.1A**). We observed that the different collateral termination patterns had different effects on the activation thresholds during conventional SCS depending on the diameter of the parent fiber in the dorsal columns (**Fig. 2.6B**; **Supp. Fig. 2.1B**). In response to conventional SCS, the termination pattern affected the percent change in threshold (i.e., collaterals vs. no collaterals) for small-diameter (i.e., 5.7 and 7.3 μm) fibers located within the ventral aspect of the dorsal columns. However, for the most dorsal fibers, which are more likely to be activated by SCS, the thresholds were largely unaffected by the relative termination pattern for all fiber sizes. For large-diameter fibers, we observed that the threshold changes due to the presence of collaterals were approximately uniform across all four termination patterns. For this reason, and to significantly reduce computational demands, we only used the PC termination pattern when including collaterals in the remaining analyses. We utilized the PC termination pattern because it was the termination pattern that was most likely to produce complex changes in the activation thresholds (**Fig. 2.6B; Supp. Fig. 2.1B**).

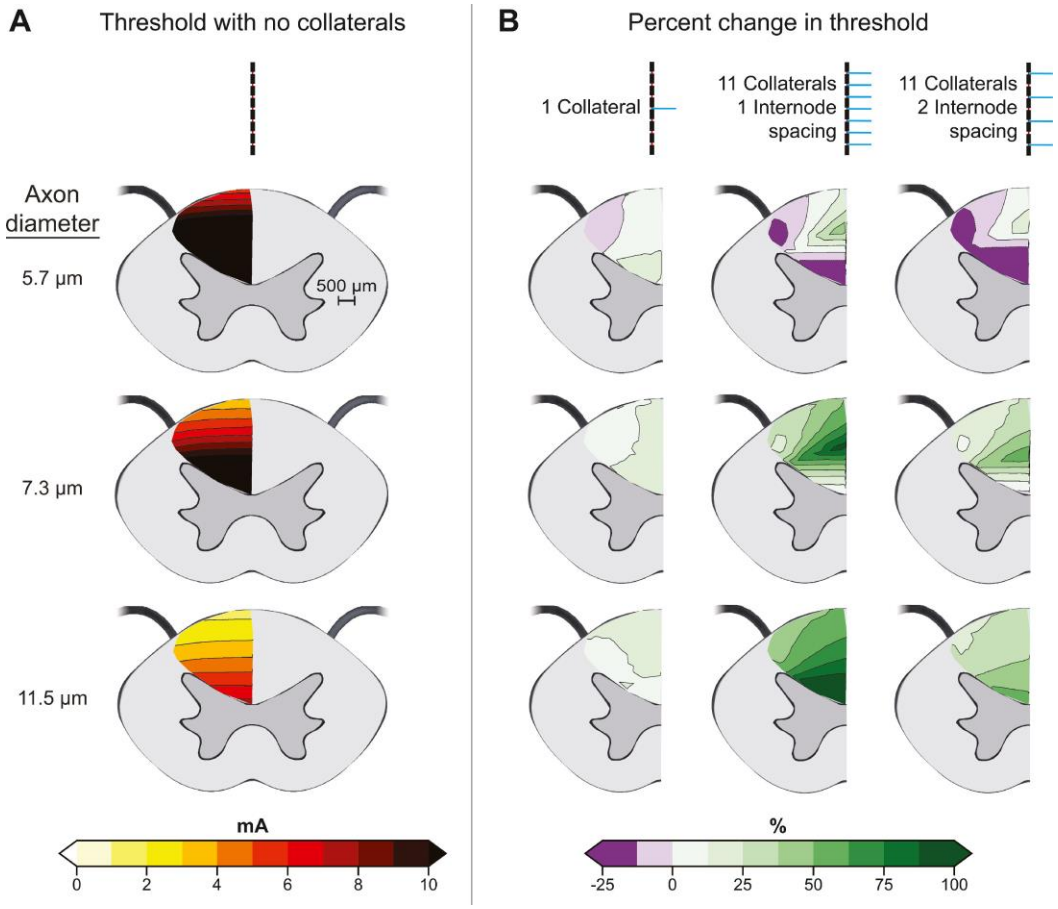

Figure 2.7: Effect of collateral number and inter-collateral spacing on the axonal response to conventional spinal cord stimulation. (A) Activation thresholds for axons with no collaterals. (B) For all parent fiber diameters, there are clear differences in the percent change in threshold for the models with 1 collateral, the fibers with 11 collaterals separated by 1 internode, and the fibers with 11 collaterals separated by 2 internodes. The results for 5.7, 7.3, and 11.5 µm axons are shown in the top, middle, and bottom rows, respectively.

Next, we investigated how the number of collaterals and the spacing between adjacent collaterals affected the activation thresholds during conventional SCS. This analysis demonstrated clear threshold differences between an axon without collaterals (**Fig. 2.7A**; **Supp. Fig. 2.2A**) relative to an axon with one single collateral, an axon with 11 collaterals separated by one internode, and an axon with 11 collaterals arising from every second node (**Fig. 2.7B; Supp. Fig. 2.2A**). For all diameters, there was a mediolateral gradient in which axon collaterals produced excitatory changes in the activation thresholds for more lateral fibers compared to medial fibers (i.e., decreases for 5.7 µm fibers and smaller increases for 7.3 – 11.5 µm fibers). Expanding the

spacing between collaterals from every node to every second node consistently reduced the relative increases in threshold (for 7.3 – 11.5 μm fibers). Finally, because SCS lead position can vary due to migration or implantation in the lateral epidural space [58,160] we performed simulations with a lateral lead placement. Although this lateral lead placement altered the spatial recruitment profile with the dorsal columns, it only produced small differences in the amplitudes necessary for DC fiber activation (**Supp. Fig. 2.2B**). Furthermore, axon collaterals produced qualitatively similar changes in the activation thresholds for both midline and lateral lead placements (**Supp. Fig. 2.2B**).

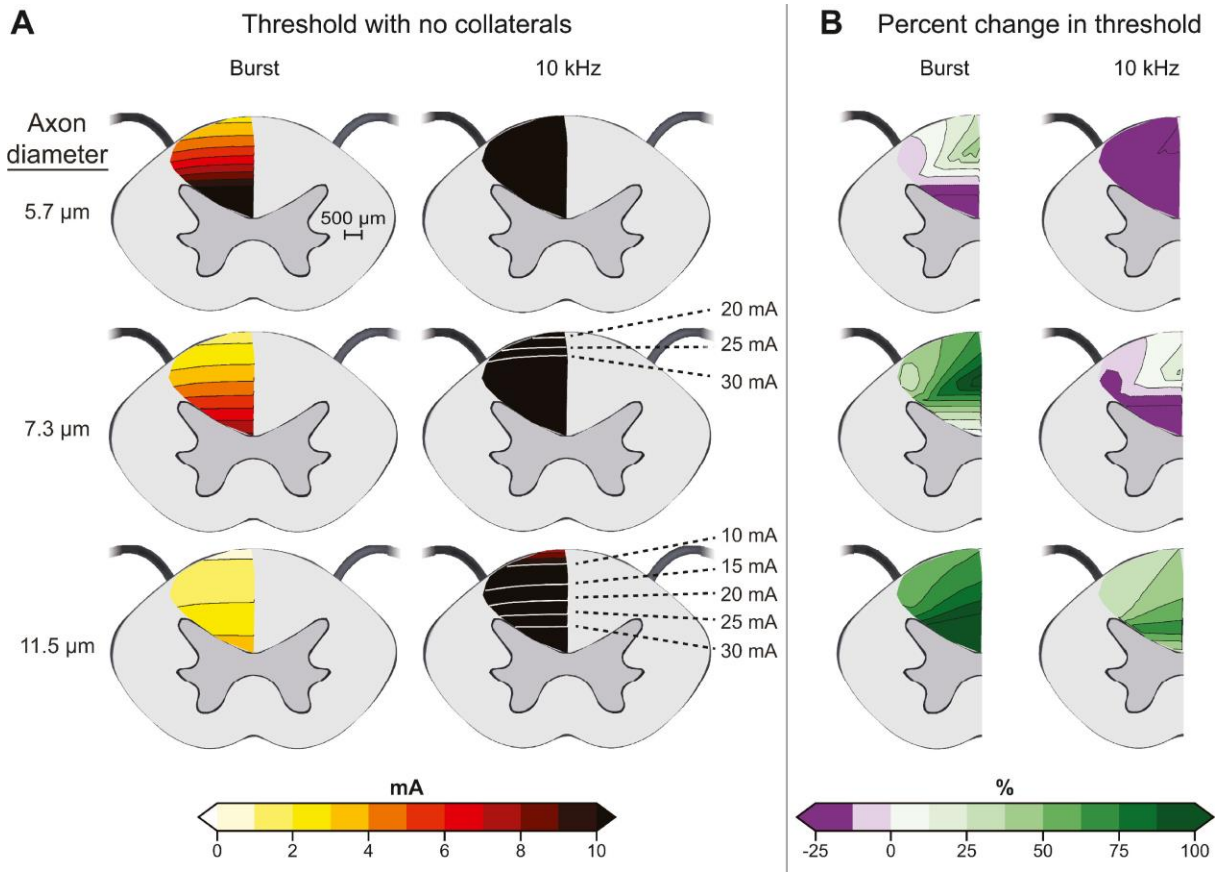

Figure 2.8: Effect of collateralization on the axonal response to burst and 10-kHz spinal cord stimulation. (A) Activation thresholds for axons with no collaterals. (B) Percent change in activation thresholds for the same axons after adding 11 collaterals separated by 1 internode. The results for 5.7, 7.3, and 11.5 μm axons are shown in the top, middle, and bottom rows, respectively.

To examine the effect of collateralization on newer forms of clinical SCS, we conducted a similar analysis to that described above for burst and 10-kHz SCS. Burst SCS always had lower

activation thresholds compared to conventional SCS, whereas 10-kHz had significantly higher thresholds (**Fig. 2.8A**; **Supp. Fig. 2.3A**). For the largest-diameter afferents, burst SCS activation thresholds were commensurate with clinical burst SCS amplitudes. This result suggests it is possible that burst SCS activates primary afferents, and the lack of paresthesia may be due to the subset of fibers activated and/or the temporal properties of activation. Conversely, we observed that 10-kHz SCS activation thresholds were higher than typical clinical stimulation amplitudes. In agreement with previous studies, this result suggests that clinical 10-kHz SCS is not directly activating afferent fibers.[83,161] Similar to conventional SCS, activation thresholds decreased monotonically as fiber diameter increased for both burst and 10-kHz SCS. During burst SCS, the effects of collateralization on activation thresholds were qualitatively similar to the effects that we observed for conventional SCS (**Fig. 2.8B**; **Supp. Fig. 2.3A**). Namely, we saw that for 5.7 μm fibers the threshold decreased for laterally positioned fibers. For larger fibers, the thresholds always increased, but once again lateral fibers had smaller threshold changes relative to medial fibers. The effects of collateralization during 10-kHz SCS were different. Thresholds decreased for all 5.7 μm fibers, for lateral and ventral 7.3 μm fibers, and the most ventral 8.7 μm fibers. Additionally, the larger diameter 10.0 and 11.5 μm fibers had smaller percent increases in activation threshold compared to conventional and burst SCS. However, it is important to note that the activation thresholds for 10 kHz SCS were always significantly higher than for conventional or burst SCS. Finally, similar to conventional SCS, we observed qualitatively similar changes in activation threshold for both midline and lateral lead placements (**Supp. Fig. 2.3B**).

The second class of primary afferents that we considered in our model analysis was DR axons that ascended throughout a dorsal rootlet. Upon entering the spinal cord, they continued ascending and traveled medially until reaching a bifurcation point in the dorsal column, at which

point the fiber divided into a rostrally ascending and caudally descending branch of smaller diameter than the parent DR fiber (**Fig. 2.4**). We assessed the activation thresholds for DR fibers with and without collateralization.

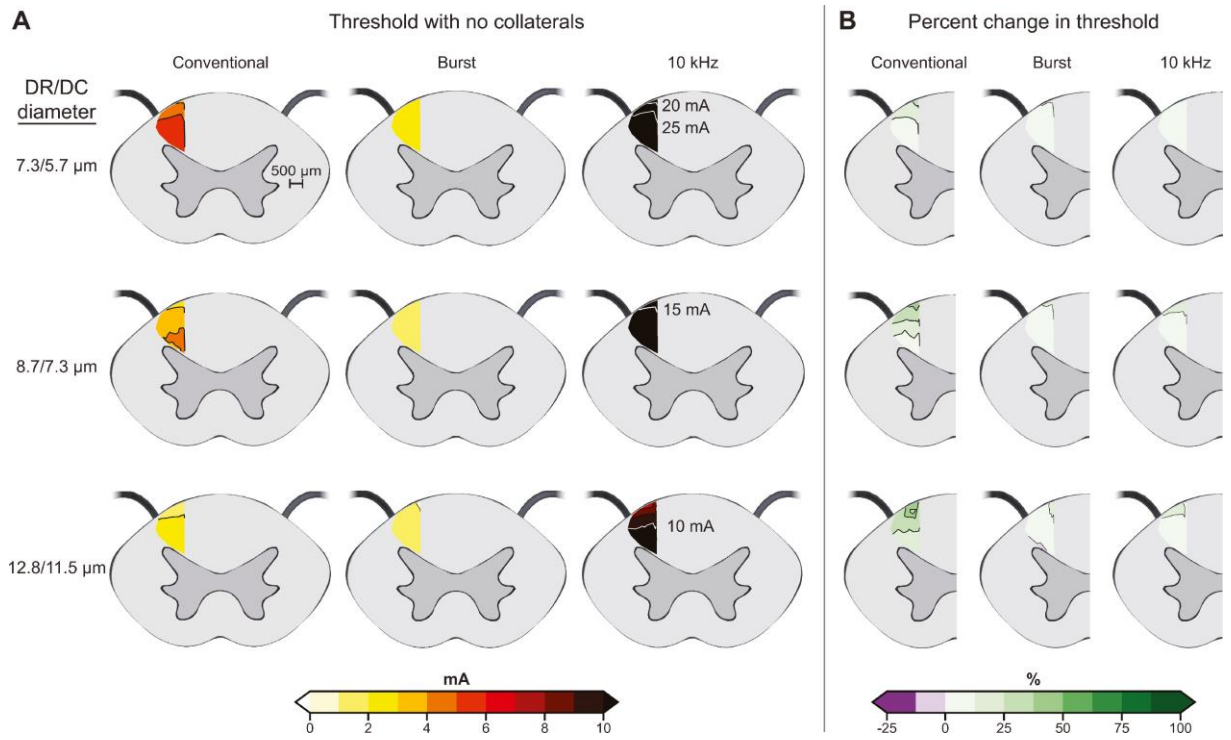

Figure 2.9: Effects of collateralization on the activation thresholds for dorsal rootlet (DR) fibers for conventional, burst, and 10-kHz spinal cord stimulation. (A) Activation thresholds for DR fibers with no collaterals. (B) Percent change in activation thresholds for the same DR fibers after adding collaterals separated by 1 internode. The results for parent/child or DR/DC diameters of 7.3/5.7, 8.7/7.3, and 12.8/11.5 µm axons are shown in the top, middle, and bottom rows, respectively.

In the DR axons, we observed that once again the lowest thresholds were for burst SCS, followed by conventional, and then 10-kHz SCS (**Fig. 2.9A**; **Supp. Fig. 2.4A**). For the DR fibers, axon collaterals produced smaller changes in activation thresholds relative to DC fibers and the DR fiber activation thresholds always increased (**Fig. 2.9B**; **Supp. Fig. 2.4A**). For conventional SCS, axon collaterals produced larger increases in activation thresholds for DR fibers with branching axons located more superficially within the dorsal columns relative to deeper axons. However, for burst and 10-kHz SCS, axon collaterals only produced, at most, small increases in activation thresholds. Finally, for DR fibers, we observed that shifting the electrode laterally

typically reduced thresholds in DR fibers (**Supp. Fig. 2.4B**). However, the effects of collateralization were very similar for midline and lateral lead placements.

2.4.2 Local cell thresholds

The motivating principle behind conventional SCS is the activation of low-threshold afferents that have collaterals synapsing on local neurons in the dorsal horn to reduce pain transmission through post-synaptic activation of inhibitory interneurons.[1,5] However, local neurons in the dorsal horn gray matter have recently been proposed as targets for both conventional and novel forms of SCS. [84,116] To investigate if local neurons are directly recruited by SCS systems, we developed multi-compartment models of interneurons and projection neurons reconstructed from the rat dorsal horn.[147] We then placed these models at six positions within a grid in the superficial dorsal horn, at five transverse cross-sectional slices ranging from the center of the anode to the center of the cathode (**Fig. 2.5**).

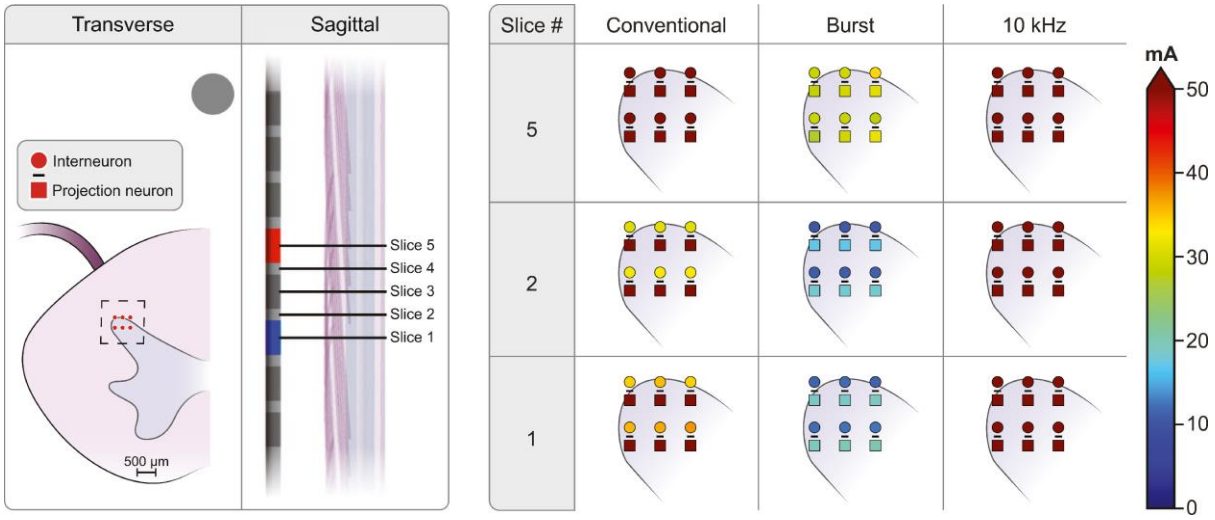

Figure 2.10: Activation thresholds for local neurons in response to burst, conventional, and 10-kHz SCS. At each position, the circle on top depicts the threshold for the interneuron whereas the square depicts the threshold for the projection neuron. The dividing line separating the interneuron and projection neuron thresholds shows the position of the cell.

For both the interneurons and projection neurons, burst SCS consistently had the lowest activation thresholds, followed by conventional SCS, and then 10-kHz SCS with notably higher activation thresholds (**Fig. 2.10**; **Supp. Fig. 2.5**). In our study, both local cell models had identical electrical biophysical properties and differed only by morphology. These morphological differences had significant effects on activation thresholds and the interneuron typically had lower activation thresholds relative to the projection neuron. Interestingly, the neurons whose somas were at caudal locations had lower activation thresholds than more rostral neurons near the level of the cathode. This trend is consistent with the notion that these neurons are being activated at the terminals of their rostrally ascending axons. Accordingly, we observed that rostrally ascending axon terminals were a common initiation point for action potentials. We observed that action potentials were typically initiated at axon terminals for all SCS waveforms. Thus, the interneuron's large, dorsally positioned and rostro-caudally oriented axonal arbor resulted in its lower activation thresholds relative to the projection neuron. Shifting the electrode laterally by 2 mm typically lowered activation thresholds. However, in all cases, the local cell thresholds were well above the activation thresholds for the primary afferents, and notably higher than the stimulation amplitudes used clinically, which is evidence against the direct activation of local cells by clinical SCS.

2.5 Discussion

It is a challenging problem with important clinical implications to identify which neural elements are directly activated by SCS. In conventional SCS, the presumed targets are large-diameter axons in the dorsal columns that carry innocuous touch information. This hypothesis is consistent with the clinical observation that overlap of SCS-induced paresthesias (due to activation of these Aβ fibers) with a patient's painful regions is associated with successful clinical outcomes.[58] Still, questions remain as to which subset of Aβ fibers are being activated, how

relevant variables (e.g., fiber collateralization) affect activation thresholds, and if dorsal horn neurons are being directly recruited. Furthermore, several new forms of clinical SCS, such as burst and 10-kHz SCS, are delivered at subparesthetic stimulation amplitudes which has been interpreted as evidence against activation of Aβ fibers.[1,5,115,161,162]

Clinical and experimental observations opposing direct activation of Aβ fibers have led to hypotheses regarding alternative neural targets and/or mechanisms of action during these newer forms of SCS. However, a lack of paresthesias does not necessarily mean a lack of Aβ fiber activation, but instead could correspond to temporal and/or spatial differences in Aβ-fiber activation that result in paresthesia-free stimulation.[163] Furthermore, it is unclear how well the stimulation amplitudes and experimental conditions utilized in preclinical testing translate to clinical implementation of these newer forms of SCS.[84,164,165] Therefore, in this study, we utilized a computational modeling approach to investigate which neurons are directly activated by these three common SCS modalities. Understanding the direct effects of SCS is a critical step to explain its mechanisms of action, to facilitate the design of future SCS systems, and to improve clinical outcomes.

2.5.1 Axon collaterals produce complex changes in activation thresholds

Previous work has indicated that DC axon collaterals consistently reduce activation thresholds.[118,140] However, our results contradict this common belief, and we found that collateralization frequently increased thresholds. Our results suggest that a major factor that has been previously overlooked is the collateral trajectory as it approaches the gray matter. This factor is evident in the mediolateral gradients in which collaterals produce larger increases in the thresholds of medial DC fibers relative to lateral fibers (**Figs. 2.6**-**2.8**; **Supp. Figs. 2.1**-**2.3**). These mediolateral gradients imply that SCS may preferentially activate lateral DC fibers. A recent study

suggested that proprioceptors and mechanoreceptors are segregated mediolaterally in the dorsal columns, with proprioceptors assuming a more lateral position and mechanoreceptors located medially.[166] This study also reported modality-based differences in diameter (proprioceptors were larger), rostrocaudal length (mechanoreceptors ascended to the brainstem, whereas proprioceptors terminated after ascending several spinal levels), and collateralization (mechanoreceptors produced collaterals while ascending several segments dorsolaterally before joining the dorsal columns, whereas proprioceptors immediately joined the dorsal columns and produced collaterals along the length of the axon). Our results demonstrated significant variation in the effect of collaterals on activation threshold due to fiber location, diameter, and the number and spacing of collaterals, which correspond to the aforementioned differences between proprioceptors and mechanoreceptors. Therefore, our results suggest that these two classes of afferents may be differentially modulated by SCS.

Aβ collaterals produce complex 3D termination patterns within the dorsal horn that vary between different physiological fiber classes.[32,139] Additionally, axon terminals are susceptible to extracellular stimulation because their polarization is driven by the first spatial derivative of the extracellular potential field, compared to the second spatial derivative that drives axons of passage.[149,167–170] Yet, to date, no studies have analyzed if these complex termination patterns are the initial targets recruited by SCS or if specific termination patterns will result in different activation thresholds between fiber subtypes. Therefore, we investigated how DC fibers with four different collateral termination patterns respond to conventional SCS. We observed that the specific collateral termination patterns produced different effects for the smallest diameter (i.e., 5.7 μm) fibers, whereas their effects were relatively uniform for the largest (i.e., ≥7.3 μm) fibers (**Fig. 2.6**, **Supp. Fig. 2.1**). Furthermore, activation of collateral terminals only occurred for ventral

fibers, specifically small-diameter fibers. Therefore, because small-diameter fibers have higher activation thresholds relative to large-diameters fibers and are less likely to be recruited in clinical SCS, our results suggest that primary afferents are not selectively recruited based upon their collateralization patterns within the dorsal horn.

With regards to DR fibers, we observed a different pattern of threshold changes due to axon collateralization. During conventional SCS, DR fiber thresholds increased with dorsal fibers having the largest increases (**Fig. 2.9**; **Supp. Fig. 2.4**). Without considering axon collaterals, these superficial fibers are closer to the stimulating electrodes and should have the lowest activation thresholds. However, our results imply that collateralization increases the activation thresholds of these superficial DR fibers. Some afferents produce collaterals more densely near their spinal cord entry level and more sparsely at rostral positions as they ascend in the dorsal columns.[139,166] Therefore, DC axons from caudal dermatomes (which have ceased producing collaterals) may have lower thresholds than a DR fiber producing several collaterals near the level of the stimulating electrode. A common goal in clinical SCS is to target medial DC fibers without concomitant activation of DR fibers, which can produce unpleasantly strong paresthesia or evoke motor responses.[171] For this reason, understanding the different effects of collateralization on DC fiber versus DR fiber activation has important clinical value, and our results suggest that densely collateralizing DR fibers will have larger increases in activation thresholds relative to DC fibers from more caudal dermatomes producing fewer collaterals.

2.5.2 Clinical SCS does not activate dorsal horn neurons

Dorsal horn neurons have been neglected as direct targets of SCS, given their distance from the electrode and because axons are more readily activated by extracellular stimulation than cell bodies.[119] However, dorsal horn neurons have recently gained popularity as potential targets for

SCS. It has been hypothesized that conventional SCS works by activating GABAergic islet cells located in lamina II [116] and experiments support the potential for 10-kHz SCS to directly recruit inhibitory interneurons.[84] Direct activation of inhibitory dorsal horn neurons, while avoiding simultaneous DC recruitment, is an attractive notion as it could bypass the typically undesirable paresthetic sensations concomitant to Aβ fiber activation.[1,172] This concept would stand in contrast to a recently developed closed-loop SCS paradigm which uses the compound action potentials produced by the activation of DC axons to determine therapeutic stimulation amplitudes.[173]

To investigate the direct response of dorsal horn neurons to SCS, we developed biophysical models of superficial dorsal horn interneurons and projection neurons. Like the afferent fiber models, we found that burst SCS always produced the lowest thresholds, followed by conventional SCS with 10-kHz SCS having notably higher activation thresholds. We observed that for all SCS waveforms and cell locations, the local cell thresholds were definitively higher than primary afferent thresholds (**Fig. 2.10**; **Supp. Fig. 2.5**). This trend suggests that local cells are not directly activated by these clinical SCS waveforms. Our results support the concept that neural elements within the gray matter are not activated because most of the applied currents are shunted through the highly conductive CSF with little current entering the spinal cord.[119]

2.5.3 Limitations and future work

This study is limited by the large parameter space, such as the spinal cord and surrounding tissue anatomy, cellular morphologies and biophysics, and stimulation configurations that can affect the predicted activation thresholds. Our study only provides results for a subset of these parameters. However, we focused our model analyses on parameters that were most relevant to clinical applications of SCS for chronic pain management. To our knowledge, this is the first study to investigate the effects of conventional, burst, and 10-kHz SCS on both afferents and local

neurons within a single modeling framework. This study represents an important step towards understanding the neural response to these common clinical SCS paradigms and provides a strong reference point for future work necessary to further validate and generalize our results.

While our model results suggest that SCS does not directly activate local cells, these cells will still have a subthreshold response to the applied electric field, and these subthreshold effects could still influence dorsal horn processing and produce analgesic effects.[174] Investigations into the mechanisms for low-intensity forms of neuromodulation reveal numerous potential effects, such as altering neuronal excitability, shifting spike timing, affecting network activity, and modulating presynaptic action potential properties and synaptic efficacy.[175–177] These potential subthreshold effects are beyond the scope of this study and future experimental and computational studies investigating these phenomena are necessary to better understand their feasibility.

2.6 Conclusions

In this computational modeling study, we compared the effects of conventional, burst, and 10-kHz SCS for pain on the activation of primary afferents and local neurons in the spinal cord. All three clinical SCS paradigms had the same relative neural recruitment, albeit with different absolute thresholds. We observed that burst SCS always produced the lowest thresholds, followed by conventional SCS, with 10-kHz SCS having the highest activation thresholds. This result suggests that these SCS modalities do not exert differential effects through distinct recruitment profiles. Additionally, our results contradict the common viewpoint that collateralization will uniformly reduce activation thresholds for primary afferents, and instead they predicted complex spatial effect patterns that often increase activation thresholds. We also observed that local cells have significantly higher activation thresholds relative to primary afferents, and this trend suggests that local cells are unlikely to be directly activated by clinical SCS. These results have important

implications for interpreting clinical observations as well as the design of future SCS systems for chronic pain management and other neurological disorders.

2.7 Supplementary Figures

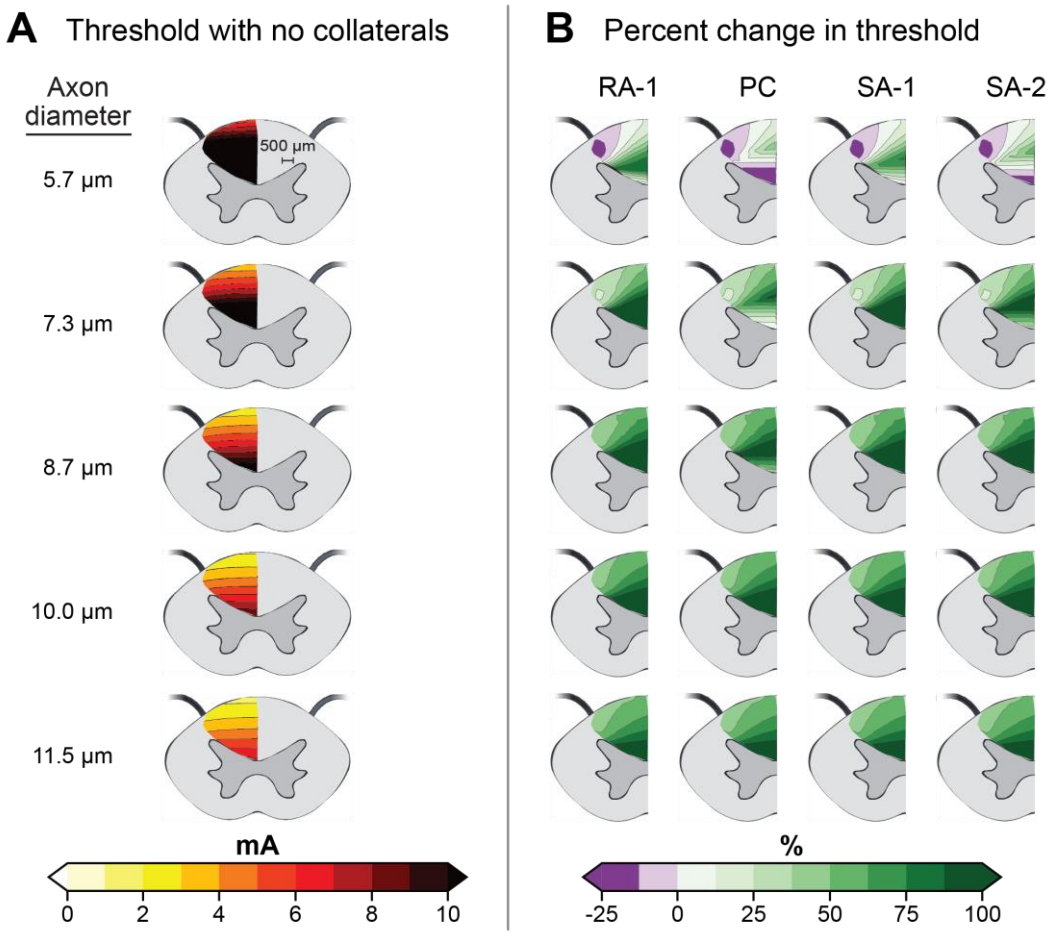

Supplementary Figure 2.1: Effect of collateral termination patterns on activation thresholds during conventional spinal cord stimulation for all diameters. (A) Activation thresholds for axons with no collaterals. (B) Percent change in the activation thresholds for four different collateral terminations patterns (rapidly adapting type I (RA-I), Pacinian corpuscle (PC), slowly adapting type I (SA-1), and slowly adapting type II (SA-II)) relative to the same axons without collaterals. These results are for collaterals at 11 nodes of Ranvier near the active SCS electrodes.

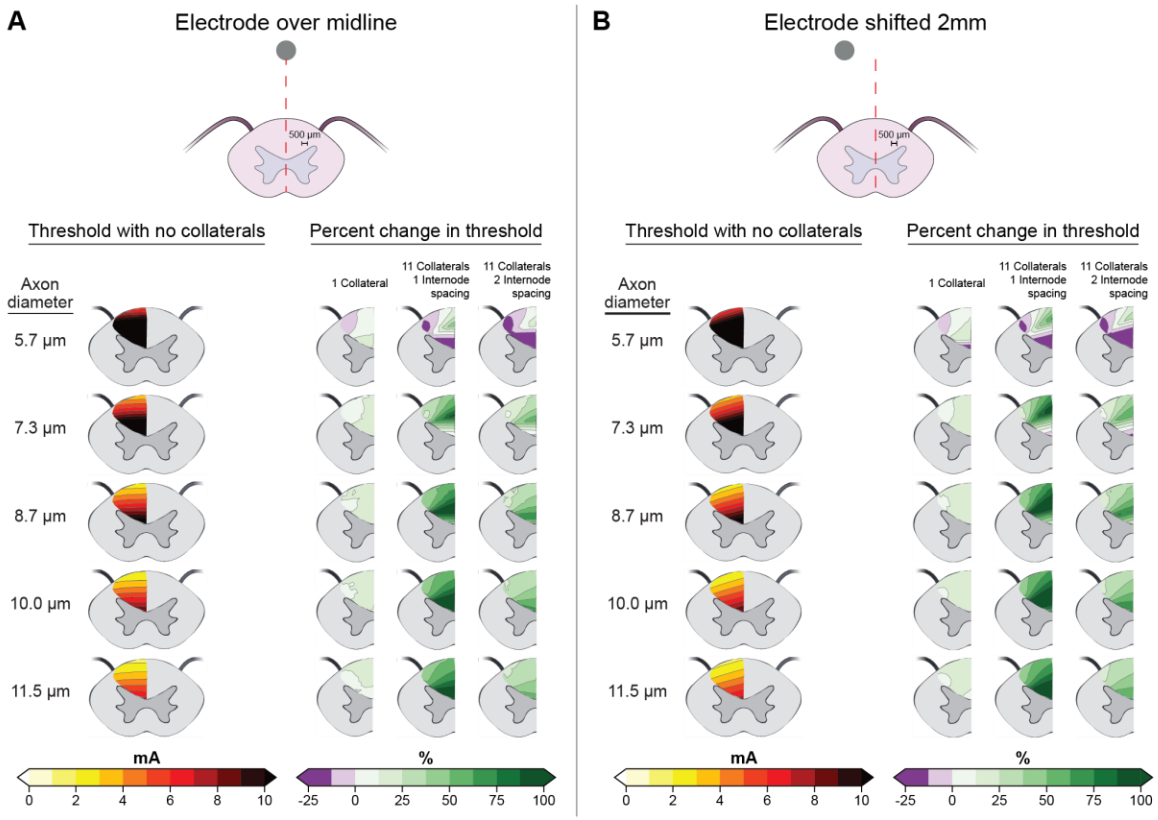

Supplementary Figure 2.2: Effects of collateral number and inter-collateral spacing on the axonal response to conventional spinal cord stimulation. (A) Results with the electrode over the anatomical midline. (B) Results with the electrode shifted 2 mm laterally.

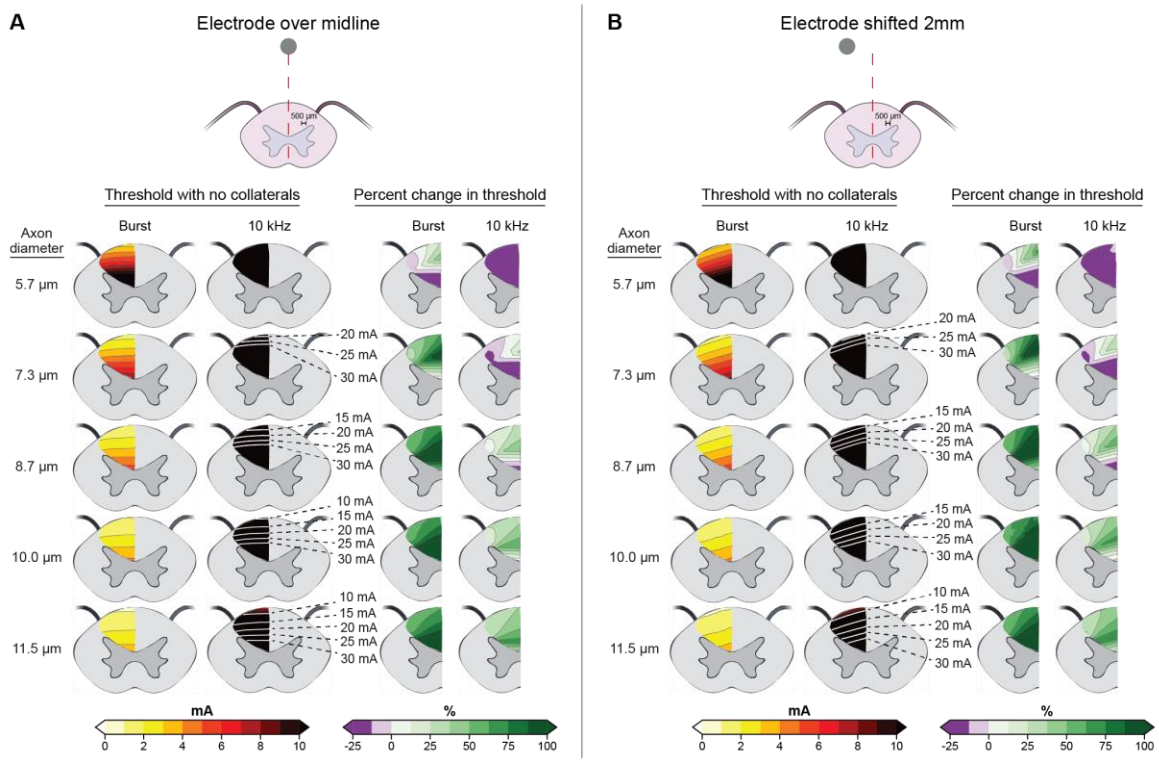

Supplementary Figure 2.3: Effect of collateralization on the axonal response to burst and 10-kHz spinal cord stimulation. (A) Results with the electrode over anatomical midline. (B) Results with the electrode shifted 2 mm laterally.

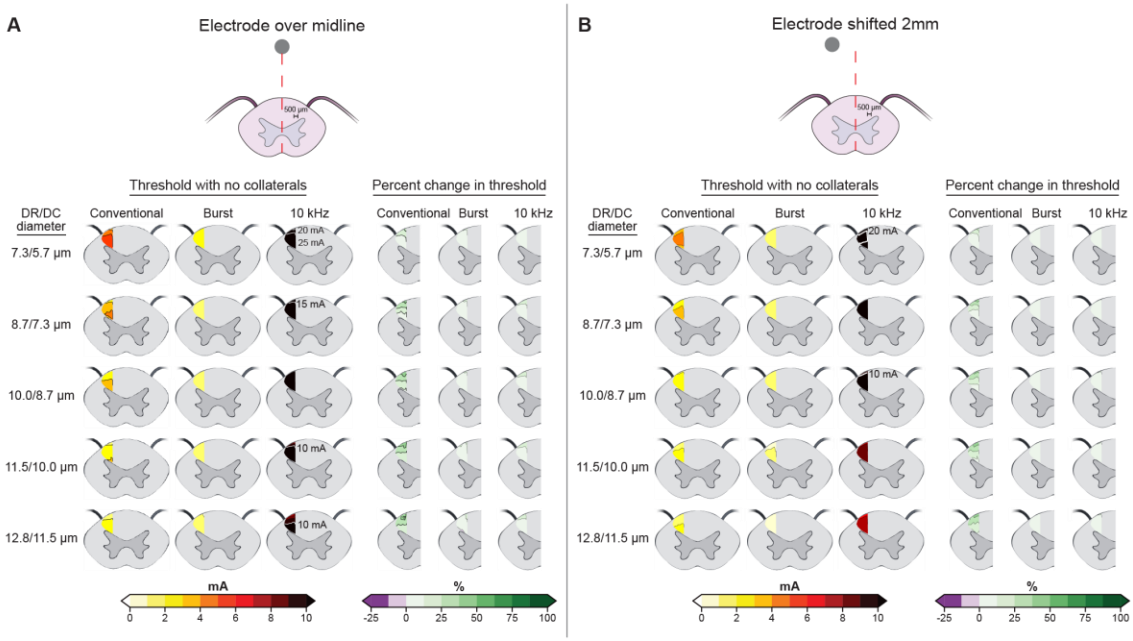

Supplementary Figure 2.4: Effects of collateralization on dorsal rootlet fibers. (A) Results with the electrode over anatomical midline. (B) Results with the electrode shifted 2 mm laterally.

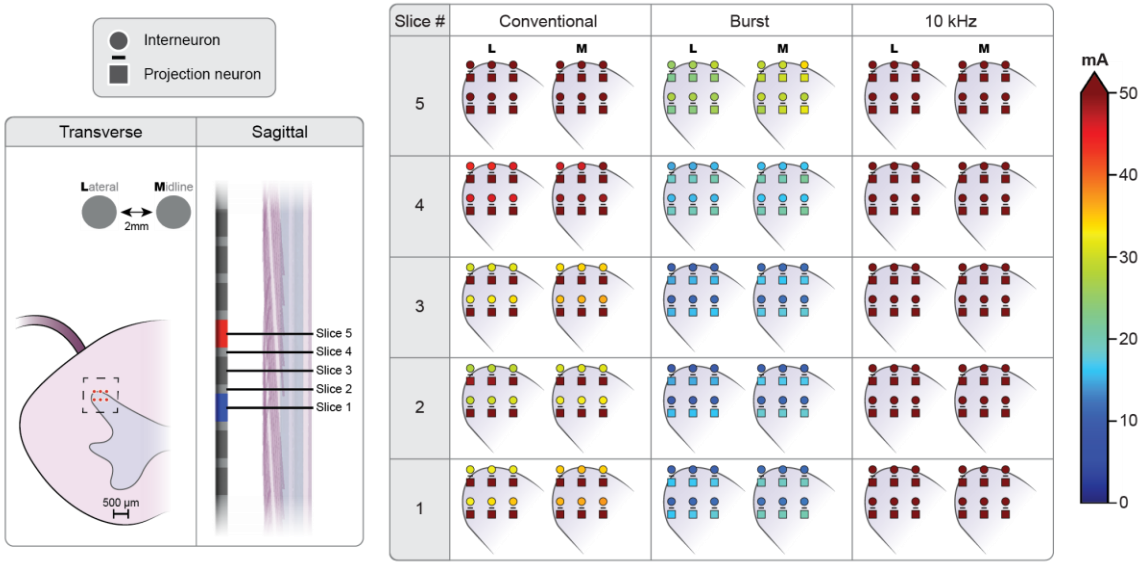

Supplementary Figure 2.5: Activation thresholds for the local interneurons and projection neurons at all positions tested in response to conventional, burst, and 10-kHz spinal cord stimulation. At each position, the circle on top depicts the threshold for the interneuron whereas the square depicts the threshold for the projection neuron. The dividing line separating the interneuron and projection neuron thresholds shows the position of the cell. For each stimulation waveform, the "M" column shows the threshold with the electrode placed over the midline, whereas the "L" column shows the threshold with the electrode shifted 2 mm laterally.

Chapter 3 - Model-based Analysis of Potential Subthreshold Mechanisms of Spinal Cord Stimulation for Chronic Pain

The project described in this chapter is currently being prepared for submission to a peer-reviewed journal.

3.1 Abstract

Introduction: Spinal cord stimulation (SCS) is a common treatment for chronic pain. For decades, SCS was designed to maximize overlap between stimulation-induced paresthesias and the patient's painful areas. However, several modern SCS paradigms relieve pain at amplitudes below the threshold for perceptible sensation. In this study, we used a computational modeling approach to investigate the neurophysiological effects and potentials mechanisms of action of three paresthesia-free SCS paradigms: burst, 1-kHz, and 10-kHz SCS.

Methods: We used the finite element method to evaluate the electric potentials generated throughout the spinal cord during SCS. We then applied these potential fields to biophysical neuron models to evaluate their response to the different forms of stimulation. Specifically, in afferent fibers (C- and Aβ-fibers), we investigated the effects of different SCS waveforms on spike timing and activation thresholds. We also investigated the effects of stochastic ion channel gating in the response of dorsal column axons to SCS. Finally, we analyzed membrane polarization of neurons within the superficial dorsal horn during stimulation.

Results: No form of SCS activated nor modulated spike timing in C-fibers. Spike timing was modulated in Aβ-fibers only at suprathreshold amplitudes. Stochastic ion channel gating had a minimal effect on Aβ-fiber activation thresholds but did produce more random spiking patterns

at suprathreshold amplitudes. Local cells were preferentially polarized in their axon terminals, and the magnitude of this polarization was dependent on cellular morphology and position relative to the stimulation electrodes.

Conclusions: The mechanisms of action of subparesthetic SCS remain unclear. No form of SCS directly activates C-fibers, and modulation of spike timings is not likely at subthreshold amplitudes. Potential subthreshold neuromodulatory effects of SCS on local cells are likely to be presynaptic in nature, as axons are preferentially depolarized by stimulation.

3.2 Introduction

Spinal cord stimulation (SCS) is a neurostimulation approach to treating chronic pain that is refractory to conventional treatment options (e.g., pharmaceuticals, physical therapy). In this technique, one or more multi-contact electrode arrays are implanted into the posterior epidural space within the vertebral column and short pulses of mild electrical current are applied to the spinal cord. Originally, SCS was conceived to exploit the "gate control theory of pain," which implies that activation of large-diameter Aβ fibers (mechanoreceptors carrying innocuous touch information in the dorsal column white matter pathway) will inhibit the transmission of painful signals to the brain.[3,49] However, the exogenous stimulation-induced action potentials in these fibers also travel orthodromically towards the brainstem, and their repetitive activation generates a buzzing or tingling percept typically referred to as paresthesia.[56] Importantly, spatial overlap of the paresthesia sensation with the painful region is associated with successful SCS outcomes.[2,56,58]

Unfortunately, there are several limitations to this standard SCS approach. Many patients find the paresthetic sensation intolerable or distracting, and paresthesia-related complications are a major reason for device explantations.[172,178] Furthermore, these paresthesias can interfere with daily functions, such as sleeping and driving,[179] and postural changes induce potentially

uncomfortable fluctuations in paresthesia sensation as the spinal cord moves relative to the implanted electrodes.[68,180] These concerns can be partially mitigated by closed-loop systems which automatically adjust stimulation parameters in response to postural changes to avoid under or overstimulation.[73] However, given the choice, many patients express a preference for pain relief without concomitant paresthesia.[181]

Recently, several novel SCS paradigms have been developed that produce pain relief at amplitudes that do not produce paresthesia.[48] Notable examples of these techniques include burst and kilohertz-frequency (KHF) SCS.[5,48] Both burst and 10-kHz SCS (a common implementation of KHF SCS) have been rapidly adopted in the clinical following successful pivotal trials demonstrating superior results compared to conventional stimulation.[72,86] There is a consensus, based on both clinical observations and preclinical evidence, that these novel waveforms likely engage different pain-relieving mechanisms compared to conventional SCS.[5] However, the specific mechanisms underlying these approaches remain largely speculative and are actively debated.

To date, many hypotheses have been proposed regarding the neural effects of these paresthesia-free stimulation waveforms.[5,48] Still, these suppositions remain largely theoretical and untested. In addition, these proposed mechanisms typically lack a biophysical basis for how these effects are achieved. For instance, working hypotheses for 10-kHz and burst SCS are selective activation of dorsal horn inhibitory interneurons and modulation of the medial pain pathway, respectively.[84,89,94] Evidence for these hypotheses is provided by rodent spinal recordings[84] and neuroimaging[90–93]. However, no available data elucidate the biophysics of how these effects would be achieved.

In this study, we used a computational modeling approach to investigate postulated sub-paresthetic mechanisms of action of SCS, which permits analyzing the biophysical effects of SCS at human scale. Specifically, we examined the following hypotheses: whether novel SCS waveforms desynchronize spike timing,[115] if C-fibers are selectively activated,[89] and direct modulation of local gray matter neurons[84,116,182] (e.g., increased excitability or activation due to direct membrane polarization[183]). Additionally, we considered the effects of including stochastic ion channel behavior in the response of dorsal column (DC) fiber models to SCS to investigate whether these properties will reduce thresholds or produce asynchronous activation. For these analyses, we evaluated the response to conventional (50 Hz), burst, 1-kHz, and 10-kHz SCS.

Overall, our results suggest C-fibers are not activated nor desynchronized by any form of stimulation. Membrane polarization of neurons within the dorsal horn were small, but strongest in their axon terminals, suggesting any local dorsal horn effects are likely to be presynaptic in nature. Finally, we found that considering stochastic ion channel properties had a negligible effect on activation thresholds but did affect the suprathreshold firing patterns during all SCS waveforms. Overall, these results help elucidate the neural response to several clinically relevant forms of SCS.

3.3 Methods

We utilized a two-stage computer modeling approach to evaluate several theoretical subparesthetic mechanisms of novel SCS technologies. First, we used the finite element method (FEM) to evaluate the spatial electric potential fields generated in the spinal cord during SCS. Then, we applied these electric potentials to biophysical multi-compartment neuron models, scaled by the appropriate temporal stimulation waveform (assuming quasi-static conditions[103,104,184]), and assessed the neural response using the NEURON computational software package[108] (v7.4) through a Python interface. We tested several potential hypotheses, including direct activation of

C-fibers, action potential desynchronization, local cell modulation, and reduced activation thresholds due to stochastic ion channel properties (**Fig. 3.1**). Each of these sub-analyses is described in more detail below.

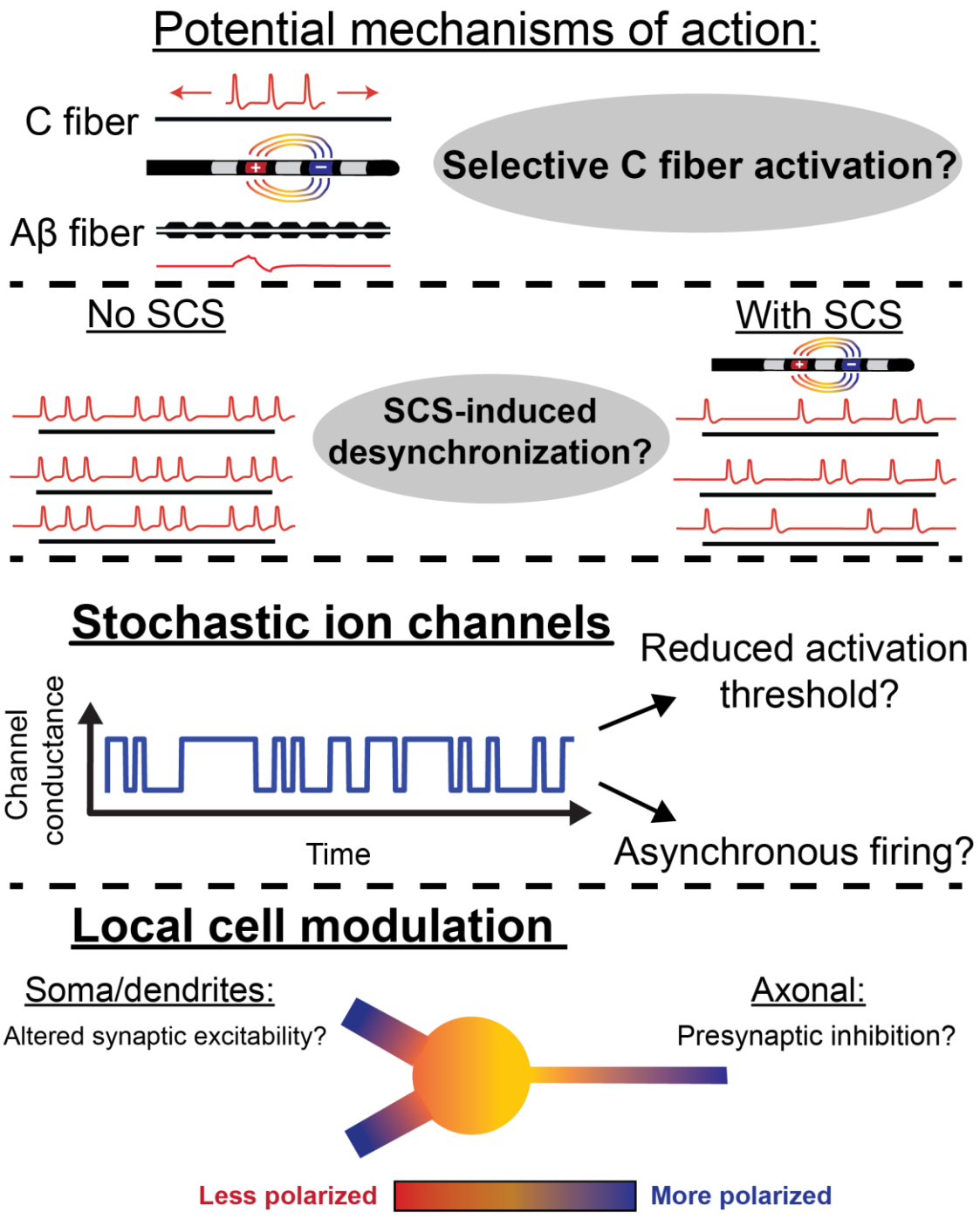

Figure 3.1: Overview of subthreshold modeling study. We evaluated four potential subparesthetic mechanisms of action: (1) Do subparesthetic waveforms SCS selectively activate C-fibers? (2) Do subparesthetic SCS waveforms

modulate spike timing and desynchronize afferent firing? (3) Do subparesthetic SCS waveforms interact synergistically with the stochastic nature of ion channel gating to reduce activation thresholds or produce asynchronous firing? (4) Do subparesthetic SCS waveforms directly modulate the excitability of neurons within the dorsal horn?

3.3.1 Volume conductor model

We utilized a previously developed volume conductor model of the lower thoracic spinal cord to evaluate the spatial electric potential field generated during SCS using a clinically relevant bipolar stimulation configuration (i.e., one cathode and one anode). This model is extensively described in its original publication.[103] Briefly, this model contains domains representing gray matter (electrical conductivity of 0.23 S/m), anisotropic white matter (including dorsal rootlets) (0.6 S/m longitudinally, 0.083 S/m transversely), cerebrospinal fluid (1.7 S/m), dura mater (0.6 S/m), epidural tissue (0.25 S/m), vertebral bone (0.02 S/m), intervertebral disc (0.65 S/m), electrode encapsulation (0.11 S/m), and a general thorax domain (0.25 S/m). Electrode contacts are 3 mm in length and 1.3 mm in diameter, separated by 1 mm edge-to-edge spacing. We used COMSOL Multiphysics (COMSOL, Inc., USA) to numerically evaluate the Laplace equation $\nabla \cdot \sigma \nabla V = 0$ to find the spatial electric potential field (V = electric potential, σ = conductivity) throughout the spinal cord. We modeled all stimulation as current-controlled, and we applied unit currents (1 mA) at active contacts, whereas we modeled the inactive contacts as equipotential surfaces with no net current and the electrode shaft as a perfect insulator. We modeled bipolar stimulation, with the cathode and anode separated by one inactive contact corresponding to a center-to-center spacing of 8 mm between the active electrodes (with the cathode positioned rostrally).

3.3.2 Stimulation waveforms

For each analysis, we evaluated the neural response to four clinically relevant SCS waveforms (**Fig. 3.2**). These stimulation paradigms were conventional, burst, 1-kHz, and 10-kHz

SCS. Importantly, conventional SCS is intended to maximize overlap between paresthesia and the painful areas, whereas the three other waveforms are delivered clinically at subparesthetic amplitudes.

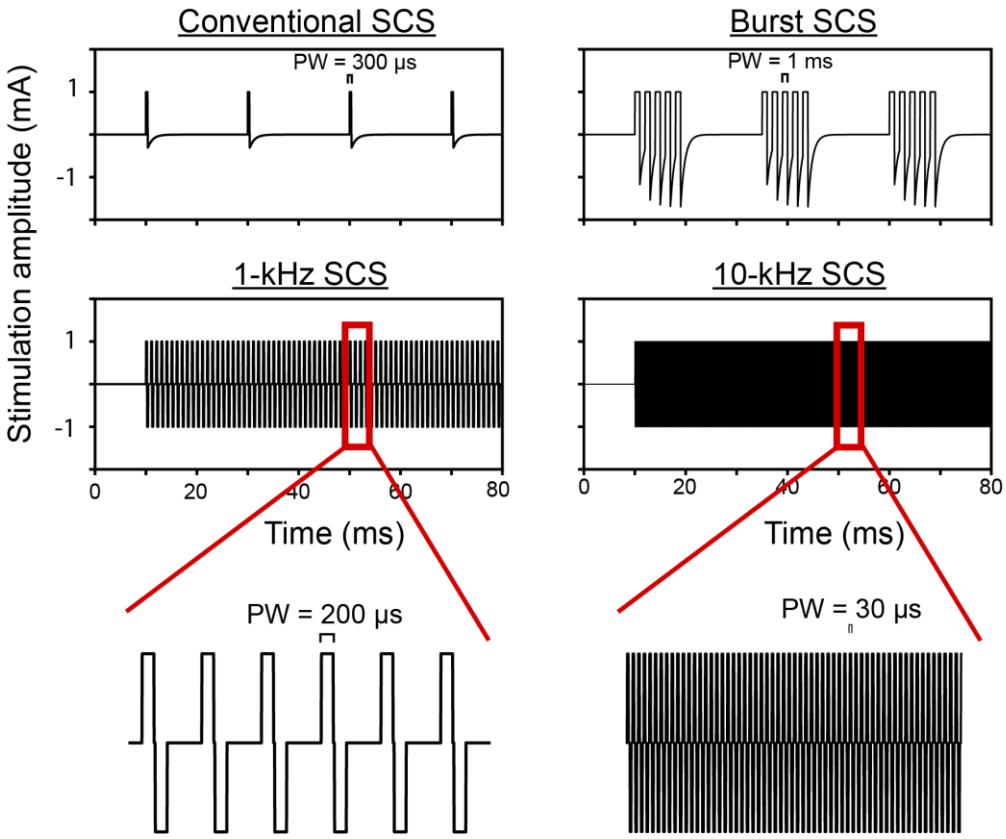

Figure 3.2: The four SCS waveforms considered in this study. Conventional SCS is delivered at an amplitudes that generate paresthesia, whereas the other waveforms are typically delivered at subparesthetic amplitudes. PW = pulse width.

We modeled conventional SCS as having a 300-µs stimulation pulse followed by a passive discharge phase. We delieved stimulation at 50 Hz. Burst SCS consisted of bursts of five pulses (pulse width of 1 ms) with passive discharging both between individual pulses and at the end of the burst. Intra-burst frequency was 500 Hz and inter-burst frequency was 40 Hz.[71] For both conventional and burst SCS, we calculated the passive discharge phase using a previously developed circuit model of bipolar stimulation.[125] We modeled 1-kHz SCS as symmetric biphasic rectangular stimulation with a pulse width of 200 µs (interphase interval of 80 µs later) delivered

at a rate of 1000 Hz.[74,75] Finally, we modeled 10-kHz SCS as symmetric biphasic rectangular stimulation, with a pulse width of 30 μs (interphase interval of 20 μs) delivered at a rate of 10,000 times per second.[72]

3.3.3 C-fiber activation thresholds

Selective activation of C-fibers has been proposed as a mechanism for subparesthetic SCS.[89] To test this hypothesis, we utilized a previously developed C fiber model[185] and evaluated the C-fiber response to the different SCS waveforms. Briefly, this nonmyelinated C-fiber model contains a passive leak conductance (1e-4 S/cm^2) and active TTX-sensitive $Na_v1.7$, TTX-resistant $Na_v1.8$, and slow TTX-resistant $Na_v1.9$ channels, as well as delayed rectifier and A-type potassium conductances. Additionally, the specific membrane capacitance and axial resistance are 1.0 μF/cm^2 and 100 Ω·cm, respectively, with an axon diameter of 1 μm.

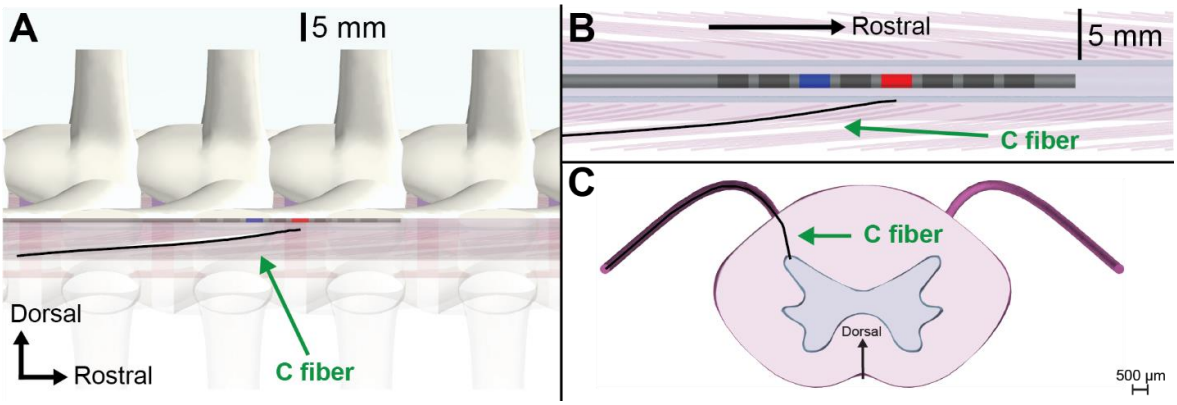

Figure 3.3: Overview of the C-fiber model. **(**A) Sagittal view of the C-fiber (black). The red electrode is the cathode, and the blue electrode is the anode. (B) Posterior view of the C fiber ascending in a dorsal root before entering the spinal cord. (C) Axial view of the C-fiber terminating in the superficial dorsal horn.

The C-fiber model ascended in the dorsal rootlets before entering the spinal cord white matter (**Fig. 3.3**). From here, the fiber ascended in the white matter dorsal to the gray matter boundary (Lissauer's tract) before finally terminating in the superficial dorsal horn at the level of the cathode. We calculated activation thresholds via a binary search algorithm with a resolution of

0.1 mA. We also shifted model fibers into the rootlet directly caudal and directly rostral to the original model to evaluate sensitivity to rostro-caudal position.

3.3.4 Spike timing

The nerve fibers in the vicinity of the SCS electrodes transmit action potentials from the periphery into the central nervous system. Thus, one plausible mechanism of subparesthetic neurostimulation is modulating spike timing of ongoing nociceptive signaling, e.g., producing analgesia by desynchronizing firing patterns in a population of nociceptive fibers.[1,89,115] For this reason, we investigated how the different SCS waveforms might affect spike timing in afferent fibers (**Fig. 3.4**).

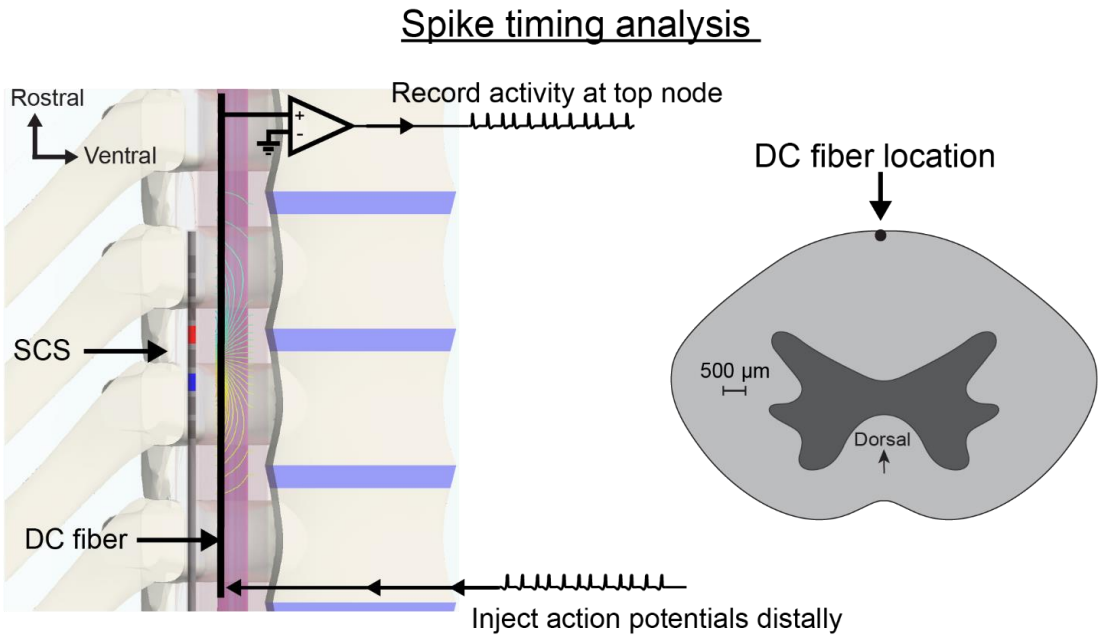

Figure 3.4: Overview of our analysis of the effects of SCS on spike timing. We injected a spike train into one end of an afferent fiber (C- or Aβ-fiber) and recorded at the terminal node of Ranvier. We used the Victor-Purpura metric to quantify differences in spike trains. On the right we show the location of the dorsal column (DC) fiber used for all analyses. The C-fiber locations are shown in **Fig. 3.3**.

For these analyses, we introduced spontaneous ongoing spike trains in the form of homogeneous Poisson processes with a mean rate of 30 spikes per second. We generated ten random spike trains with these parameters (**Fig. 3.5**). Thirty spikes per second is in the range for

spontaneous firing of human large-diameter myelinated afferents[186,187] and various classes of C-fibers[188] that have been observed in microneurography experiments. We performed this analysis for both C-fibers and DC Aβ-fibers.

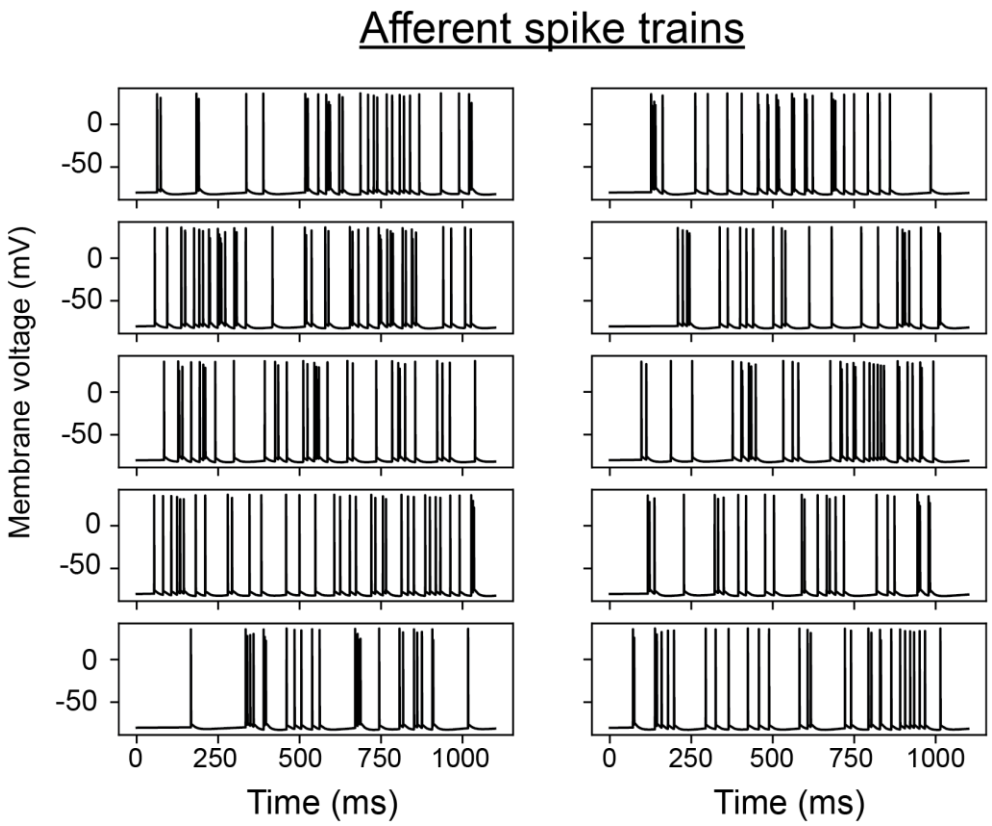

Figure 3.5: Afferent spike trains. We generated ten random spike trains to model ongoing activity in afferent fibers. We generated spike trains as homogeneous Poisson processes with a mean rate of 30 spikes per second.

We assessed the effects of the various SCS waveforms on spike timing by comparing simulations with and without concomitant SCS. We quantified dissimilarities between spike trains using the Victor-Purpura (VP) distance.[189] This metric calculates the minimum "cost" to transform one spike train into another using three basic operations: spike insertion (cost = 1), spike deletion (cost = 1), and spike shifting (cost = $q|\Delta t|$, where Δt is the time-shift interval and q is the cost of shifting per time unit). Here, we set q = 1. We standardized the dissimilarities by first finding the average pairwise VP distance between the ten randomly generated spontaneous spike trains. We then divided all further VP distances by this average value. Thus, a value close to 1 suggests

dissimilarity that is close to the average dissimilarity score of random spike trains generated by an identical homogeneous Poisson process.

3.3.5 Stochastic ion channel gating in dorsal column fibers

Typically, neuron models are parameterized using deterministic sets of differential equations, often derived from averaging a collection of recordings. However, ion channels are inherently stochastic in nature, and the state of an ion channel (i.e., whether it is open or closed) fluctuates over time in a probabilistic fashion.[190] Importantly, the impact of these fluctuations will be larger in smaller fibers as they have fewer ion channels, thus magnifying the impact of fluctuations in individual channels.[191] This stochastic gating can affect both activation threshold as well as firing patterns in activated fibers, potentially generating pseudo-spontaneous and asynchronous firing.[192] For this reason, the interaction of stochastic ion channel properties with novel high-frequency stimulation paradigms has been proposed as a potential mechanism underlying paresthesia-free analgesia.[83]

We utilized a previously developed diffusion approximation approach to incorporate stochastic ion channel properties into the MRG axon model.[193] In short, this approach uses stochastic differential equations to model the fraction of channels in each state, which is considerably more computationally efficient than methods utilizing Markov Chains. The time evolution of the fraction of channels in each state is modeled by the combination of a deterministic component, which use the same voltage-dependent rate constants in the traditional model, and a stochastic component, which includes Gaussian noise processes to introduce stochasticity. The precise details of this approach, and its mathematical derivation, are provided by Orio and Soudry.[193]

We evaluated the effects of stochastic ion channels on superficial DC fibers. Specifically, we placed modeled fibers at the midline of the DC white matter and 100 μm ventral to the surface of the spinal cord. We modeled fibers using a modified version of the MRG model, developed in a previous study to improve the dynamics of the potassium conductance.[194,195] Channel densities were identical to those in the original MRG model: 2000 channels per μm^2 for nodal fast sodium and 100 channels per μm^2 for nodal potassium.[195] We evaluated thresholds for fiber diameters between 5.7 and 11.5 μm by running 50 simulations for each diameter and stimulation waveform, each with a unique random seed. Additionally, to evaluate the effect of stochasticity on firing patterns, we also ran simulations at an amplitude 10% greater than the deterministic threshold determined for each SCS stimulation waveform and fiber diameter (i.e., 10% greater than the amplitude necessary to generate at least one action potential in the standard fiber model). We ran all simulations with a time step of 1 μs.

3.3.6 Local cell polarization

We developed models of five cells within the superficial dorsal horn based on morphological reconstructions of superficial dorsal horn neurons (**Fig. 3.6**). Three of these neurons were interneurons and two were projection neurons. These morphologies were downloaded from Neuromorpho (Neuromorpho ID numbers NMO_61486, NMO_34018, NMO_34025, NMO_34017, NMO_61481).[147,196,197] We validated the cell models by comparing their responses to injected current clamp recordings[158] as well as extracellular microstimulation of central neurons[198] (**Fig. 3.7**). For extracellular microstimulation, we positioned 100 point sources randomly in three-dimensional space around the neurons and calculated the activation threshold for a 200-μs cathodic pulse.[149] Time constants for these models ranged from 34.4 to 43.2 ms, which is in excellent agreement with the 40 +/- 5 ms reported by Prescott and De Koninck for tonic-firing

lamina I neurons.[40] We also developed a vertical cell model, which is a class of neurons residing in lamina II of the superficial dorsal horn and that have been implicated in pain processing.[35] These neurons are characterized by their ventrally projecting dendritic arbor. To generate this model, we simplified the axonal and dendritic structure of one of the interneuron models (**Interneuron 1 in Fig. 3.6**), and then re-oriented the cell to have a dorsally-directed axon and ventrally-directed dendritic arbor.

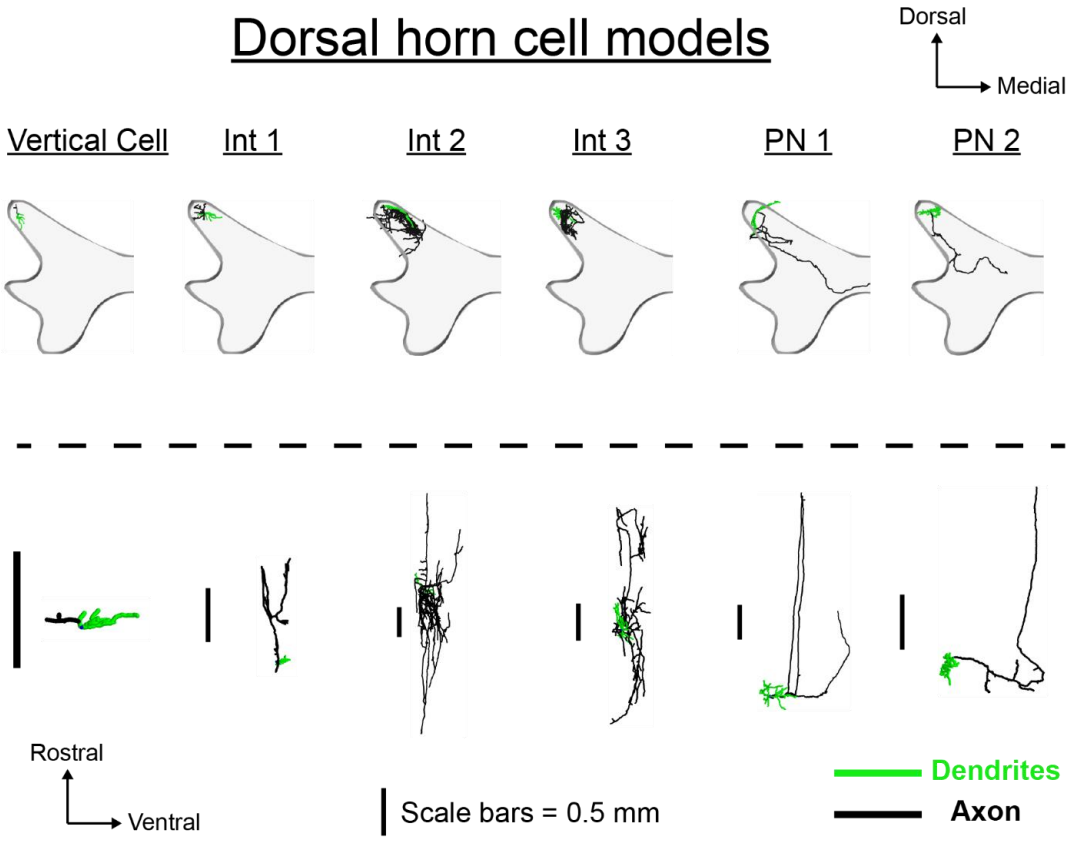

Figure 3.6: Local cell models in the dorsal horn. Top and bottom rows show axial and sagittal views, respectively, of neurons within the dorsal horn. Dendrites are shown in green and axons in black. The vertical cell is a simplified version of Interneuron 1 (Int 1). All other cell models were based on experimental reconstructions. Scale bars in the sagittal view each correspond to 1 mm for the adjacent neuron. Int = interneuron, PN = projection neuron.

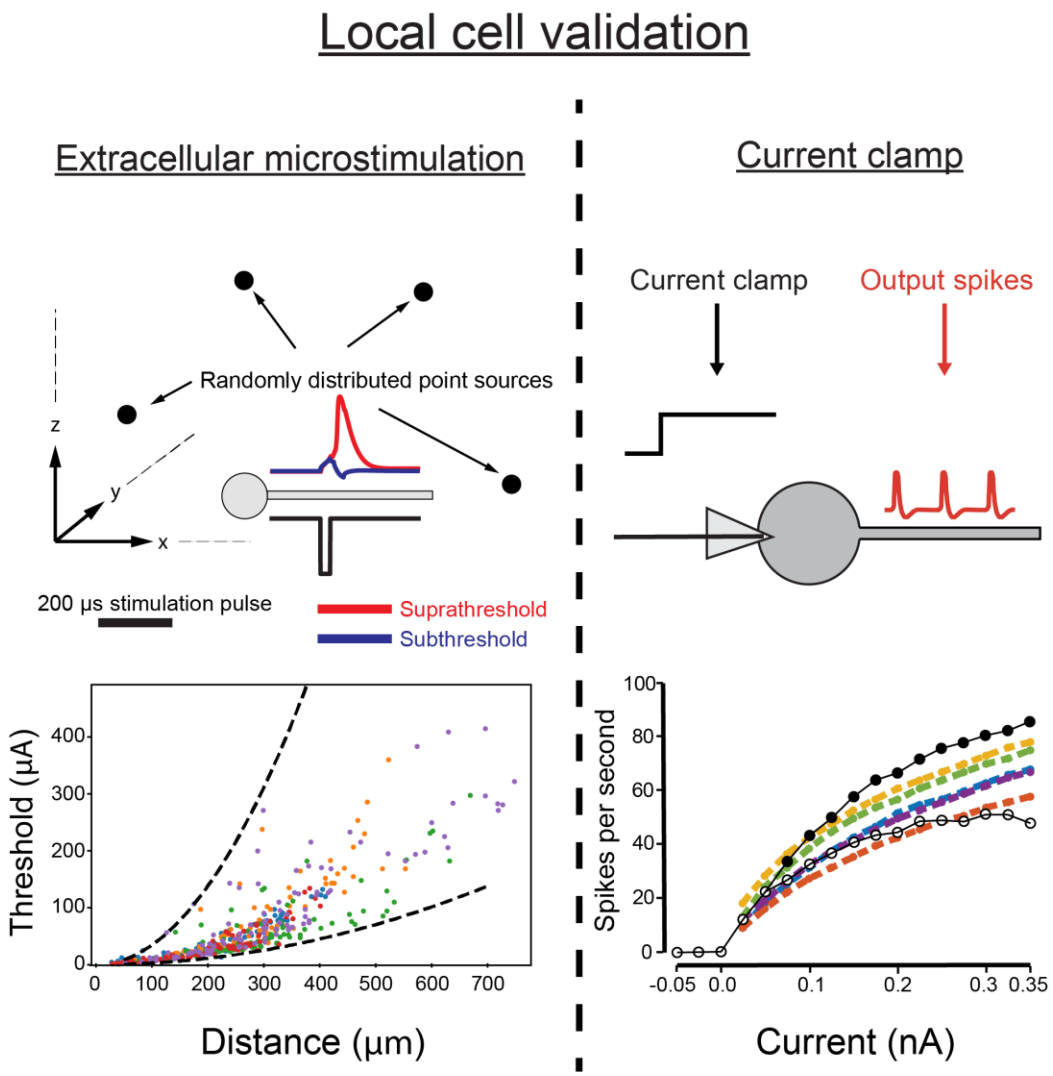

Figure 3.7: Validation of local cell models. Left: Activation thresholds during extracellular microstimulation with a 200-µs cathodic pulse. We randomly placed 100 point-source electrodes in the vicinity of each of the five neuron models. As shown in the bottom left plot, we calculated the activation threshold (ordinate) for each neuron model (color coded) and the distance between the corresponding point-source electrode and site of activation (abscissa). The dashed black lines correspond to the minimum and maximum experimental values given by Stoney et al.[198] Right: Firing rate of each of the five model neurons during simulated current clamp conditions compared to experimental recordings of dorsal horn tonic firing neurons by Ruscheweyh and Sandkühler[158] (open circle = lamina I neurons, filled circles = deeper neurons). Microstimulation thresholds and current clamp results are color-coded for each of the five model neurons.

All local neuron models had identical biophysical properties and thus varied solely in morphology. Axons were myelinated following the algorithm described by Aberra et al.[149] and myelinated compartments had a specific membrane capacitance of 0.02 µF/cm^2 and membrane resistance of 1.25 MΩ·cm^2. Unmyelinated neuron compartments had a membrane capacitance of

0.85 μF/cm^2 and membrane conductivity of 1.8e-5 S/cm^2.[156] Active currents were fast sodium and delayed rectifier potassium, which are sufficient to generate tonic firing patterns found in superficial dorsal horn neurons.[154] Sodium conductances were 1.8, 0.008, and 0.008 S/cm^2, and potassium conductances were 0.3, 0.0043, and 0.1 S/cm^2 in the nodes of Ranvier, soma, and dendrites, respectively. Axial resistance was uniformly 200 Ω·cm.

We positioned the model neurons in the superficial dorsal horn. We shifted the cell models rostro-caudally in 500 μm increments from 5 mm caudal to the center of the anode to 5 mm rostral to center of the cathode. For each compartment in the neuron models, we calculated the maximum polarization from the resting membrane potential during each stimulation waveform.

3.4 Results

3.4.1 C fibers are not activated by SCS

We calculated activation thresholds for a C-fiber model as the stimulation amplitude necessary to generate at least one action potential in the fiber during SCS. For all of the SCS waveforms, the activation thresholds for C-fibers were far beyond those stimulation amplitudes necessary to activate myelinated DC Aβ-fibers. We found that burst SCS had the lowest thresholds, followed (in order) by conventional SCS, 1-kHz SCS, and then 10-kHz SCS. We performed sensitivity analysis to C-fiber rostro-caudal level by placing the C-fiber in several adjacent dorsal rootlets. Of all the C-fiber positions and SCS waveforms tested, the lowest observed threshold for a C-fiber was ~60 mA during burst SCS, more than an order of magnitude higher than the amplitude necessary to activate the myelinated afferents underlying paresthesia. These data provide strong evidence that C fibers are not activated by clinical SCS.

3.4.2 SCS modulated spike timing in Aβ-fibers at supra-threshold amplitudes, and did not modulate spike timing in C-fibers

We evaluated the effects of conventional, burst, 1-kHz, and 10-kHz SCS on spike timing in C-fibers as well as DC Aβ-fibers. We placed the Aβ-fiber superficially in the DC white matter, 100 μm ventral to the surface and at the mediolateral midline of the spinal cord. We modeled the response of a single 10-μm fiber, which corresponds to the upper range of fiber diameters found in the dorsal columns.[199] We then calculated the activation threshold for this model fiber to generate at least one action potential. The activation thresholds were 1.92, 0.96, 2.20, and 8.15 mA for conventional, burst, 1-kHz, and 10-kHz SCS, respectively.

We then evaluated the effects of spike timing on fibers with ongoing spontaneous activity (10 separate iterations of a 30 Hz homogeneous Poisson process) during SCS with the stimulation amplitude set to 0.05 mA below the activation threshold for each waveform. We quantified dissimilarity between spike trains using the VP distance, which we standardized so that a value close to 1 suggests the dissimilarity is close to the average dissimilarity between the ten randomly generated input spike trains (see Methods).

For subthreshold stimulation (i.e., SCS amplitude 0.05 mA below the amplitude necessary to generate an action potential), we found that spike timing modulation was negligible. For conventional, burst, 1-kHz, and 10-kHz SCS, the average standardized VP distances (mean +/- SD) were 0.002 +/- 0.005, 0.004 +/- 0.007, 0.011 +/- 0.003, and 0.017 +/- 0.024, respectively.

Next, we investigated the effects on spike timing when the amplitude was increased to slightly above threshold, as it possible that SCS may activate DC fibers without concomitant paresthesia.[200] We repeated the same analysis as in the subthreshold case, but at amplitudes 0.1, 0.3, and 0.5 mA above the activation threshold for each of the SCS waveforms. In this case,

appreciable differences in spike timings were observed compared to the spontaneous input spike trains (summarized in **Table 3.1**). We observed two clear trends. First, for all SCS waveforms, as the stimulation amplitude was increased, the dissimilarity between the original input spike train and output spike train increased. Second, burst and 1-kHz SCS had similarly large effects on spike trains, whereas conventional and 10-kHz SCS produced notably smaller standardized VP distances at each amplitude. A representative example for stimulation 0.3 mA above threshold is provided in **Fig. 3.8**.

Table 3.1: Average standardized VP distances between spontaneous spike trains with and without applying simultaneous SCS. Data are given as mean ± SD.

	0.05 mA below threshold	0.1 mA above threshold	0.3 mA above threshold	0.5 mA above threshold
Conventional	<0.01	0.04 ± 0.02	0.17 ± 0.04	0.40 ± 0.02
Burst	<0.01	0.10 ± 0.04	0.53 ± 0.10	1.25 ± 0.13
1-kHz	0.01 ± 0.00	0.10 ± 0.06	0.44 ± 0.15	1.58 ± 0.15
10-kHz	0.02 ± 0.02	0.06 ± 0.04	0.07 ± 0.04	0.13 ± 0.05

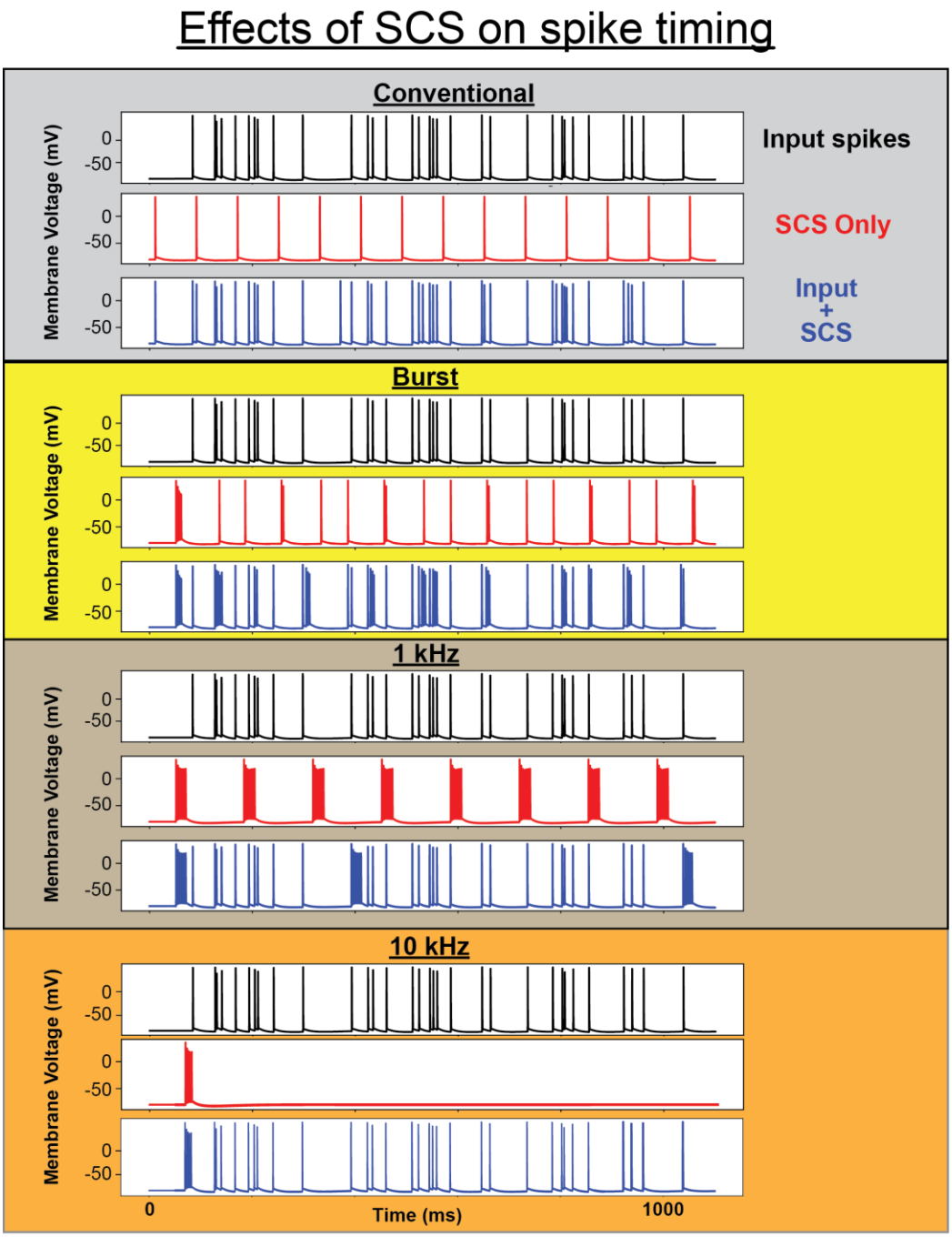

Figure 3.8: Effects of suprathreshold SCS (0.3 mA above activation threshold) on spike timing during conventional, burst, 1-kHz, and 10-kHz SCS. For each SCS waveform, three membrane voltage traces are provided: (Top) The ongoing spontaneous input within the fiber, which corresponds to the spike train in third row of the first column of Fig. 3.5. (Middle) The response of the fiber to SCS with no ongoing spontaneous input. (Bottom) The response of the fiber when the stimulation is provided while there is simultaneous spontaneous activity.

Finally, it has been proposed that novel SCS waveforms can desynchronize nociceptive signaling in C-fibers. To this end, we repeated the above analysis in the C-fiber models. For each

SCS waveform, we performed this analysis with an amplitude of 120% the necessary amplitude to activate the 10-μm DC fiber. Alterations in spike timing were negligible (data not shown).

3.4.3 Stochastic ion channel behavior affected firing patterns, but not activation thresholds

We incorporated stochastic ion channel behaviors into superficial DC fibers between 5.7 and 11.5 μm in diameter (50 fibers per diameter). Overall, the activation thresholds were highly similar to those found in the deterministic model, with a tendency for stochastic models to have slightly lower thresholds. Differences between the stochastic model and the deterministic model were negligible for the largest-diameter fibers (e.g., fibers ≥ 8.7 μm) (**Fig. 3.9**). Smaller-diameter fibers had slightly larger variation in thresholds (i.e., larger standard deviations), but the order of recruitment was always the same as for the deterministic model (**Table 3.2**).

Table 3.2: Activation thresholds for a superficial dorsal column fiber using the deterministic (D) and stochastic (S) models**.** Thresholds are in mA. For the stochastic models, thresholds are given as mean ± SD.

Axon diameter	5.7 μm		7.3 μm		8.7 μm		10.0 μm		11.5 μm	
	D	S	D	S	D	S	D	S	D	S
Conventional	5.60	5.22 (±0.09)	3.27	3.09 (±0.04)	2.34	2.23 (±0.03)	1.92	1.83 (±0.02)	1.66	1.59 (±0.01)
Burst	2.67	2.43 (±0.04)	1.59	1.52 (±0.02)	1.17	1.12 (±0.02)	0.96	0.92 (±0.01)	0.84	0.81 (±0.01)
1-kHz	6.88	6.61 (±0.11)	3.90	3.81 (±0.04)	2.71	2.65 (±0.03)	2.20	2.16 (±0.02)	1.88	1.85 (±0.02)
10-kHz	27.49	27.25 (±0.48)	15.43	15.37 (±0.20)	10.32	10.29 (±0.11)	8.15	8.12 (±0.08)	6.72	6.70 (± 0.06)

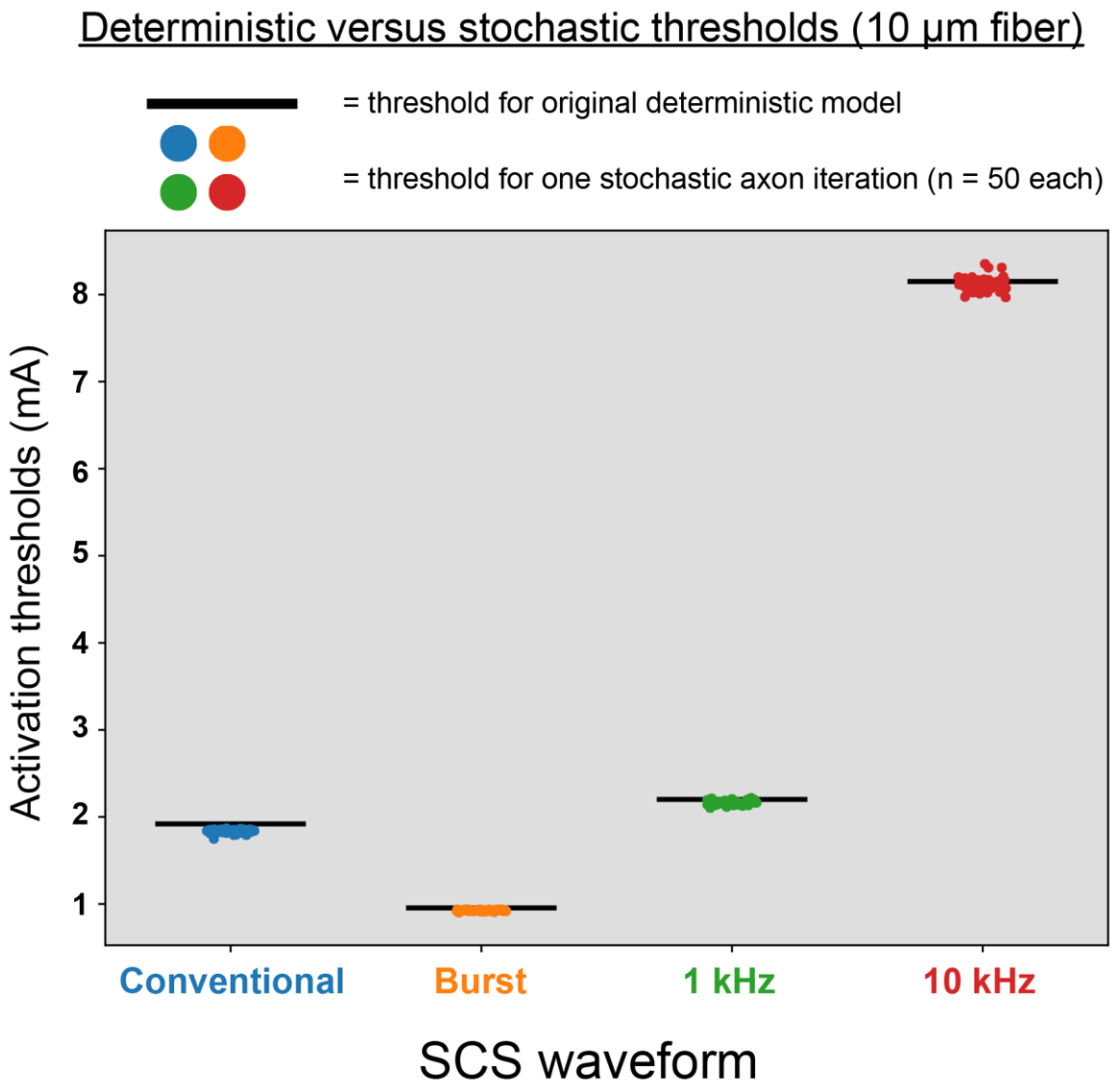

Figure 3.9: Deterministic (black lines) versus stochastic (circles) model thresholds for a superficially positioned 10-µm dorsal column fiber. For each SCS waveform, we found thresholds for 50 randomly seeded stochastic models.

Next, we evaluated how incorporating stochastic ion channel gating affected firing properties by modeling 10-µm DC fibers with a stimulation amplitude 10% greater than the deterministic threshold. We found that firing patterns were qualitatively similar for stochastic models compared to the original deterministic model, but we observed slight differences in spike timing and the number of spikes (**Fig. 3.10**).

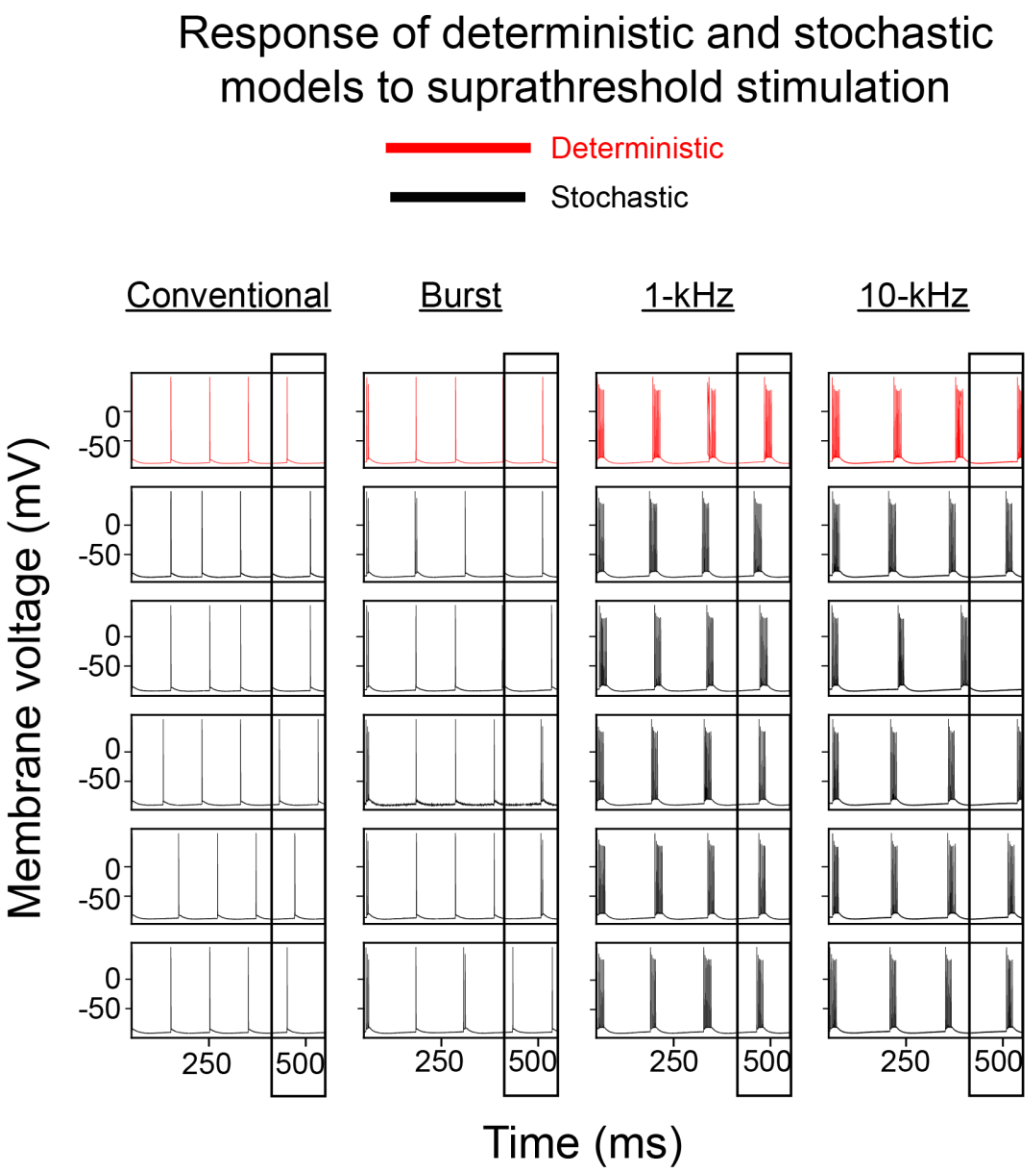

Figure 3.10: Comparison of the response of a 10-µm dorsal column fiber to conventional, burst, 1-kHz, and 10-kHz SCS using deterministic (red) and stochastic (black) ion channel models. The stimulation amplitude was 10% above the activation threshold for the deterministic model. For each SCS waveform, we randomly selected five stochastic simulations represented by each row in the plot above. Boxes at the end of each simulation highlight differences in spike timing between the deterministic and stochastic models.

3.4.4 Local cell polarization was largest in the axon

Direct modulation of rostrally-oriented dorsal horn neurons has been proposed as a mechanism of action for several SCS paradigms.[84,116,182] To test this hypothesis, we generated models of five neurons within the dorsal horn (three interneurons, two projection neurons) based

upon previously published morphological reconstructions, as well as a vertical cell model with dorsally-oriented axon (see Methods). Neurons spanned from 5 mm caudal to the center of the anode to 5 mm rostral to the center of the cathode in 500 μm increments (total of 37 locations).

In agreement with previous work,[110] we found that activation thresholds for all of the dorsal horn neurons were well above those for DC fibers for all SCS waveforms (data not shown). However, a neuron does not need to be directly activated to have its behavior modulated by the stimulation,[177,201] and thus we assessed membrane polarization through the soma, dendrites, and axonal arbor to investigate whether a neuron was likely to experience subthreshold modulation (e.g., activation due to spatiotemporal summation of subthreshold currents, increased excitability to synaptic input, or altered presynaptic transmitter release). For each waveform, we evaluated the maximum depolarization (and hyperpolarization) throughout the cell during stimulation at 1 mA (responses can be scaled to estimate the response at a higher stimulation amplitude).

Table 3.3: Maximum depolarizations in the different compartments during the various forms of SCS for each neuron. Note, these are the overall maximum depolarizations observed across all rostrocaudal levels. C = conventional, B = burst, 1K = 1-kHz, 10K = 10-kHz.

	Axon				Dendrites				Soma			
	C	**B**	**1K**	**10K**	**C**	**B**	**1K**	**10K**	**C**	**B**	**1K**	**10K**
Vertical cell	0.43	0.47	0.41	0.24	0.07	0.11	0.06	0.03	0.03	0.06	0.04	0.01
Interneuron 1	0.71	1.02	0.60	0.22	0.09	0.19	0.07	0.02	0.02	0.05	0.03	0.01
Interneuron 2	0.39	0.68	0.31	0.10	0.09	0.12	0.07	0.03	0.04	0.07	0.03	0.01
Interneuron 3	0.30	0.73	0.43	0.12	0.09	0.19	0.07	0.03	<0.01	0.02	<0.01	<0.01
Projection Neuron 1	0.20	0.38	0.16	0.09	0.10	0.18	0.08	0.03	0.01	0.02	0.01	<0.01
Projection Neuron 2	0.28	0.65	0.22	0.08	0.12	0.17	0.10	0.06	0.02	0.05	0.02	0.01

Overall, the polarization magnitudes were small, and were varied across the different neurons, which affirms that cellular morphology is important to consider for neurostimulation applications (**Table 3.3**). We found that in all cases, burst SCS produced the strongest polarization, whereas 10-kHz SCS always produced the smallest polarization. Importantly, polarizations were

always largest in the axon and negligibly small in the soma, whereas dendritic polarizations were typically non-negligible but substantially smaller than in the axon. The largest axonal depolarizations during a unit amplitude (1 mA) stimulus for conventional, burst, 1-kHz, and 10-kHz SCS, were 0.71, 1.09, 0.6, and 0.22 mV, respectively (all in the same neuron; Interneuron 1 in **Fig. 3.6**). For dendrites, maximum depolarizations (across all neuron morphologies and rostrocaudal positions) were approximately 0.2 mA for burst SCS, 0.1 mA for conventional and 1-kHz SCS, and 0.05 mA for 10-kHz SCS.

Finally, we found that local cell polarization was strongly dependent on rostrocaudal position as well as cellular morphology and orientation (**Fig. 3.11**). For neurons with rostrocaudal orientations (e.g., interneurons 1-3 in **Fig. 3.6**), polarization in the axon was strongest approximately midway between the two active electrodes. On the other hand, the dorsally-directed vertical cell axon was maximally depolarized at rostrocaudal levels near the outer edges of the active contacts.

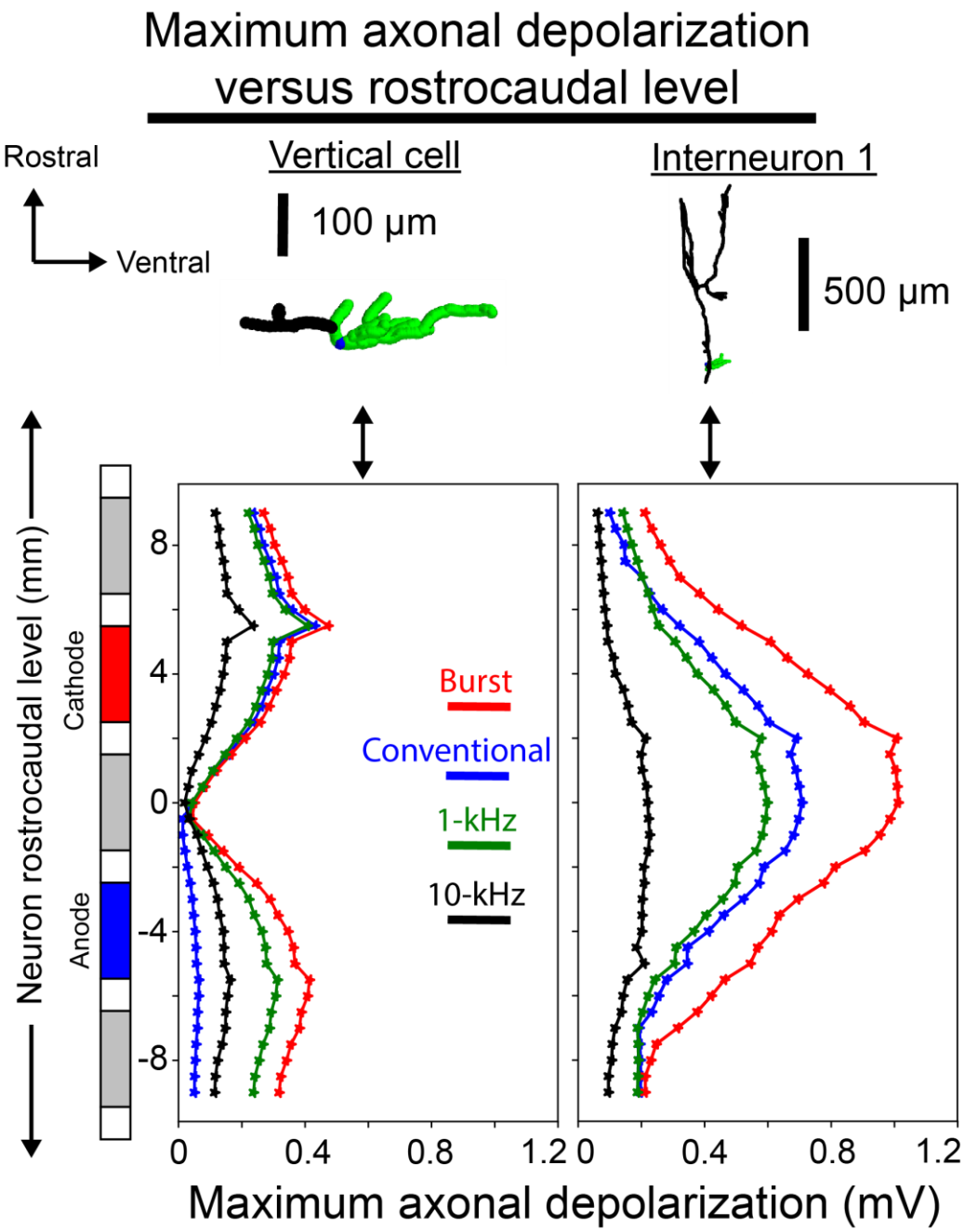

Figure 3.11: Effects of rostrocaudal position on maximum axonal depolarization for (Left) the vertical cell and (Right) a rostrocaudally oriented interneuron. The interneuron corresponds to Interneuron 1 in **Fig. 3.6**, which was the most strongly polarized of all neuron models. Different colored lines correspond to the different SCS waveforms. Filled markers indicate the maximal depolarization from rest within the axon at a given rostrocaudal level. Simulations were sampled at 500 µm increments from 5 mm caudal to the center of the anode to 5 mm rostral to the center of the cathode.

3.5 Discussion

Several new forms of SCS produce analgesia without producing the concomitant paresthesia inherent to conventional stimulation. These therapies offer promising options for patients who do not tolerate these paresthesias and may even produce superior pain relief compared to conventional SCS.[74,86,179] Still, little is known about the neurophysiological effects and underlying mechanisms of action of these paradigms. A better mechanistic understanding of these stimulation waveforms will facilitate the development of optimized stimulation settings to maximize pain relief, tailored to an individual patient's condition, while minimizing power consumption and prolonging battery life.

Unfortunately, direct experimental testing of these hypotheses is often infeasible, and anatomical differences between humans and animal models complicate direct translation of the available preclinical evidence. Therefore, in this study, we used a computational modeling approach to investigate the neurophysiological effects and potential mechanisms of action of three subparesthetic SCS paradigms (burst, 1-kHz, and 10-kHz SCS), as well as conventional paresthesia-based SCS. We found that no SCS waveform directly activates C fibers, nor modulates or desynchronizes ongoing activity within these unmyelinated afferents. Additionally, these novel SCS waveforms did not interact synergistically with stochastic ion channel properties to affect activation thresholds or alter the recruitment order of fibers. However, including these stochastic properties did alter firing patterns at suprathreshold amplitudes to produce realistic fluctuations in spiking patterns resembling recent experimental recordings of afferent fibers during SCS.[200,202] Finally, we characterized the polarization of neurons in the superficial dorsal horn during SCS. We found that axons (specifically their terminals) were preferentially polarized during stimulation to a much stronger extent than the dendrites and soma. Additionally, burst SCS reliably produced

the strongest polarization and 10-kHz the weakest, with conventional and 1-kHz SCS moderately polarizing the membrane. Taken together, these results help elucidate the neural response to various clinically relevant SCS waveforms.

3.5.1 C fibers are not activated or modulated by SCS

Activation thresholds for C fibers were well beyond the activation thresholds of Aβ-fibers in the dorsal columns, refuting the notion that C-fibers are selectively activated by subparesthetic SCS waveforms. Similarly, the timing of ongoing spikes in C-fibers were not affected by any form of SCS. One consideration is that these waveforms have been suggested to activate non-noxious C fibers that convey pleasant touch,[203] whereas we utilized a model derived for a nociceptive C fiber.[185] However, while differences in their biophysical properties could affect their response to stimulation, it is unlikely that these differences would reduce thresholds at least an order of magnitude to be comparable to Aβ fibers, as their small diameter and unmyelinated structure strongly oppose activation by extracellular stimulation.

3.5.2 Local cell membrane polarization is primarily in the axon

We analyzed membrane polarization during conventional, burst, 1-kHz, and 10-kHz SCS for six models of local dorsal horn cells. These were three rostrocaudally oriented interneurons, two projection neurons, and one dorsoventrally oriented interneuron (a vertical cell). For all neurons, activation thresholds were notably higher than those for Aβ-fibers in the dorsal columns, suggesting that it is unlikely that these neurons are activated during clinical SCS (data not shown).

It has been hypothesized that SCS will preferentially activate or increase excitability in the dendrites of local dorsal horn neurons.[116,182] Our results demonstrated that dendrites were weakly polarized by unit 1-mA stimulation, with an overall maximum depolarization of ~0.2 mV during

burst SCS, and maximum polarizations were less than or equal to 0.1 mV during 1-kHz and 10-kHz SCS. Clinical SCS is often delivered at higher amplitudes than 1 mA and these depolarizations would increase at these higher stimulation amplitudes. However, maximum depolarization in the axon was always at least twice as large as the depolarization in the dendrites, and often at least four or five times larger. Additionally, we note that maximum depolarization in the dendrites of the vertical cell, which are directed ventrally, were comparable to those for the other neurons, suggesting that bipolar stimulation will not preferentially modulate dendrites in rostrocaudally oriented neurons. From these results, we conclude that a presynaptic mechanism of action (e.g., altering neurotransmitter release) is more likely than effects on somatodendritic processing. It is worth noting that primary afferent collaterals will also produce rostrally oriented arborizations in the superficial dorsal horn.[32,139] Thus, any presynaptic effects on local cells could plausibly be mirrored in these afferent fiber terminals, and these effects warrant consideration in future studies.

We also observed a strong effect of rostrocaudal position on axonal polarization. Specifically, in this bipolar configuration, the strongest axonal polarization for the rostrocaudally oriented cells was approximately at the midpoint between the electrodes. On the other hand, polarization for the dorsally-directed vertical cell axon was maximal near the lower and upper borders of the anode and cathode, respectively. This vertical cell polarization was of a similar magnitude to that observed for the other cells. Intuitively, these observations are consistent with the notion that these axon terminals will be most strongly polarized where the electric field parallel to the terminating axon is maximized.[204] Thus, these results demonstrate that modulation of local neurons in the dorsal horn is not necessarily selective for specific neuron orientations, but that different cell morphologies will be modulated simultaneously at different locations in the spinal

cord. This insight should be kept in mind when comparing recordings of heterogeneous dorsal horn neurons in preclinical SCS models.

3.5.3 Stochastic ion channels produce small changes in thresholds, but noticeably modulate suprathreshold responses

We found that incorporating stochastic ion channel behavior did not alter activation thresholds but did affect firing patterns in DC fibers. Specifically, stochastic ion channels produced slight alterations in the timing and number of spikes, although firing patterns were qualitatively similar (**Fig. 3.10**). Recent experiments have demonstrated that stimulating DC fibers at amplitudes just above activation threshold will produce asynchronous firing responses.[202] While deterministic fiber models provide qualitatively accurate approximations of the response to SCS, incorporating the stochastic ion channel properties produced results that demonstrated fluctuations in spike timing that more closely resemble experimental recordings.[200,202]

The asynchronous and random fluctuations in firing behavior observed by incorporating stochastic ion channels have several important clinical and technical implications. First, Gilbert and colleagues demonstrated *in silico* that asynchronous firing patterns more effectively reduced output of the dorsal horn pain processing network than synchronous DC fiber activation.[202] This result highlights the need to understand realistic DC fiber firing patterns during SCS to better maximize pain relief, which our results demonstrate are noticeably affected by including stochasticity. Next, recent evidence suggests that paresthesia may rely on the synchrony of DC fiber activation.[200] Thus, asynchronous firing due to these stochastic ion channel properties could increase the paresthesia perception amplitude, and future waveforms could be designed exploit these properties to reduce synchronization and thereby increase the therapeutic range of stimulation at subparesthetic levels. Finally, novel closed-loop SCS systems utilize evoked

compound action recordings which measure the synchronous firing of the DC fibers. Analyses that estimate neural recruitment using deterministic models may produce population firing rates that are more synchronized than stochastic models, thus leading to an overestimate of fiber recruitment. Thus, these results suggest that future modeling studies should consider incorporating these stochastic properties to better estimate the neural response to SCS.

3.5.4 Limitations and future directions

The results presented in this study further elucidate the biophysical effects of various clinically relevant SCS waveforms. However, there are some limitations to our approach that should be considered. First, we modeled the neural response to a single percutaneous electrode array using a bipolar stimulation configuration, whereas modern SCS systems often employ more than one electrode array and/or complex multipolar stimulation configurations.[48] Still, bipolar stimulation is ubiquitous, and this model represents a reasonable starting point for future work comparing the effects of different configurations on the neural response to SCS. Furthermore, while DC fibers are sensory fibers, we used a motor axon model (i.e., the MRG model).[195] The MRG model is the gold standard for mammalian axons, but future work developing validated sensory fiber models will be important to understand the importance of considering electrophysiological differences in these fiber classes. Finally, while we are investigating the mechanisms of subparesthetic SCS, very little is known about the precise neural activation profile that generates paresthesia. Thus, we were unable to define a precise stimulation range that corresponds to subparesthetic SCS, which should be considered when interpreting our results. For example, we analyzed our results for the local cell models by comparing depolarizations in the different cellular substructures (i.e., the soma, axon, and dendrites) in response to a unit (1 mA) stimulus, and we found that the axons were notably more depolarized than the soma and dendrites.

However, if the perception threshold amplitude is high, it is possible that the soma and dendrites will be sufficiently depolarized to modulate neural behavior. Future work investigating the neural correlates of paresthesia will better inform future studies and clinical SCS systems.[200]

3.6 Conclusions

In this study, we utilized an *in silico* approach to evaluate several hypothesized mechanisms of action of conventional, burst, 1-kHz, and 10-kHz SCS. Our results strongly refute the proposal that novel SCS waveforms preferentially activate C-fibers.[89] Additionally, we found that no waveform desynchronized or modulated spike timings in C-fibers, and only substantially did so in Aβ-fibers at suprathreshold amplitudes. Relative to deterministic models, including stochastic ion channel properties into DC fiber models did not appreciably affect activation thresholds but did produce variable and asynchronous firing patterns at suprathreshold amplitudes. Future work will be necessary to understand the effects of these realistic spiking fluctuations on pain relief and paresthesia during SCS. Finally, we found that axons were considerably more polarized during stimulation than the soma or dendrites. From this result, we conclude that any SCS-induced modulation of cells within the dorsal horn is likely to be presynaptic in nature (i.e., altered neurotransmitter release). Additionally, we found that cellular morphology and orientation strongly affected both the magnitude of this polarization as well as the rostrocaudal level at which specific cell types were most strongly affected by stimulation. Thus, the heterogeneous cellular populations of the dorsal horn may be differentially modulated at various locations during SCS due to these properties. Overall, the results presented this study help provide a more complete understanding of the neural response to various clinically relevant SCS waveforms.

|

Chapter 4 - Biophysical Modeling Explains Clinical Observations of the Effects of Frequency on Spinal Cord Stimulation

The project described in this chapter is currently being prepared for submission to a peer-reviewed journal.

4.1 Abstract

Spinal cord stimulation (SCS) delivers pulses of electrical current to the dorsal spinal cord to relieve chronic neuropathic pain. Despite its clinical prevalence, the effects of the applied stimulation on the nervous system are poorly understood. Here, we investigated the effects of stimulation frequency on neural behavior during SCS. We used a computational modeling approach to comprehensively examine the effects of frequency on the neural response to SCS. Specifically, we modeled the response of dorsal column axons to SCS applied at various pulse frequencies, the frequency-following behavior at their supraspinal synapses in the dorsal column nuclei, pain processing in the dorsal horn, and the ability of action potentials to faithfully propagate through the complex terminal arbors of their collaterals in the dorsal horn. We also collected self-reported perception, comfort, and discomfort paresthesia thresholds from human subjects with permanently implanted SCS systems at a range of frequencies. For frequencies less than or equal to 100 Hz, we found that perception thresholds were similar with a slight tendency to decrease as frequency increased, but they were notably lower at the highest frequencies tested (500 and 1000 Hz). Our modeling analysis found that these decreased perception thresholds at high frequencies were reflected in reduced DC activation thresholds, and additionally that axons fired asynchronously in a frequency-dependent manner at amplitudes just above threshold. By including

realistic DC fiber firing patterns into a dorsal horn network model, we found that stimulation frequencies up to 1000 Hz could effectively reduce painful signaling, but variability in the network response was observed due to incongruities in axonal firing responses. Finally, we conclude that high frequency action potential conduction failure is likely within primary afferent collateral terminals in the dorsal horn, especially at the higher pulse frequencies utilized in novel stimulation waveforms.

4.2 Introduction

Spinal cord stimulation (SCS) is a common neurostimulation treatment for refractory chronic pain. One or more multi-electrode arrays are implanted into the epidural space dorsal to the spinal cord, and a subcutaneously implanted pulse generator delivers electric current pulses through the electrodes to target the spinal cord. SCS was designed to relieve pain by exploiting the "gate control theory of pain."[49] In brief, large diameter mechanoreceptive primary afferent fibers transmit innocuous touch information from the periphery to the brainstem through the ascending dorsal column (DC) white matter pathways located in the dorsomedial spinal cord. As these afferent fibers ascend, they produce small caliber collaterals which travel into the spinal cord gray matter and repeatedly divide into tortuous, ramified axonal arbors that interact with local neurons.[32,139] According to the gate control theory of pain, action potentials generated in these mechanoreceptive afferents will, through their collaterals, activate inhibitory interneurons in the dorsal horn, which will in turn inhibit transmission of nociceptive signals from the spinal cord to the brain. These mechanoreceptive afferents also synapse on second order projection neurons in the dorsal column nuclei (DCN) that relay the signal to the thalamus (and ultimately the cortex), generating a tingling sensation ("paresthesia") that should overlap the painful region for optimal pain relief.[58] This framework is typically referred to as "conventional" or "tonic" SCS, which was

the only option available to patients for several decades. Newer SCS paradigms do not produce paresthesia, suggesting that they may provide pain relief via different mechanisms of action.[70,71,205,206]

Although SCS has been used for over 50 years, there are many unanswered questions regarding the neural response to the applied stimulation. Unfortunately, this scientific uncertainty manifests as suboptimal clinical SCS outcomes, and only about 60% of patients successfully respond to SCS (typically defined as having at least 50% reduction in self-reported pain scores).[6] To improve clinical outcomes, we need a better understanding of how SCS interacts with the nervous system. Specifically, it is imperative to understand how the various adjustable system parameters (e.g., pulse width, pulse frequency, stimulation configuration) influence the neural response.

One crucial parameter to SCS systems is the pulse frequency, i.e., the number of pulses applied per second.[174] For conventional SCS, the prototypical frequency is 50 Hz.[174] However, the stimulation frequency for conventional SCS varies according to patient preference,[64] and novel waveforms can utilize frequencies ≥ 1 kHz.[5,48] Importantly, both preclinical experimental work and human neuroimaging studies indicate that SCS-induced neural modulation is frequency-dependent, and it is known that optimal pain relief depends on proper frequency selection.[155,207,208] Recent clinical evidence has demonstrated that increasing stimulation frequency leads to decreased perception thresholds (as well as comfort and discomfort thresholds) and a stronger perceived stimulus strength.[209,210] However, somewhat paradoxically, evoked compound action potential magnitude per pulse (a measure of the evoked dorsal column fiber response) decreases monotonically with increased frequency,[209] and novel subparesthetic systems often utilize high (≥ 1 kHz) stimulation frequencies.[5,48,174]

In this study, we investigated the role of frequency in the neurophysiological response to SCS by comparing computational modeling results with self-reported data from 16 human subjects undergoing SCS as part of their clinical care. First, we measured paresthesia thresholds (perception, comfort, and discomfort) as a function of frequency between 2 and 1000 Hz in these subjects. SCS-induced paresthesias are thought to reflect DC fiber activation, and the various SCS implementations are often broadly categorized into those paradigms that produce paresthesia and those that do not.[5] However, despite the clinical relevance of paresthesia, how the temporal and spatial patterns of DC fiber activation affect both paresthesia threshold and quality is poorly understood. Here, we implemented a computational model to assess the firing behavior of DC fibers at stimulation amplitudes close to activation threshold. These firing rates were then introduced into a previously validated dorsal horn network model[155] to evaluate how variation in DC fiber activation will affect pain processing. We also developed and validated a biophysical DCN projection neuron model, the supraspinal postsynaptic target of these DC afferent fibers, and analyzed the frequency dependent transmission properties at this synapse. Finally, we assessed frequency-dependent conduction failure within dorsal column fiber collaterals, motivated by recent experimental evidence demonstrating branchpoint conduction failure in these collaterals at frequencies employed in both conventional and novel SCS systems.[211]

The relationship between DC fiber activation during SCS and their role in paresthesia development (or lack thereof) and pain relief is an area of active and exciting research.[202,212] Comparison of our modeling results with paresthesia thresholds in SCS patients suggests that perception thresholds at different frequencies can be explained by activation thresholds at each frequency, as higher frequencies had reduced DC fiber activation thresholds that closely matched clinical observations. DC fibers also exhibited heterogeneous, frequency-dependent firing patterns

at amplitudes slightly above threshold. In the DCN, neurons were able to reliably follow low SCS frequencies, but the DCN population firing rate became asynchronous at the highest frequencies. In the dorsal horn pain processing network, we found that accounting for realistic firing patterns in dorsal column fibers generated variation in network output during the various SCS frequencies. Finally, our model of DC collaterals demonstrated that branch point failure in these terminals is common at high frequencies and is highly sensitive to several biophysical and morphological neuronal properties. Overall, our results elucidate the neurophysiological effects of SCS stimulation frequency and offer a biophysical basis for the effect of frequency on both paresthesia and pain relief.

4.3 Methods

In this study, we investigated the effects of stimulation frequency on the neural response to SCS. We collected paresthesia thresholds from SCS patients at various frequencies between 2 and 1000 Hz. We also modeled the activation properties of DC fibers at the same frequencies, as well as the synapse between these fibers and projection neurons in the DCN, and we compared the model predictions with the clinical data. We additionally considered the effects of realistic axonal firing rates on the output from dorsal horn pain projecting neurons. Finally, we produced models of DC fiber collaterals and analyzed their ability to faithfully propagate spike trains of various frequencies throughout their arbors. A simplified overview of the computational modeling study is provided in **Fig. 4.1**.

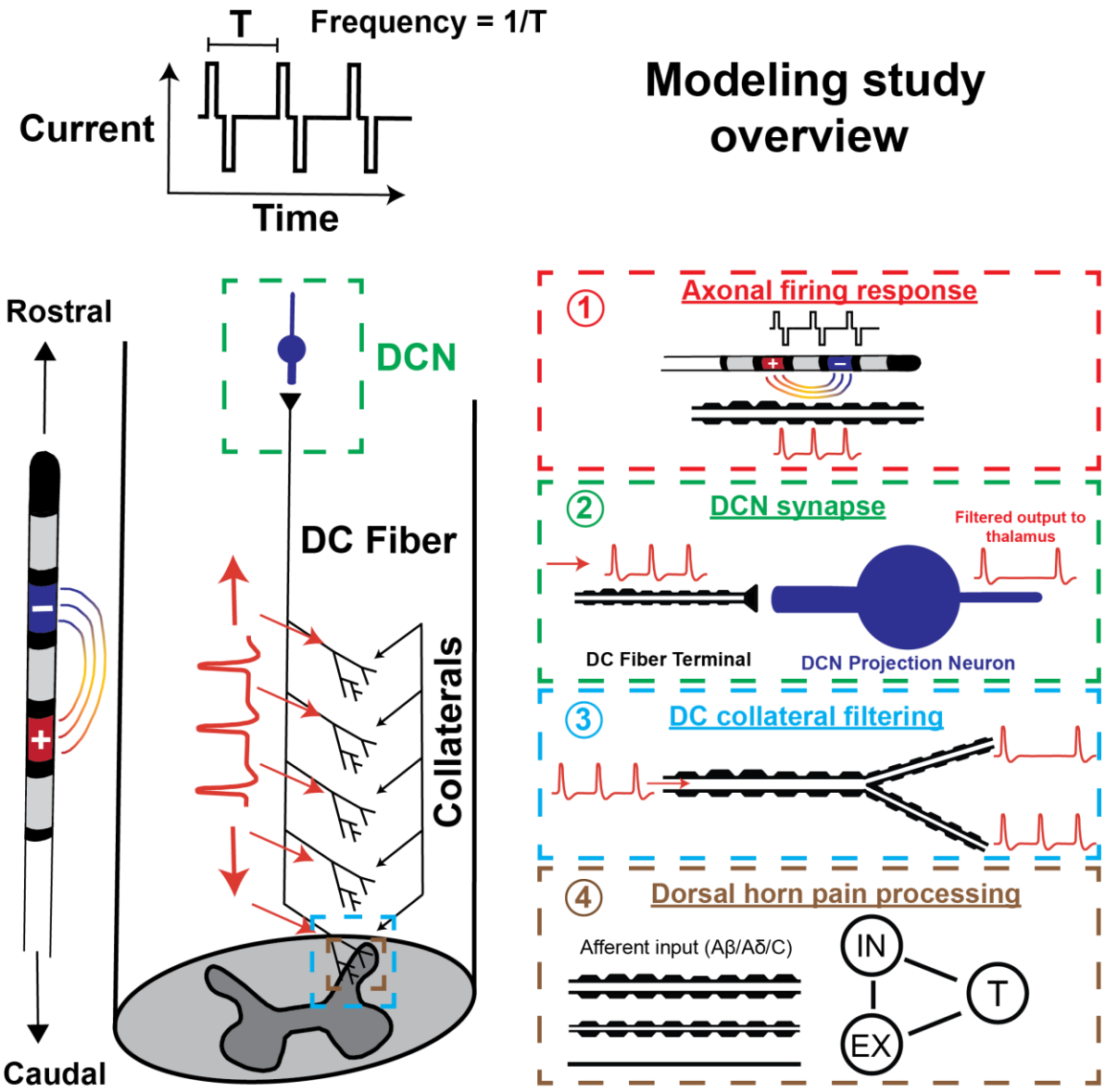

Figure 4.1: Overview of modeling study. We evaluated the effects of stimulation frequency on four relevant phenomena: (1) The DC fiber firing response (red dashed box). (2) Synaptic transmission at the DC-to-DCN synapse (green dashed box). (3) Action potential conduction failure at the axon terminals of DC fiber collaterals (blue dashed box). (4) Output of the dorsal horn pain processing network (brown dashed box).

4.3.1 Human paresthesia thresholds

We asked 16 SCS patients to report relevant thresholds related to the SCS-induced paresthesia while undergoing stimulation at frequencies between 2 and 1000 Hz. Data were collected as part of two separate studies conducted at the University of Michigan (Ann Arbor, Michigan, USA) after obtaining approval from the medical Institutional Review Board. One study

was a clinical trial registered at ClinicalTrials.gov (https://clinicaltrials.gov/show/NCT04732325). All participants provided written informed consent prior to participation in either study. These subjects all had permanently implanted SCS systems for treatment of chronic pain per the standard clinical care. We instructed the participants to lie supine. Then, using a fixed pulse width of 200 μs, we applied SCS at frequencies of 2, 10, 50, 100, 500, and either 900 or 1000 Hz (depending on hardware capabilities). Ten subjects were tested with 1000 Hz and six with 900 Hz.

We randomized the order of the frequencies and allowed a rest period of at least one minute between testing different frequencies. We asked participants to report three different thresholds: 1) perception threshold (PT), when subjects first felt a stimulation-induced sensation; 2) comfort threshold (CT), the maximum stimulation amplitude that participants would comfortably run continuously; and 3) discomfort threshold (DT), the amplitude at which the stimulation became acutely uncomfortable. For each frequency, we first collected PT using a triangulation method (increase amplitude in 0.1 mA increments until perception, decrease until the sensation was lost, and then increase until sensation returned). The amplitude was then incrementally increased until DT was reported and then immediately decreased to CT.

Given the small sample size, non-normally distributed data, and outliers, we employed non-parametric statistics to compare thresholds at the various frequencies. Specifically, we used the Wilcoxon signed-rank test to perform pairwise comparisons of thresholds at the different frequencies. We did not correct for multiple comparisons due to the exploratory nature of the analysis.

4.3.2 Direct axonal response to SCS at various frequencies

When stimulated at pulse amplitudes close to their activation threshold, axons will typically not fire an action potential in response to each stimulation pulse. Instead, the axon will often show

more complex behavior, such as bursting, firing asynchronously, or spiking at a subharmonic frequency.[202] Here, we utilized an existing SCS modeling infrastructure to evaluate firing behavior in DC axons at stimulation amplitudes close to activation threshold ("juxtathreshold"). In brief, we modeled the SCS axonal response using the MRG axon model, a standard and validated model for mammalian axons.[102,194] We placed the axon in a previously developed three-dimensional volume conductor model of the human lower thoracic spinal cord,[103,110,127] approximately at midline and 100 μm ventral to the surface of the spinal cord white matter. We then used finite element analysis (COMSOL Multiphysics, Burlington, Massachusetts, USA) to evaluate the electric potential generated along the axon by SCS applied via a standard bipolar configuration, and we quantified the axonal response using the software package NEURON (version 7.4) through a Python interface.[99,108] The model fiber had a diameter of 10 μm. We simulated one second of SCS, utilizing a time step of 5 μs. We utilized symmetric biphasic stimulation pulses. Each phase had a pulse width of 200 μs that were separated by an interphase interval of 80 μs (**Fig. 4.2**). To mimic our clinical data, we tested the axonal response to frequencies of 2, 10, 50, 100, 500, and 1000 Hz.

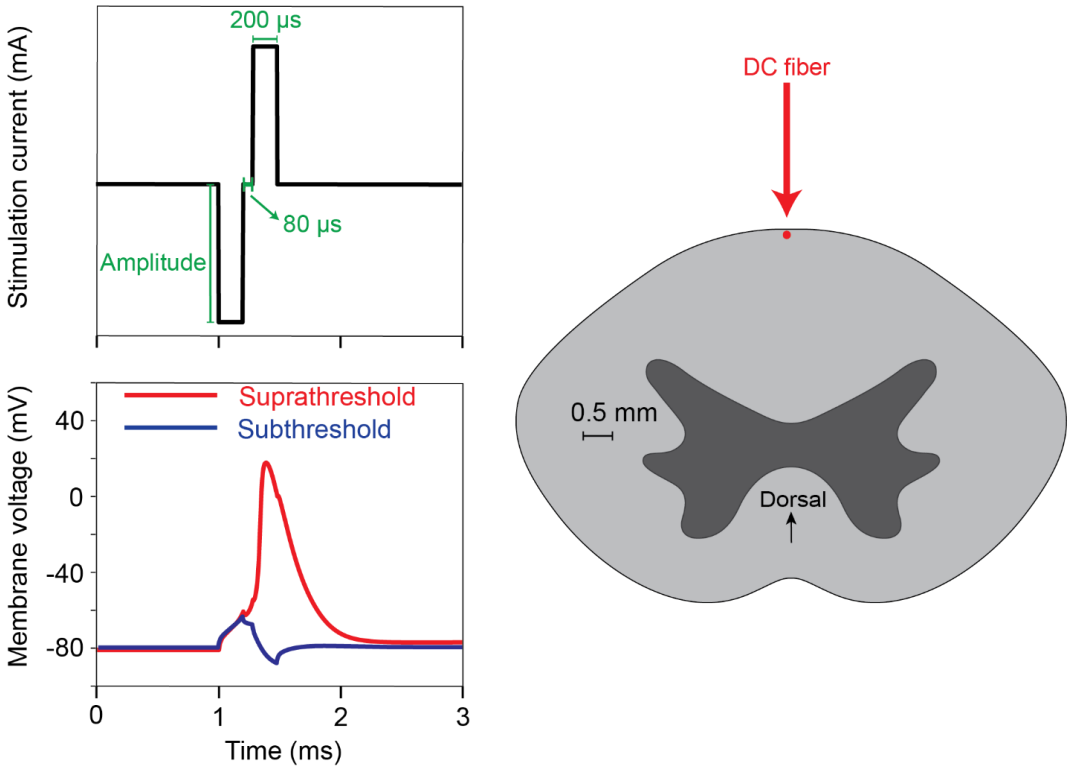

Figure 4.2: Overview of modeling axonal juxtathreshold response. On the left, we show the symmetric, biphasic pulse used at all SCS frequencies, which had a pulse width of 200 µs and an interphase interval of 80 µs. Below this, we show a sub- and supra-threshold axonal response to stimulation just below and above the threshold amplitude, respectively. On the right we show the location of the DC fiber in the model spinal cord.

4.3.3 DCN model

Synaptic transmission properties are frequency dependent.[213] Therefore, a comprehensive understanding of the frequency varying effects of SCS must consider the synaptic transmission properties between DC fibers and their postsynaptic targets. In this study, we specifically considered the synapse between DC fibers and their postsynaptic targets in the DCN (i.e., the gracile and cuneate nuclei). These nuclei contain the first synapse in the pathway linking innocuous mechanical stimuli carried by DC fibers to perception. [32] Thus, their frequency filtering properties should affect the quality (and initial perception threshold) of sensation in paresthetic SCS, as well as contribute to supraspinal feedback loops regulating descending pain inhibition.

To investigate the synaptic transmission properties at the DCN synapse during SCS-relevant frequencies, we constructed a DCN projection neuron model using published experimental data. We began by adopting a model previously generated for pallidal deep brain stimulation, as this neuron was morphologically similar to those described in the DCN and displayed similar electrophysiological properties and active conductances.[214] We then adjusted the model parameters to produce a final DCN projection neuron model that demonstrated excellent agreement with published experimental data (input resistance, spontaneous firing frequency, resting membrane potential, action potential duration and amplitude, and membrane time constant; **Table 4.1**).[215,216] We provide the active channel properties in **Table 4.2**. Next, we incorporated an experimentally derived model of the synapse between DC afferents and a DCN-to-thalamus projection neuron. In line with similar investigations in deep brain stimulation, we employed a Tsodyks-Markram (TM) phenomenological synapse model.[217,218] We then tuned this model to recreate experimentally recorded properties of excitatory postsynaptic potentials (EPSPs) in DCN projection neurons. Specifically, we calibrated the EPSPs to closely match EPSP rise time, decay time, and amplitude, accounting for frequency dependent EPSP amplitude variation (**Table 4.3**, **Fig. 4.3**).[215,216] Finally, we evaluated the synaptic transmission properties at a range of frequencies between 10 and 400 Hz and assessed sensitivity of the model to unitary EPSP amplitude. Post-hoc comparison of the final model to experimental results demonstrated excellent agreement between model firing rates in response to DC fiber stimulation and available published data.[219–223]

Table 4.1: Comparison of the DCN computational model parameters with experimental data.

Parameter	**Model**	**Experimental values**	**Reference**
Soma diameter	18.0	19.0 ± 1.8 µm	Nuñez & Buño[216]
Soma length	30.0	33.2 ± 5.8 µm	Nuñez & Buño[216]

AP amplitude	76.0 mV	75.3 ± 0.89 mV	Nuñez & Buño[216]
AP duration	0.8 ms (FWHM)	0.7 ± 0.05 ms	Nuñez & Buño[216]
Membrane time constant	5.7 ms	5.2 ± 1.8 ms	Bengtsson[215]
Input resistance	78 MΩ	96 ± 43 MΩ	Bengtsson[215]
Spontaneous firing rate	9.7 Hz	~10.0 Hz	Bengtsson[215]
Resting potential	-55.5 mV	-52.8 ± 1.0 mV	Bengtsson[215]
EPSP rise time	1.04 ms	1.08 ± 0.15 ms	Bengtsson[215]
EPSP decay time	5.55 ms	6.40 ± 1.90 ms	Bengtsson[215]
EPSP amplitude (baseline)	4.0 mV	3.7 ± 1.5 mV	Bengtsson[215]

Table 4.2: Ionic conductances in the DCN cell model soma. Conductances were equal in the dendrites, where NaF was 1e-7 S/cm^2.

Current	**Description**	**g_{ion} (S/cm^2)**
NaF	Fast sodium	0.028
NaP	Persistent sodium	0.0005
HCN	Hyperpolarization-activated inward cation current	0.002
KDR	Delayed rectifier potassium	0.006
iKCa	Calcium-activated potassium channel	2.5e-5
CaL	L-type calcium	0.0001
CaN	N-type calcium	0.001
CaT	T-type calcium	0.0001

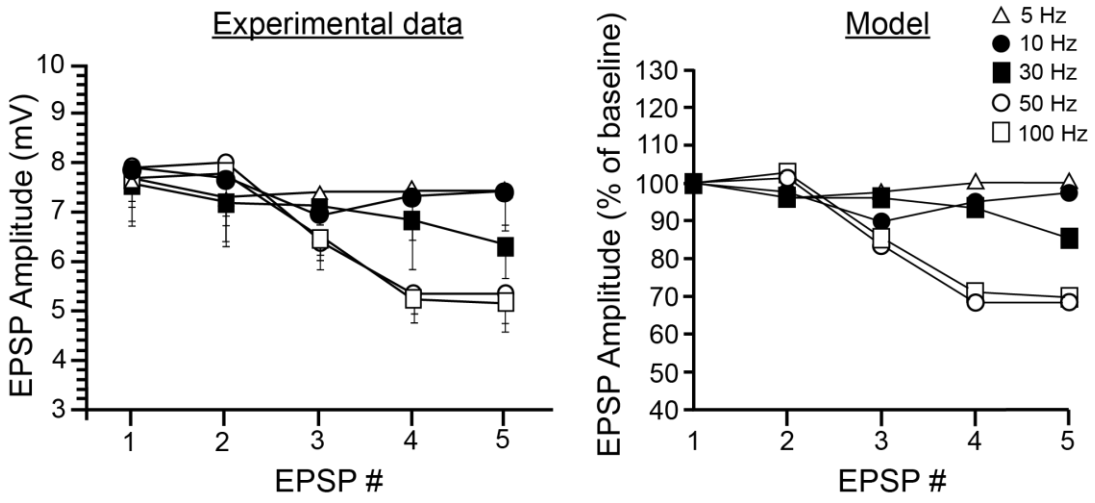

Figure 4.3: Comparison of frequency dependent excitatory post-synaptic potential (EPSP) amplitude between experimental data (left) and our computational model (right). Experimental data and figure are re-created from Nuñez and Buño, 1999.[216]

4.3.4 Dorsal horn pain processing

The overall goal of conventional SCS is to reduce painful signaling in the dorsal horn. Thus, we investigated the effects of juxtathreshold, frequency-dependent firing properties on dorsal horn transmission. To do this, we utilized the validated dorsal horn network model developed by Zhang et al.[113] Briefly, the output of this model is the firing rate of the wide dynamic range transmission ("T") neuron. The WDR neuron receives input from local inhibitory and excitatory interneurons, as well as direct inhibition from a surround receptive field inhibitory interneuron. Input to the network comes from 15 local receptive field Aβ fibers, 15 surround receptive field Aβ fibers, 15 Aδ fibers, and 30 unmyelinated C fibers.

To apply input into the model, we generated random input in the Aδ and C fibers according to homogeneous Poisson processes with mean rates of 2.2 and 1.5 spikes/s, respectively.[155] For the Aβ fibers (both local and surround receptive fields), we randomly sampled (with replacement) the firing behavior of a population of DC fibers in our model, only choosing from fibers that were activated by the SCS. Local Aβ fibers had a baseline spontaneous firing rate of 2.2 spikes/s to

model neuropathic pain).[155] For each frequency tested, we repeated this process 50 times to account for variation in fiber firing frequencies.

4.3.5 Axon collateral models

To examine action potential fidelity within DC collateral terminal arbors, we stochastically generated branching axon structures within the dorsal horn of a lower thoracic spinal cord model (described in detail in several previous publications[103,110,127]). We then introduced trains of action potentials at frequencies between 10 and 250 Hz into these collateral models and observed the firing properties at the axon terminal nodes.

Primary afferent collaterals produce morphologically diverse termination patterns within the dorsal horn.[139,143] Cellular morphology affects bioelectric activity and thus we generated a set of morphologically heterogeneous collateral termination models to account for variable responses in different terminal arbors. In total, we produced 25 afferent collateral models. Published descriptions of collateral terminal arbor geometries typically provide only gross anatomical descriptions and specific quantitative measurements are sparse.[139,143,144,224] Therefore, we used a simple algorithm to stochastically generate realistic collateral termination patterns. We modeled the collaterals as connected smooth curves (B-splines) located within the dorsal horn gray matter of a lower thoracic volume conductor model of the spinal cord. The volume conductor model has been described in detail in several previous publications.[103,110,127] The number of branch points, as well as the location of the branch points, were randomly selected from uniform distributions. The maximum number of branches off the first order collateral was 7. Second order branches produced a maximum of 3 branches, and third order branches produced a maximum of 2. The total number of branch points within the collaterals ranged from 3 to 34 (median = 16). Parameters were chosen

based on previously published collateral reconstructions.[139,143,144,166,211,224] Cross-sections of the 25 collateral models are shown in **Supp. Fig. 4.1.**

We derived the axon electrophysiological properties from the MRG model, which includes electrically active nodes of Ranvier with fast and persistent sodium conductances, a slow potassium conductance, and passive leak channels and membrane capacitance.[102] We used a version of the MRG model that included small modifications to node dynamics that was developed in a previous study to produce more realistic axonal behavior.[194] The nodes are connected by electrically passive internodes which consist of a double-layer structure, incorporating both passively conducting axolemma and myelin sheath, as well as a periaxonal current pathway in the submyelin space. We modeled the internodal regions using the same properties of the internodal region in the original MRG model.[102] Finally, we reduced the persistent sodium conductance by 50%, because it is known that in small diameter MRG axon models the default persistent sodium can produce hyperexcitability, and previous work has shown that action potential following frequency in branched axon models is strongly robust to variations in this parameter.[225]

The diameter of the primary collateral as it entered the dorsal horn was 3 μm, and at each branching point the diameter of the child collaterals were 60% of that of the parent axon. Experimental measurements of afferents have shown first-order collaterals that are approximately one third of the parent axon diameter.[226,227] Thus, we chose the 3 μm collateral diameter to correspond to the approximate 8-11 μm DC fiber diameter range which has been implicated in therapeutic closed-loop SCS.[127,228] We restricted internodal lengths (i.e., distances between nodes of Ranvier) to be between 40 and 120 times the ratio of the internodal diameter (with a typical ratio of 100, in line with measurements from Ia fiber collaterals).[226] Nodes were 1 μm long and their diameters were 70% of their parent axons, in line with small diameter MRG axon

models.[229,230] We performed a sensitivity analysis to investigate the robustness of our results to variations in fast sodium conductance, internodal length, fiber diameter, nodal length, and the ratio of diameters between child and parent axons at branch points.

We introduced action potentials at specific frequencies by applying a high-amplitude, short-duration current injection at a proximal node. We analyzed frequencies between 10 and 250 Hz. For this sensitivity analysis, we ran 500 milliseconds of simulation time, with a time step of 5 μs, and a temperature of 37 °C. In this analysis, we also decreased the time step to 2 μs and approximately halved the spatial discretization to ensure that the results were robust to these factors.

4.4 Results

4.4.1 Perception threshold was decreased at high frequencies

We asked 16 participants undergoing SCS as part of their clinical care, to report at what amplitude they first felt paresthesia (i.e., PT) using a fixed pulse width of 200 μs at six frequencies between 2 and 1000 Hz. For participants with implanted systems that could not produce 1000 Hz stimulation at this pulse width, we reduced the maximum stimulation frequency to 900 Hz. To simplify analysis, we combined results collected at 900 and 1000 Hz based on their similar interpulse intervals (1 ms versus 1.1 ms) and similar thresholds between the two frequencies shown in a previous study.[210] Additionally, we also asked participants to self-report their comfort and discomfort thresholds (CT and DT, respectively). Results for these thresholds are presented in **Fig. 4.4**. Mean group PT decreased monotonically with increasing frequency: 2.85 (±1.83), 2.71 (±1.81), 2.64 (±1.78), 2.56 (±1.60), 2.27 (±1.46), and 2.24 (±1.44) mA at 2, 10, 50, 100, 500, and

900/1000 Hz, respectively (±SD). This decreasing pattern was maintained when analyzing within-subject differences (**Table 4.3**).

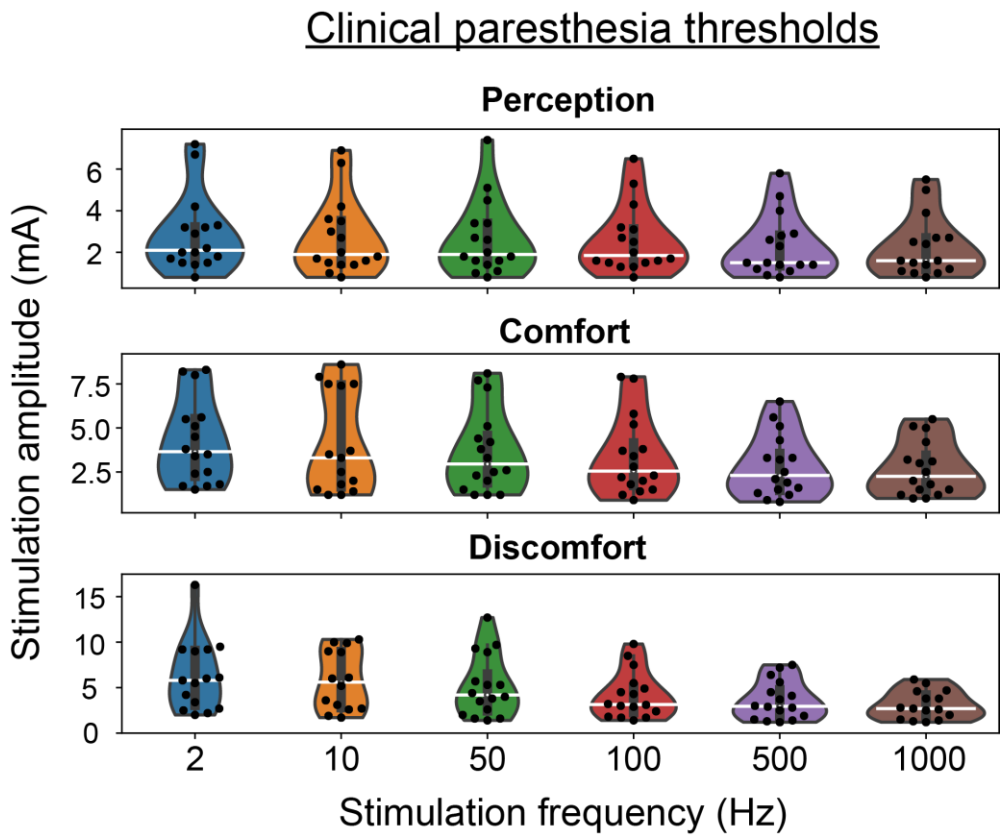

Figure 4.4: Perception (top row), comfort (middle row), and discomfort (bottom row) thresholds in 16 SCS patients. White line in each violin plot corresponds to the median values. Black circles represent individual data points. As described in the Methods, 1000 Hz stimulation includes results obtained for 900 Hz SCS.

Table 4.3: Pairwise means of within-subject differences. A negative value indicates a lower value (i.e., decrease in the corresponding threshold) at the higher frequency (f_2) relative to the lower frequency (f_1). P-values were calculated for the Wilcoxon signed-rank test, and p-values less than or equal to 0.05 are bolded.

f_1 (Hz)	f_2 (Hz)	Mean: $PT(f_2) - PT(f_1)$	p-value	Mean: $CT(f_2) - CT(f_1)$	p-value	Mean $DT(f_2) - DT(f_1)$	p-value
	10	-0.138	0.098	0.100	0.774	0.264	0.405
	50	-0.213	0.187	-0.569	**0.002**	-1.380	**0.009**

2	100	-0.294	**0.003**	-0.863	**<0.001**	-2.327	**<0.001**
	500	-0.581	**<0.001**	-1.400	**<0.001**	-2.833	**<0.001**
	1000	-0.606	**<0.001**	-1.544	**<0.001**	-2.636	**<0.001**
10	50	-0.075	0.523	-0.660	0.274	-1.486	**0.008**
	100	-0.156	**0.050**	-0.873	0.096	-2.293	**<0.001**
	500	-0.444	**<0.001**	-1.400	**<0.001**	-2.650	**<0.001**
	1000	-0.469	**<0.001**	-1.547	**<0.001**	-2.900	**<0.001**
50	100	-0.081	0.278	-0.294	**0.006**	-0.975	**0.003**
	500	-0.369	**<0.001**	-0.831	**<0.001**	-1.519	**<0.001**
	1000	-0.394	**<0.001**	-0.975	**<0.001**	-1.520	**<0.001**
100	500	-0.288	**<0.001**	-0.534	**<0.001**	-0.544	**0.003**
	1000	-0.313	**<0.001**	-0.681	**<0.001**	-0.673	**<0.001**
500	1000	-0.025	0.714	-0.144	**0.041**	-0.267	0.078

4.4.2 Clinical comfort and discomfort thresholds

We determined CT and DT by asking participants to report when the stimulation amplitude was the maximum level that they could run continuously and when it became acutely uncomfortable, respectively. In rare instances, participants maximized their stimulator output before reaching either CT and/or DT. This happened once for CT (at 10 Hz) and four times for DT (once at 2 Hz, twice at 10 Hz, once at 1000 Hz). These individual data points were not included in the analysis but should be considered when interpreting our results.

Interestingly, we observed that 2 and 10 Hz had similar thresholds for both CT and DT, and the mean paired difference within subjects was slightly higher for 10 Hz for both measures

(mean within-subject differences were 0.1 and 0.26 mA for CT and DT, respectively; **Fig. 4.4** and **Table 4.3**). Mean CT and DT consistently and appreciably decreased as frequency was further increased, and the mean paired difference was negative for all frequencies higher than 10 Hz. For instance, compared to 2 Hz, the mean within-subject differences in CT were -0.57, -0.86, -1.40, and -1.54 mA for 50, 100, 500, and 900/1000 Hz stimulation. For DT, these mean differences were -1.49, -2.29, -2.65, and -2.9 mA. Additionally, we considered the therapeutic window as CT – PT.[231] The average therapeutic windows were 1.37, 1.37, 1.01, 0.80, 0.55, and 0.43 mA for 2, 10, 50, 100, 500, and 900/1000 Hz SCS, once again showing similar thresholds between 2 and 10 Hz, followed by sustained decreases at higher frequencies.

4.4.3 Dorsal column fiber firing properties

First, we simulated the firing behavior of a single superficially located DC fiber in response to SCS amplitudes just above activation threshold at 2, 10, 50, 100, 500, and 1000 Hz (**Fig. 4.5**). The fiber was 10 µm in diameter and located 100 µm ventral to the white matter boundary. For this fiber, the activation threshold to fire at least one action potential was equal for 2, 10, 50, and 100 Hz SCS (2.47 mA). At 500 Hz and 1000 Hz, threshold decreased to 2.32 and 2.25 mA, respectively. Interestingly, these reduced activation thresholds at 500 and 1000 Hz appear to result from interaction of temporal summation during the high-frequency stimulation and transient subthreshold depolarizing currents that reduce the axonal threshold for activation (data not shown).

We observed that, despite having an equivalent 2.47 mA activation threshold, the axonal firing behavior varied subtly between 2, 10, 50, and 100 Hz stimulation as the amplitude was incrementally increased to slightly higher juxtathreshold stimulation amplitudes (**Fig. 4.5**). At 2 Hz, the subthreshold versus suprathreshold response was a sharp binary, and the axon immediately began firing in response to each SCS pulse as soon as the amplitude was above the axonal

threshold. In contrast, all other frequencies produced slight changes in axonal behavior as amplitude was incrementally increased. At juxtathreshold amplitudes, both 10 and 50 Hz SCS produced tonic axonal firing at a lower rate. During 10 Hz, just above threshold stimulation (2.5 mA) produced a 5 Hz firing rate in the axon, which sharply converted to a tonic 10 Hz firing response at 2.7 mA. In contrast, 50 Hz SCS produced a graded increase in axonal firing rate as the stimulation amplitude was increased. As we increased the amplitude from 2.5 to 2.8 mA in 0.1 mA increments, the firing rates were approximately 7, 9, 11, and 13 Hz during 50 Hz SCS. We did not observe tonic 50 Hz firing until the activation threshold was increased to 3.3 mA. Finally, 100 Hz SCS produced a distinct axonal response. Specifically, we observed that the axon fired in spike doublets (pairs of spikes separated by 10 ms) at just-above-threshold stimulation. At 2.5 mA, these doublets occurred at approximately 6 Hz. Increasing the amplitude to 2.6 and 2.7 mA slightly increased the frequency of these doublets to approximately 8 and 9 Hz, respectively. Further increasing the amplitude converted these doublets into bursts, with higher amplitudes having more spikes in a burst (2.8, 2.9, and 3.0 mA SCS produced bursts with 3, 4, and 5 spikes, respectively), until the axon began firing tonically at 100 Hz at 3.1 mA.

As previously discussed, 500 and 1000 Hz SCS had reduced thresholds compared to these lower frequencies (2.32 and 2.25 mA, respectively). We observed that these two frequencies produced qualitatively similar axonal firing behavior. At juxtathreshold amplitudes, SCS at both frequencies generated burst firing patterns. As the stimulation amplitude is increased, the number of spikes within a burst increases while the time between bursts decreases. Eventually, the axon begins tonically firing at a subharmonic frequency of the applied stimulus, and further amplitude increase eventually produces a maximum tonic firing frequency in the axon, with the upper firing

rate limited by the axonal biophysics. In this model, the maximum axonal firing frequency was 500 Hz for both 500 and 1000 Hz SCS.

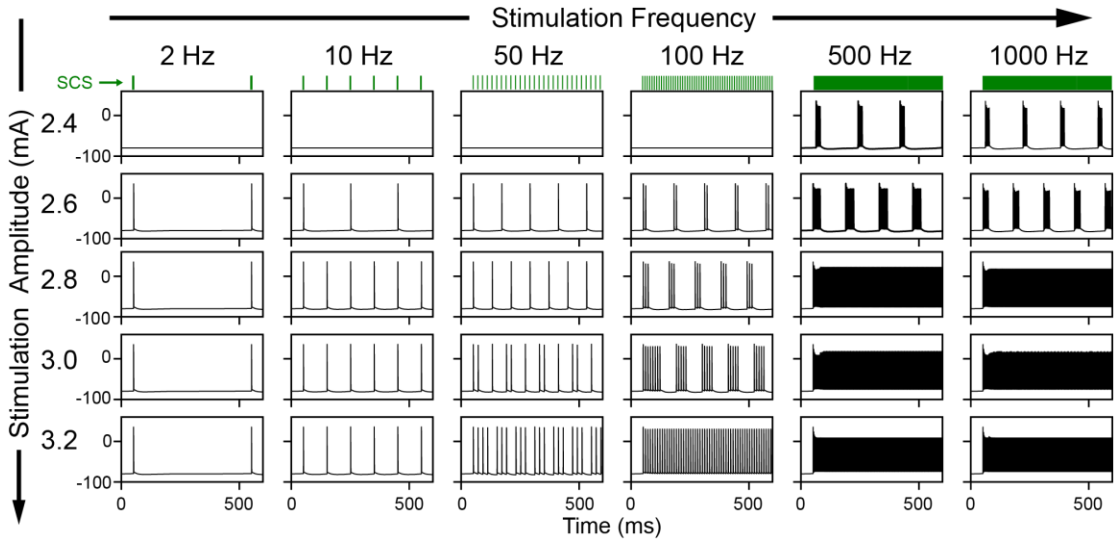

Figure 4.5: Response of a model superficial DC fiber to SCS between 2 and 1000 Hz at juxtathreshold amplitudes. These results correspond to the DC fiber location depicted in Figure 2 (located at midline and 100 µm ventral to the white matter surface).

Next, we expanded our model to explore the effects of both spatial position and fiber diameter on axonal firing behavior. First, we produced an identical 10 µm fiber located 200 µm ventral to the original fiber model. We found that this slight difference in dorsoventral position corresponded to a notably higher threshold, and that the two fibers fired asynchronously at frequencies of at least 50 Hz (**Fig. 4.6**).

Finally, we evaluated the firing characteristics of a population of DC fibers. To do this, we used identical positions and densities to those described by Anaya et al.[127] in the 7.3 to 11 µm diameter range, which themselves were derived from histology of the human dorsal columns.[199] Overall, our model population included 346 total fibers. Similar to the previous analysis, we found that firing behavior was asynchronous at high frequencies at amplitudes near thresholds. To investigate the effects of frequency on stimulation perception threshold, we determined model PT as the amplitude necessary to activate 10% of DC fibers in our population model to fire at least

one action potential.[105,131] We found that this model PT was identical for 2, 10, and 50 Hz, and then decreased slightly at 100 to 1000 Hz. Importantly, we found that the activation thresholds of model fibers activated closely correspond with clinical PT at the various tested frequencies (**Fig. 4.7**). Raster plots of the frequency-specific firing behavior of DC fibers activated at PT are shown in **Supp. Fig. 4.2.**

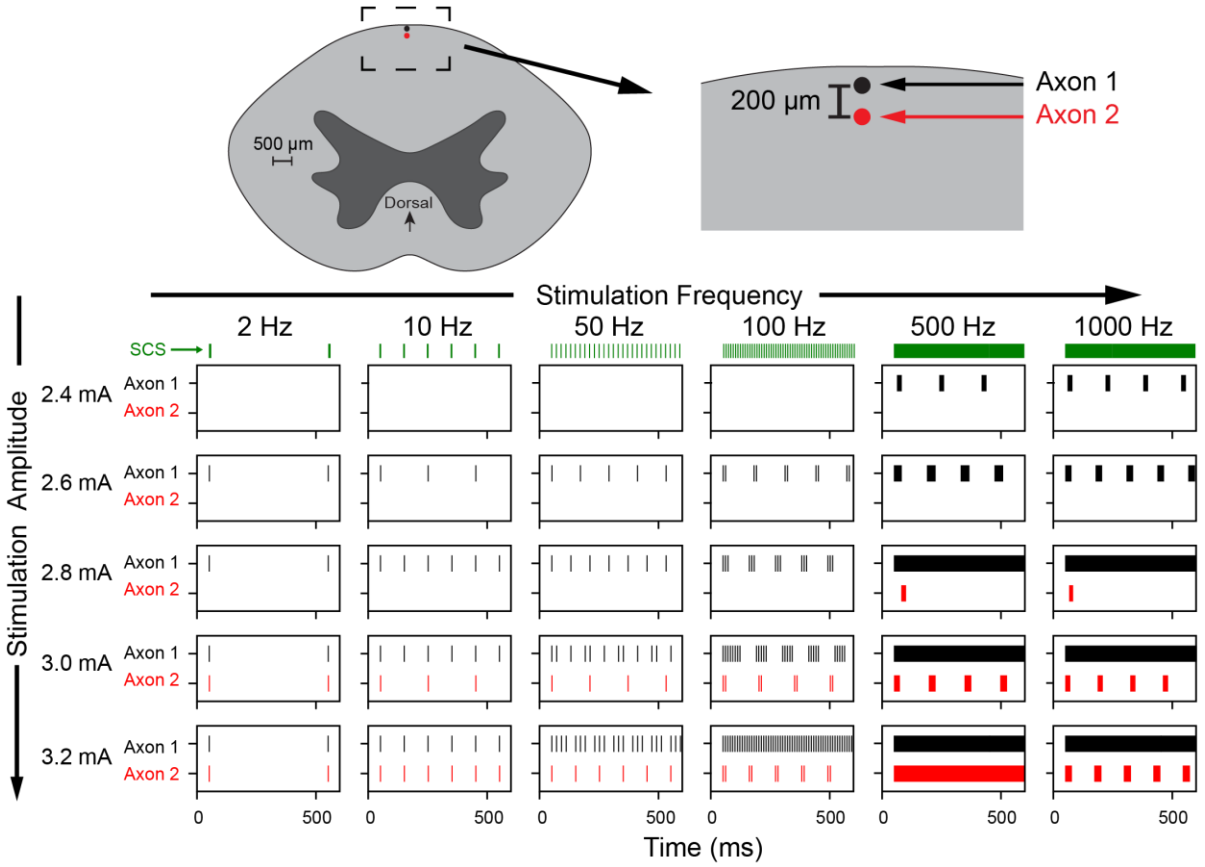

Figure 4.6: Raster plot showing firing behavior for two identical axons separated by 200 µm. The black spikes represent the firing of the original axon (same axon as **Fig. 4.5**), whereas the red spikes are those for a second axon, located 200 µm ventral to the first axon. The stimulation amplitudes are equivalent to those in **Fig. 4.5**: The top row corresponds to 2.4 mA stimulation, which is increased in 0.2 mA increments to a maximum of 3.2 mA.

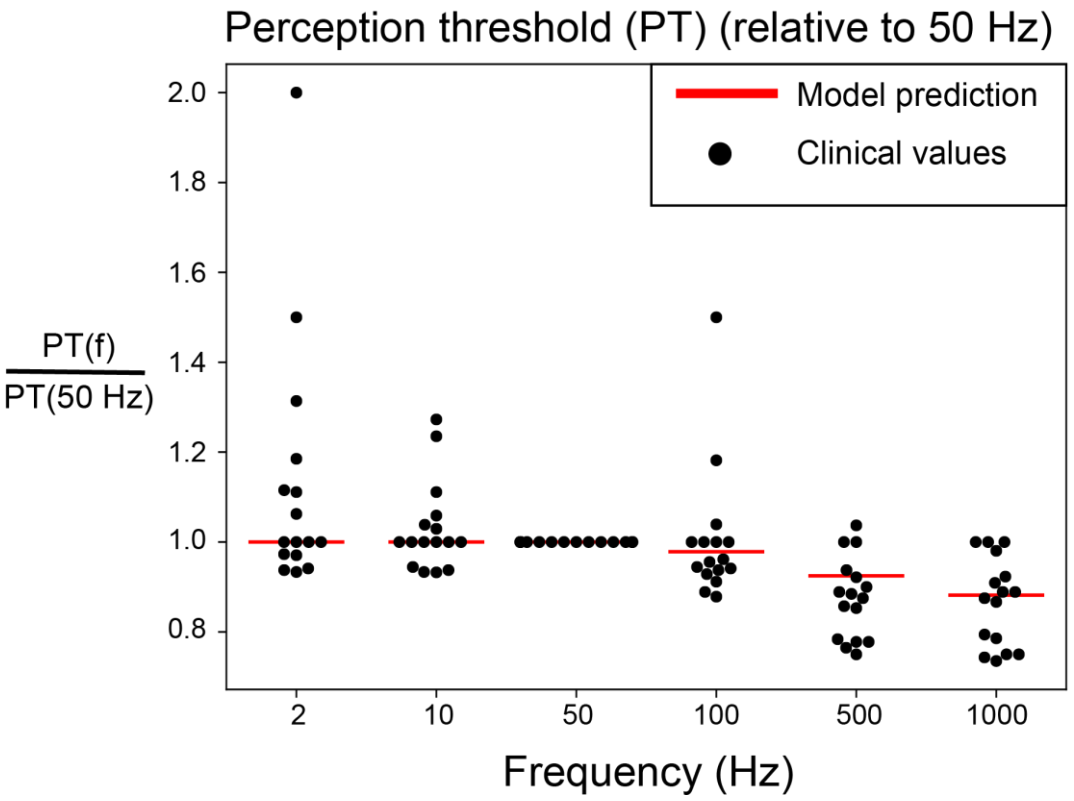

	2 Hz	10 Hz	50 Hz	100 Hz	500 Hz	1000 Hz
Clinical median	1.0	1.0	—	0.96	0.88	0.88
Model	1.0	1.0	—	0.98	0.92	0.88

Figure 4.7: (Top) Scatterplot showing individual perception thresholds (PTs) for each human subject. PTs are given as relative to conventional 50 Hz SCS for each individual to account for inter-subject variation in baseline thresholds and model activation thresholds. Red lines indicate the model PT when 10% of fibers fire at least one action potential. (Bottom) Comparison of model PT predictions with clinical medians.

4.4.4 Dorsal column nucleus model

The first connection point in the chain linking peripheral mechanoreceptive stimuli to perception is the synapse between the DC afferent fibers and the second-order neurons in the DCN (i.e., the nucleus gracilis and nucleus cuneatus).[32] We developed a model of this synaptic connection to investigate how the synaptic transmission properties affect SCS-induced paresthesia. First, we developed a model of a DCN projection neuron that captured electrophysiological and

spiking properties of recorded DCN neurons.[215,216] Next, we included a Tsodyks-Markram phenomenological synapse model which was parameterized to fit experimentally determined synaptic properties (EPSP amplitude, rise time, and decay time, as well as frequency dependent plasticity)[215–217] (**Fig. 4.3**; **Tables 4.1- 4.2**). Finally, we applied spike trains to the synaptic model at a range of frequencies and recorded the DCN cell response (**Fig. 4.8**).

The base synaptic transmission model demonstrated reliable action potential transmission at 2, 10, and 50 Hz, with 100% of presynaptic action potentials producing a postsynaptic spike in the DCN neuron. At 100 Hz, the postsynaptic neuron could no longer be driven in a one-to-one fashion by the incoming presynaptic spike train, and the postsynaptic firing rate was decreased to approximately 70 Hz. Further increasing the presynaptic firing frequency marginally increased the postsynaptic firing rate, with 200, 300, 400, and 500 Hz presynaptic spike trains producing postsynaptic firing between approximately 70 and 75 Hz (**Fig. 4.6**).

Next, we ran simulations increasing the EPSP amplitude, modeling a stronger synaptic connection and/or coherent activation of additional afferent fibers. When the monosynaptic EPSP amplitude was doubled, the DCN neuron was able to reliably follow a 100 Hz presynaptic spike train. However, at 200, 300, 400, and 500 Hz, the DCN firing frequency plateaued at slightly higher than 100 Hz, which agrees with similar preclinical experimental recordings.[219–223] Further increasing the synaptic strength showed similar patterns, suggesting that intrinsic electrophysiological properties place an upper limit of ~100 Hz on the maximum reliable transmission frequency at this synapse.

Finally, to evaluate the effects of frequency on the DCN population response, we expanded this model from a single DCN neuron to a population of 100 DCN neurons. Each of these neurons received synaptic input from 1-3 activated DC fibers (chosen randomly), based on evidence that

synaptic input in DCN neurons is dominated by a small number of strong connections.[215] We accounted for variation in synaptic strength by allowing unitary EPSP amplitude to vary between 2-6 mV as sampled from a uniform distribution.[215] We evaluated firing properties at perception and discomfort thresholds (DT was calculated by scaling the model PTs by the average clinical ratio between DT and PT for each stimulation frequency).

We found that low-frequency SCS produced highly synchronized activity at 2, 10, and 50 Hz (**Fig. 4.9**). At 100 Hz, the response became less synchronized, but the responses to each individual pulse were still distinguishable, whereas at 500 and 1000 Hz the DCN response is almost completely asynchronous. Unsurprisingly, at DT, population firing rates tended to be higher as more fibers were recruited, and activated fibers fired at higher frequencies.

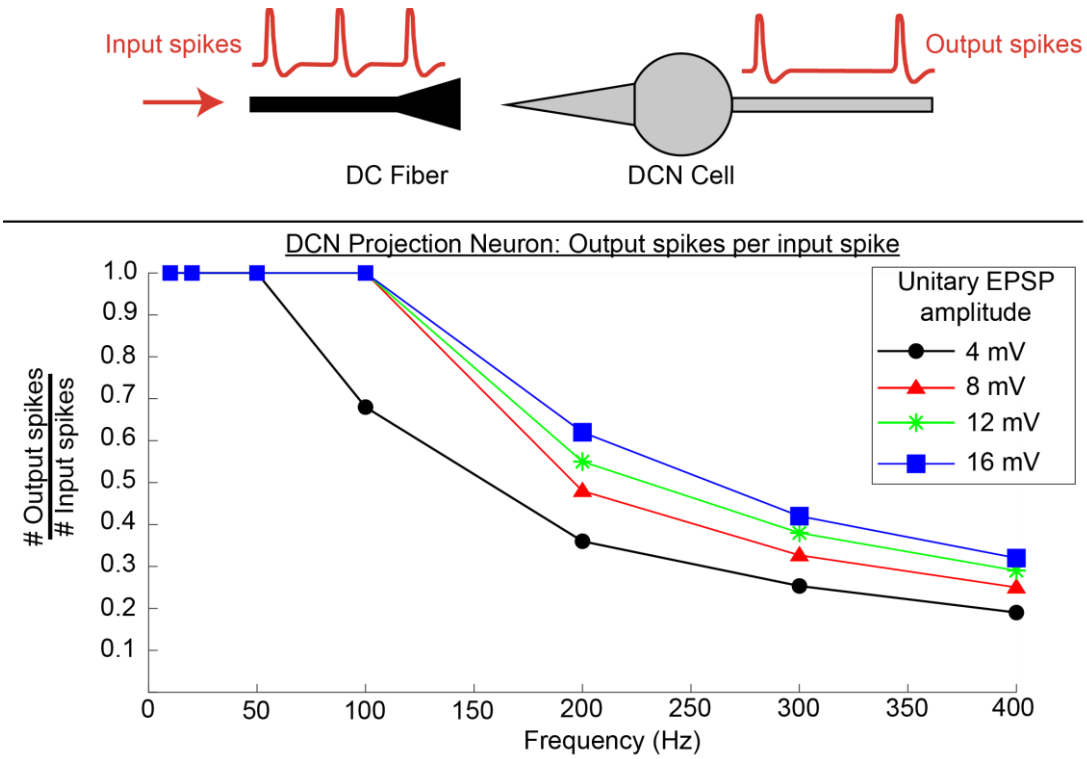

Figure 4.8: DCN projection neuron firing rates for DC afferent fiber input spike trains of varying frequencies. Note, data are given as the ratio between the number of output spikes to the number of input spikes at a given frequency. Color-coded lines correspond to different strengths of the synaptic connection.

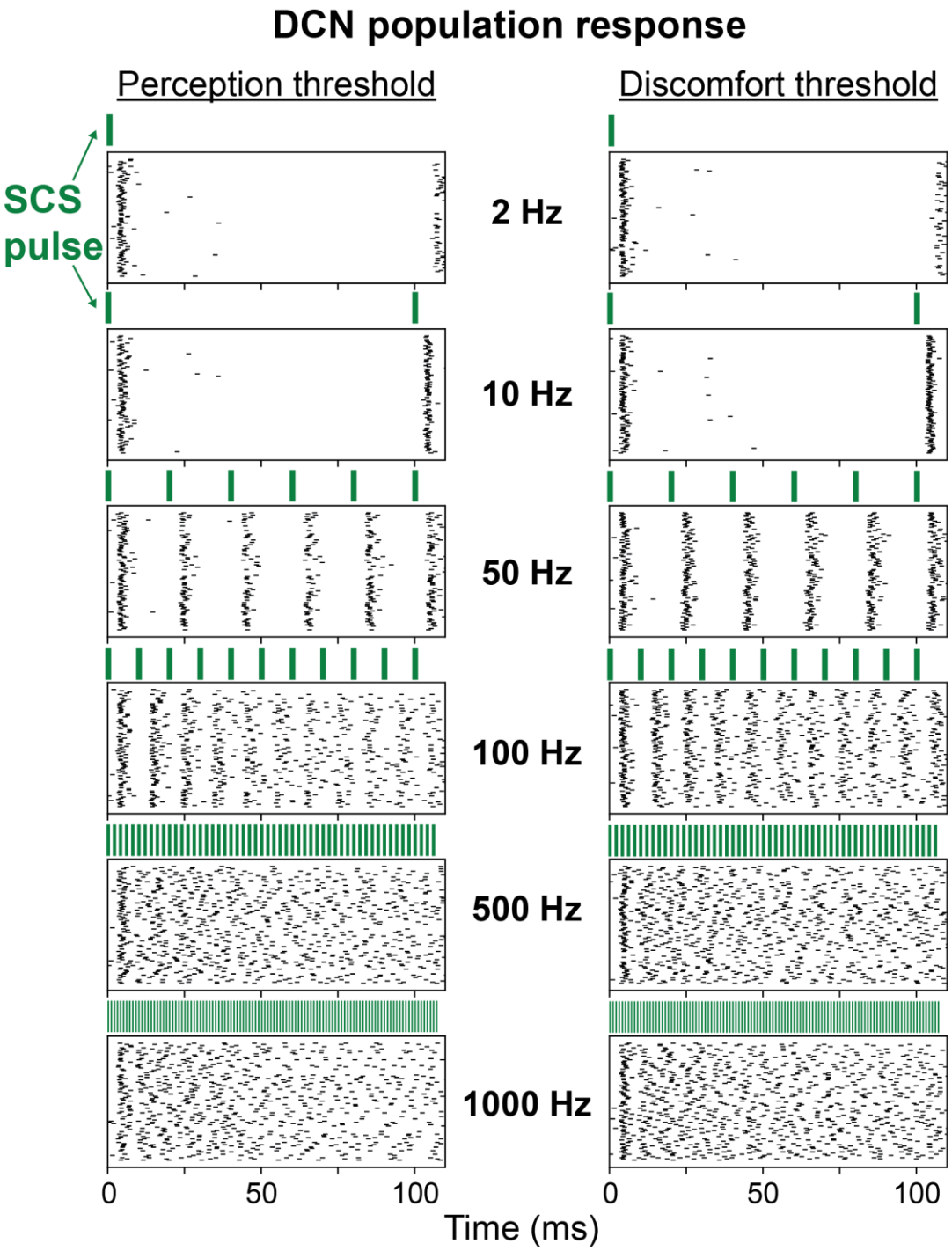

Figure 4.9: Model DCN neuron firing patterns at perception (left) and discomfort (right) thresholds. Green lines indicate SCS pulses at the various frequencies.

4.4.5 Effects of stimulation frequency on dorsal horn output

Overall, the goal of SCS is to reduce pain. Therefore, we used a previously validated circuit model to investigate the effects of stimulus frequency on the output of the dorsal horn pain-processing network.[155] To do this, we modeled realistic DC fiber firing patterns at model CT, as this would correspond to a stimulation amplitude that patients would utilize clinically. We calculated CT by scaling the model PT by the average ratio of CT to PT observed in the human subjects at each individual frequency. These scaling factors were 1.56, 1.56, 1.41, 1.29, 1.24, and 1.22 for 2, 10, 50, 100, 500, and 1000 Hz, respectively. We ran 50 simulations, each time randomly selecting 15 local Aβ fibers from the population of DC fibers that were activated by the stimulation (out of the 346 total fibers in the population), and 15 surround-field Aβ fibers from the overall population of DC fibers. Network model output was the firing rate in the network transmission ("T") neuron, which is a proxy for pain[155,232] (**Fig. 4.10**).

Like Zhang[155], we found that network output varied with frequency, with low frequencies (2 and 10 Hz) producing small decreases in network output, but 50 and 100 Hz SCS (i.e., the standard clinical range) more strongly reducing painful transmission. Additionally, we found that high frequencies (>100 Hz) did not effectively reduce network output and instead had highly variable responses that often were increased compared to baseline. Importantly, compared to the original model by Zhang, we found that applying randomly sampled DC fiber firing patterns led to variability in the network output in which different simulations could produce drastically different output neuron firing rates (most evident at 50, 500, and 1000 Hz) (**Fig. 4.10**). These fluctuations in network output due to variability in the DC fiber response at conventional 50 Hz stimulation could partially explain the heterogeneous pain relief in SCS patients observed clinically.

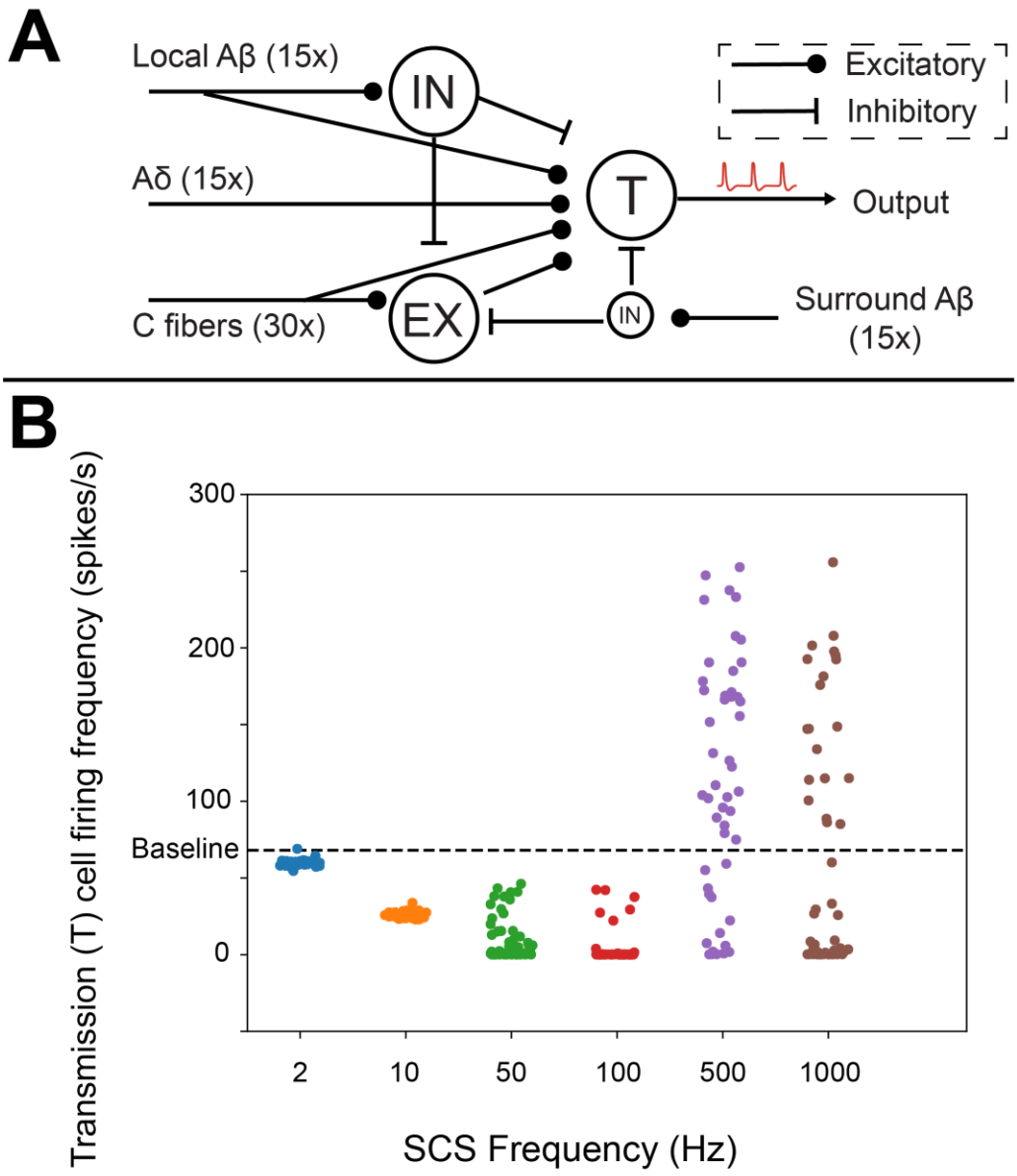

Figure 4.10: Inhibition of dorsal horn pain processing network was frequency dependent. (A) The network architecture and biophysics were identical to that developed by Zhang et al., 2014 (ModelDB accession number 168414).[155] IN = inhibitory interneuron; EX = excitatory interneuron; T = transmission (output) neuron. Network model output was the firing rate of the transmission neuron. (B) Model dorsal horn output at frequencies from 2 to 1000 Hz. Baseline firing rate was determined in a model with no SCS-induced input. At each frequency, the network was simulated 50 times with randomly selected afferent input. Each point corresponds to the output for one individual model simulation.

4.4.6 Frequency following properties in DC collaterals

A putative mechanism of action for conventional SCS is inhibiting noxious transmission at the spinal level through the activation of DC fibers. Recent recordings of DC fiber collaterals

suggest that action potentials are prone to failure at high frequencies in these terminal arbors.[211] To investigate action potential fidelity in these arbors, we generated 25 collateral arbors with random geometries and observed their responses to stimulus trains between 10 and 250 Hz (**Fig. 4.11**). We introduced action potentials by short current injections at a proximal node. The base collateral models were 3.0 μm in diameter upon their entry into the dorsal horn, and the fiber diameter decreased by 40% at each branch point (down to a minimum of 0.5 μm. We performed a sensitivity analysis to test how stable these responses were to various parameters. We considered collateral models to demonstrate failure if at least one of their terminals failed to fire in response to at least 90% of input spikes at a given frequency.

In the base model, greater than 90% of collateral models demonstrated faithful conduction fidelity up to 125 Hz. Branch point failure became increasingly common at higher frequencies, and increasing the input train frequency to 150, 175, 200, and 250 Hz decreased the proportion of models able to follow reliably to 84, 72, 52, and 36%, respectively (**Fig. 4.11**)

Our sensitivity analysis demonstrated that high-frequency action potential failure was strongly influenced by several factors. Decreasing fast sodium conductance by 25% greatly increased spike failure. In the reduced sodium conductance model, at 50 Hz (corresponding to conventional SCS), 68% of collateral models could faithfully follow the input train. This proportion decreased to approximately half (13/25; 52%) at 100 Hz, 36% at 150 Hz, and only 12% at the maximum frequency tested (250 Hz) (**Fig. 4.11**).

Adjusting collateral geometry also robustly modified collateral firing properties. Increasing the ratio of the child branch diameter to 80% of the parent branch diameter greatly increased the ability of collaterals to follow high-frequency stimulation, with only one collateral model demonstrating failure at 200 Hz and five models failing at 250 Hz. Relatedly, increasing nodal

length from 1 to 2 µm increased following frequency to approximately 100% at 250 Hz for all models (data not shown). Decreasing the diameter of the collateral as it entered the spinal cord from 3.0 µm to 2.0 µm increased failures percentages at the highest frequencies (≥ 150 Hz). Conversely, increasing the diameter improved following fidelity compared to the baseline model (**Fig. 4.11**).

Failing axons often fired at a subharmonic frequency of the input spike train. However, more complex patterns were also observed, such as bursting patterns produced by failing at fixed patterns within the input train (e.g., the green trace failing every third spike in **Fig. 4.12**). Interestingly, we observed that different branches within the axonal arbor could fire at different frequencies and patterns in response to the same input stimulus (**Fig. 4.12**). This was common in axons exhibiting branch point failure. In models tending to fail at branch points (particularly the model with reduced fast sodium conductance), high-frequency trains commonly functionally silenced terminal nodes (i.e., produced no spikes) after a transient burst of spikes.

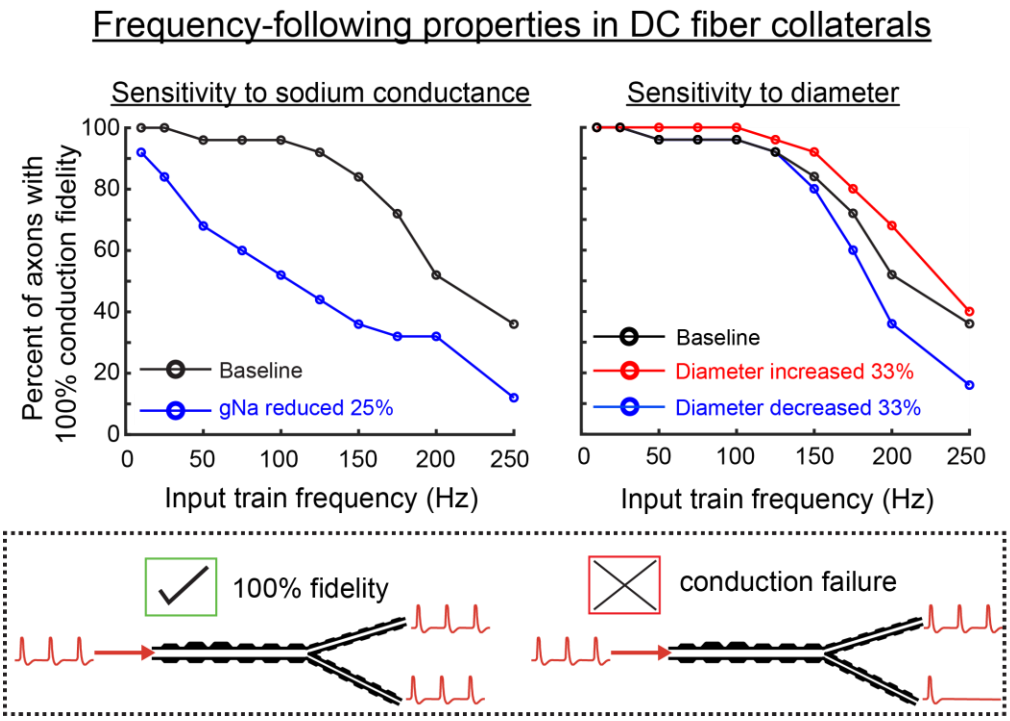

Figure 4.11: Frequency following properties within 25 DC fiber collateral models. Output data represent the percentage of collateral models that were able to respond faithfully to a given spike train frequency. A collateral was considered to respond faithfully if each of its terminal nodes of Ranvier generated a spike in response to at least 90% of input spikes. The left figure shows the results for the base model (blue) as well as the model with a 25% decrease in fast sodium conductance at all nodes of Ranvier (decrease from 3.0 to 2.25 S/cm^2). The right figure shows the results for the base model (blue) compared to a model in which the collateral diameters were either increased by 33% (red) or decreased by 33% (blue).

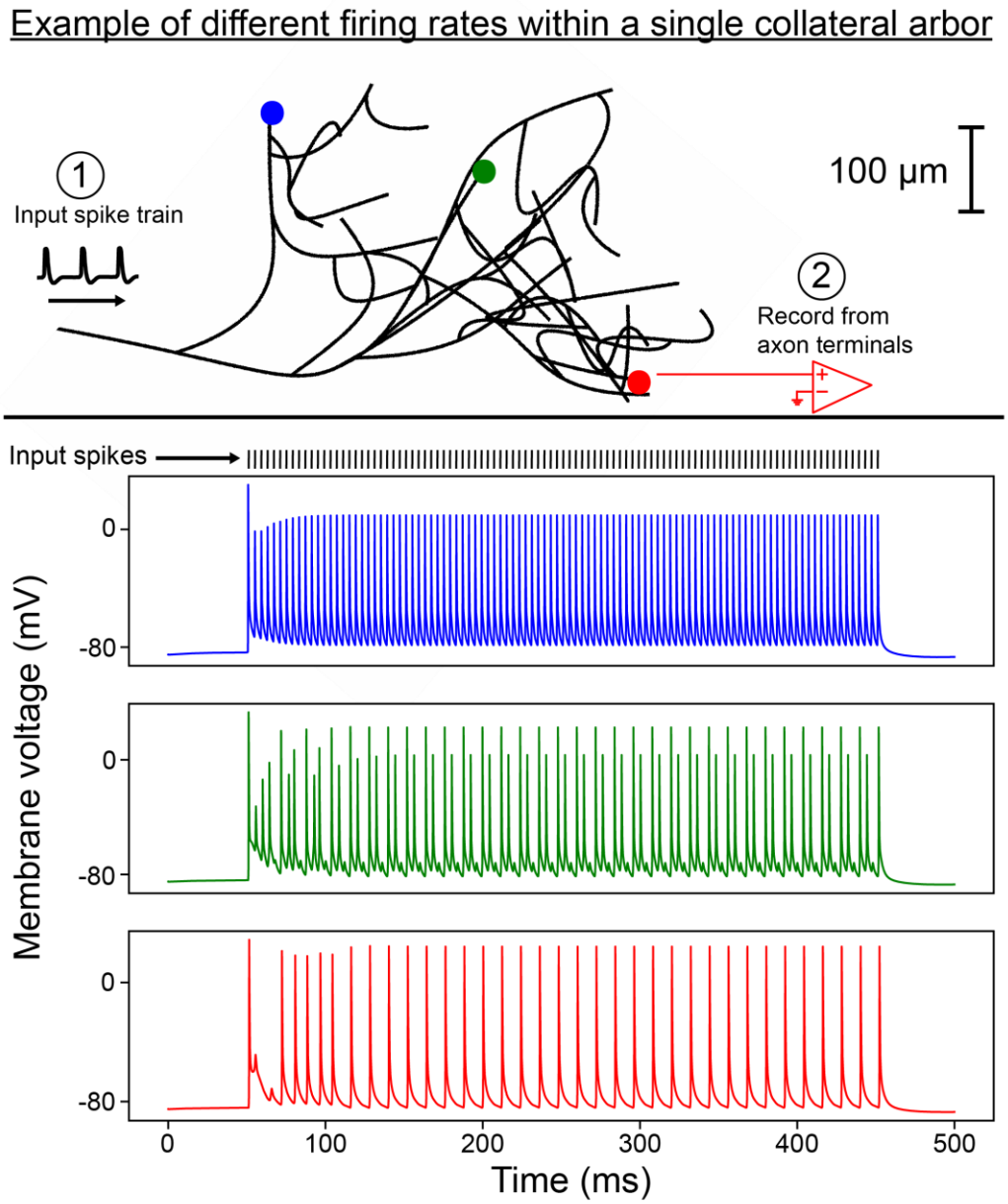

Figure 4.12: Different firing patterns within an individual collateral model. This figure shows this response of one model collateral (using baseline model parameters) to a 250 Hz input spike train. The voltage traces at the bottom correspond to the time-dependent membrane voltage of the matching-color terminal nodes marked in the illustration of the collateral at the top.

4.5 Discussion

Chronic pain is a major societal burden that is inadequately treated. SCS can provide substantial analgesia, yet clinical success rates remain suboptimal.[6] Despite decades of research and clinical experience, the neural response to SCS is not well understood. In this study, we investigated *in silico* how varying SCS frequency affects the neural response to stimulation. Specifically, we evaluated four distinct but interrelated phenomena: (1) the axonal response to juxtathreshold stimulation at various frequencies, (2) synaptic transmission between DC fibers and their postsynaptic DCN targets, (3) dorsal horn network output, and (4) conduction fidelity within the branching terminal arbors of DC fiber collaterals. Additionally, we collected paresthesia thresholds from 16 subjects with SCS implants at frequencies between 2 and 1000 Hz, which were compared with modeling results. Major results and their clinical implications are summarized below.

4.5.1 High-frequency SCS reduced DC fiber activation threshold, mirroring clinical perception thresholds

Paresthesia-free SCS systems have recently been developed, which is preferred by many patients.[233] On the other hand, some patients choose paresthesia-based stimulation, and exciting work continues to be done for paresthesia-based stimulation, notably in closed-loop systems that monitor evoked compound action potentials (ECAPs) to target consistent neural activation.[233–235] Still, the precise specific neural correlates of PT and why some SCS-induced sensations are more tolerable than others remain open questions with important implications for clinical SCS systems. Evidence from ECAPs recorded in the human spinal cord demonstrates a close relationship between the threshold to measure an ECAP and the amplitude necessary to generate perception (i.e., measurable ECAPs typically only manifest at stimulation amplitudes for which the patients

perceive the stimulation).[236] Given that the signal from an individual axon is too small to record, this observation suggests that SCS-induced paresthesia is generated by the synchronized activation of at least a small population of fibers. On the other hand, microstimulation experiments have suggested that activation of individual afferent fibers is sufficient to generate a perceivable stimulus.[237]

One plausible explanation for decreased PT at higher frequencies is temporal summation at the DCN synapse, thereby facilitating postsynaptic action potential generation at higher stimulation frequencies. However, our modeling results suggest that this is not the case. We observed that DC-to-DCN synaptic transmission was robust to both single presynaptic action potentials and low-frequency trains, with the postsynaptic neuron firing following each presynaptic spike in these scenarios (**Fig. 4.8**). Contrarily, at higher frequencies, we began observing synaptic failure, and postsynaptic firing frequency achieved a maximum plateau frequency lower than the incoming spike train frequency. Thus, another factor must explain the lower PT at higher frequencies.

Our model suggests that DC fiber activation thresholds better explain the effects of frequency on PT, based on congruence between model predictions (amplitude necessary to activated 10% of DC fibers) and our clinical data on PT versus frequency (**Fig. 4.7**). Other plausible explanations for perception are the DC fiber population firing rate or the synchrony of DC fiber responses.[200] However, our data are less consistent with these explanations. We found that high-frequency stimulation reliably produced lower PTs than low-frequency stimulation, even though high-frequency stimulation produced asynchronous responses at low amplitudes (**Fig. 4.6**; **Supp. Fig. 4.2**), which contrasted with the synchronous response produced at low frequencies. Furthermore, the average clinical ratio of PT at 1000 Hz compared to 2 Hz was ~79%, yet high-

frequency SCS produces firing rates at least an order of magnitude higher than 2 Hz, suggesting population firing rate alone does not explain differences in perception.

4.5.2 Juxtathreshold fiber responses explain decreased ECAP amplitude and increased sensation magnitude with increased firing frequency

Clinical observations have demonstrated increased sensation magnitude accompanied by decreased ECAP magnitude with increased stimulation frequency.[209] This seeming paradox is neatly resolved by the juxtathreshold frequency-specific response to SCS.

Specifically, we observed that higher frequency stimulation monotonically produced higher firing frequencies within individual DC fibers (and at a population level) (**Fig. 4.5-4.6**; **Supp. Fig. 4.2**). Recently, Graczyk and colleagues demonstrated a close correspondence between activated nerve fiber population firing rate and the magnitude of perceived sensation.[238] Thus, these greater firing rates will produce stronger sensations.

However, at the same time, as frequency increased the tendency for a DC fiber to fire one-to-one with any individual stimulation pulse decreased and the DC population firing response became increasingly unsynchronized (**Fig. 4.5-4.6**; **Supp. Fig. 4.2**). As a result, this asynchronous behavior will result in decreased ECAP magnitudes.[127]

4.5.3 High-frequency SCS produced asynchronous DCN population firing

Higher-frequency SCS producing an increased firing rate is a seemingly reasonable explanation for the observed relationship between frequency and sensation intensity. However, our DCN synaptic model and existing experimental evidence suggest that an upper frequency limit on the order of 100 Hz exists at this synapse. Therefore, higher frequency stimulation will not lead to faster supraspinal signaling beyond a certain point and could even reduce the overall number of

spikes transmitted as the synapse is depleted. Interestingly, several studies have found a positive relationship between the magnitude of sensation during electrical stimulation versus stimulation frequency, with plateaus or diminishing returns at frequencies on the order of 100 Hz.[209,238–241] Our results provide evidence that synaptic filtering at the DC-to-DCN synapse could contribute to this effect by placing an upper limit on DCN projection neuron firing rates. With this in mind, we investigated the DCN population response at these high frequencies in which the DCN neurons cannot reliably fire in response to individual presynaptic action potentials.

We found that at ≤50 Hz, the DCN population response was highly synchronized with the SCS pulses at both ST and DT (**Fig. 4.9**). As frequency increased beyond this point, the DCN population became less time-locked to the stimulation pulses. At 100 Hz, the DCN population response to individual SCS pulses could still be discerned, but firing became more irregular. However, at 500 and 1000 Hz, the DCN neurons fired in an almost completely uncorrelated manner.

These results have implications for both paresthesia sensation and pain relief during SCS. Regarding paresthesia, both our data and that from Abejón[210] demonstrate that SCS becomes increasingly unpleasant at higher frequencies. While it is known that stimulation becomes increasingly intense at higher frequencies,[209] the descriptive quality of paresthesia also frequently changes.[242] We posit that these differences in DCN synchronization contribute to differences in sensation quality, although future work will be needed to validate this hypothesis. However, once again, given the uncorrelated firing patterns at PT for 500 and 1000 Hz SCS, we conclude that DCN synchrony is unnecessary for stimulation-induced paresthesia.

4.5.4 Dorsal horn network output is sensitive to realistic variation in DC fiber firing

Conventional SCS frequency is typically on the order of 50 Hz,[5] but to-date there is little scientific understanding as to why some frequencies are more effective than others. To this end, we investigated the effects of SCS on dorsal horn pain network output using a previously developed and validated model (**Fig. 4.10**).[155]

We found that dorsal horn output was frequency-dependent, but also demonstrated variation within frequencies due to variability in fiber firing patterns. Stimulation at 100 Hz produced consistent suppression of transmission neuron activity, suggesting the potential unique clinical utility of stimulation at this frequency and robustness to variability in fiber firing patterns. In most simulations, conventional 50 Hz stimulation also effectively reduced transmission neuron firing, but responses varied due to the heterogeneous responses in different fibers. At the highest frequencies (i.e., 500 and 1000 Hz), we found that network output was highly variable when randomly sampling input from the dorsal column fibers, in which some iterations almost completely inhibited transmission neuron firing whereas other iterations produced large increases compared to baseline. Overall, these results highlight the importance of considering realistic variation in firing patterns during SCS-induced analgesia, as different simulations predicted noticeably different network output. Importantly, these results can potentially help explain the heterogeneous and variable responses observed clinically in SCS patients.

4.5.5 Spike trains fail in collateral arbors at high frequencies

Recent experimental evidence suggests that sensory afferent collateral terminal arbors in the dorsal horn are prone to spike failure during high-frequency action potential trains.[211] Several SCS paradigms are thought to produce analgesia by activating inhibitory interneurons in the dorsal horn via DC fiber collaterals (i.e., “gate control”). Hence, if action potentials fail to invade these axon terminals, SCS would not be able to achieve its intended effects. Here, we investigated the

relevance of this phenomenon during SCS by generating model DC fiber collateral arbors (n = 25 model collaterals) and quantifying their behavior during spike trains between 10 and 250 Hz.

The base collateral models demonstrated excellent conduction fidelity within the typical frequency range for conventional SCS (**Fig. 4.11**). Spike failure became increasingly common at higher frequencies, and at 200 Hz only 52% successfully propagated the spikes throughout their arbors. Sensitivity analysis demonstrated that action potential conduction reliability was strongly influenced by both morphological and electrophysiological parameters. For instance, increasing nodal length to 2.0 μm and increasing the diameters of post-bifurcation axon branches to 80% of their parent axon (compared to 60%) both produced almost perfect spike conduction. Conversely, decreasing the fast sodium conductance by 25% (i.e., 2.25 S/cm^2) greatly reduced the frequency-following ability of the collaterals, and spike failure was common in the conventional SCS frequency range (**Fig. 4.11**). Little is known about the nodal conductances within these terminal arbors, and thus this lower sodium model should be considered as potentially translatable to in vivo conditions. For instance, in their study of branched DC afferent axons, Hari et al. used a much lower nodal sodium conductance (1 S/cm^2) which they found matched their action potential recordings.[211] Decreasing fast sodium conductance within our model to 1.5 S/cm^2 produced robust branch point failure at conventional SCS frequencies (data not shown).

Another interesting consideration is that diameter clearly affected following frequency in DC collaterals, where the collaterals were able to follow higher frequencies when the collateral diameters was increased, and failure was more common when diameter decreased (**Fig. 4.11**). Thus, one must take caution when extrapolating experimental data collected from species with different axonal sizes, such as those found in rodents, as the smaller diameters may increase their tendency to fail at high frequencies.

Unfortunately, human-based experimental measurements of DC fiber collateral geometries (e.g., diameter, branching structure, myelination patterns) and electrophysiology are unavailable, thus precluding direct analysis of spiking behavior within humans at specific frequencies. Our data suggest that branch-point failure during human SCS is plausible and warrants further study. We sought to capture much of the potential variance in responses by utilizing a stochastic approach to generate collateral models and sensitivity analysis of relevant parameters. However, our model could not account for all variables that could promote spike failure. For instance, we used a structured approach in which each child branch diameter at a bifurcation was a fixed and equivalent ratio of the parent axon diameter, and nodal diameter was 70% of parent axon diameter. Animal measurements in the brain and spinal cord show that these are oversimplifications and child branches often exhibit sharply asymmetric changes in diameter and could even be larger than the parent axon.[243,244] Electron microscopy of spinal cord afferents further suggests variability in ratio of inner axonal diameter to myelinated fiber diameter (i.e., "g-ratio"), nodal diameter compared to axonal diameter, enlarged nodes (i.e., boutons), and axonal diameter tapering, all of which could affect frequency following.[243] Lastly, feline electron microscopy also reveals frequent trifurcations (or even up to four child branches) at branch points, which would likely increase branch-point failure.[226,245] Novel SCS approaches can utilize frequencies above those considered in this study.[246] Although these waveforms are typically applied at subparesthetic amplitudes, that does not necessarily imply the absence of DC fiber activation[202,212], and our results suggest that these would be prone to conduction failure.

4.5.6 Limitations

The results presented in this study are important for understanding the neural effects of SCS, yet several study limitations warrant further consideration. In our modeling, we utilized a

canonical approach based on average measurements. However, a patient-specific approach would better capture differences between participants that could account for variations in PT, CT, and DT at different frequencies. Exciting work is currently being done in the field investigating the utility of patient-specific models in understanding paresthesia thresholds as well as clinical characteristics in SCS patients.[105,247] Additionally, while the MRG model[102] is the gold standard for modeling mammalian axons, it was developed based on data from motor axons, whereas we seek to investigate the response of sensory fibers. While development of an accurate sensory fiber model will be of great value to the field,[248] several studies demonstrate that the utility of MRG model for predicting the DC response to SCS.[83,105,202] Finally, the participants in this study clinically employed various SCS programs. Thus, the subjective measurements reported in this study (i.e., PT, CT, and DT) may be affected by whether patients are accustomed to experiencing paresthesia. For instance, participants who run paresthesia-based programs may be more accustomed to stimulation-induced sensation and find it more tolerable, thus raising their CT and/or DT. Nevertheless, all patients had at least been familiar with SCS-induced paresthesia from previous experience with their SCS implants.

4.6 Conclusions

Stimulation frequency is an important but inadequately understood parameter during SCS. To investigate the effects of frequency, we modeled the firing characteristics of DC fiber axons, signal transmission at the synapse between DC fibers and their postsynaptic DCN targets, dorsal horn pain-processing network output, and the frequency following properties within the terminals of their collaterals in the dorsal horn. We found that DC fiber activation thresholds provide a close match to observed clinical paresthesia perception thresholds. Moreover, when comparing the firing properties of two closely separated axons as well as a distributed population, we observed that

higher frequency stimulation produced both higher firing rates and asynchronous activity. Given that high-frequency SCS is less tolerable than low-frequency SCS, even beyond the upper rate for reliable DCN synaptic transmission, we propose that asynchronous firing is a likely neurophysiological rationale for decreased comfort at higher SCS frequencies. Additionally, we found that frequencies between 10 and 1000 Hz could reduce painful output from the dorsal horn network, with optimal results at ~100 Hz. However, we found that pain relief was sensitive to realistic fluctuations in DC fiber firing patterns, potentially contributing to heterogeneity in clinical outcomes. Finally, our base collateral predicted high fidelity at the frequencies typically utilized in conventional SCS (i.e., <100 Hz). However, sensitivity analysis showed that following frequency was strongly affected by electrophysiological and/or geometric parameters (e.g., sodium conductance, diameter, branching ratio). These results suggest that conduction failure within these collateral terminals during conventional SCS is possible and warrants further investigation, and conduction failure is probable at the highest pulse frequencies utilized in contemporary SCS systems. These results are relevant to both understanding clinical observations, as well as future design of subparesthetic and paresthesia-based stimulation paradigms.

4.7 Supplemental Figures

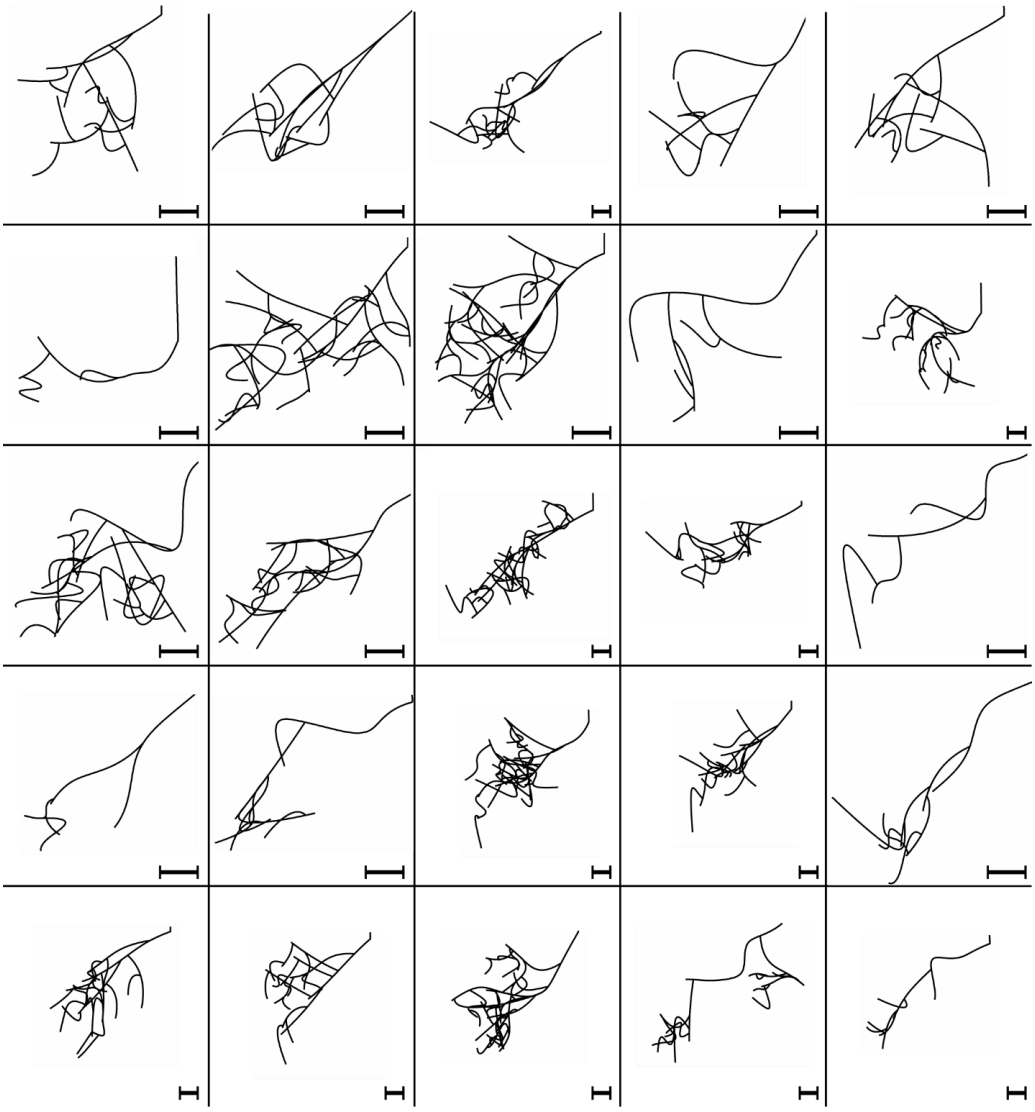

Supplementary Figure 4.1: Two-dimensional transverse cross-section of the 25 stochastically generated collateral models. The scale bar for each collateral is 100 μm.

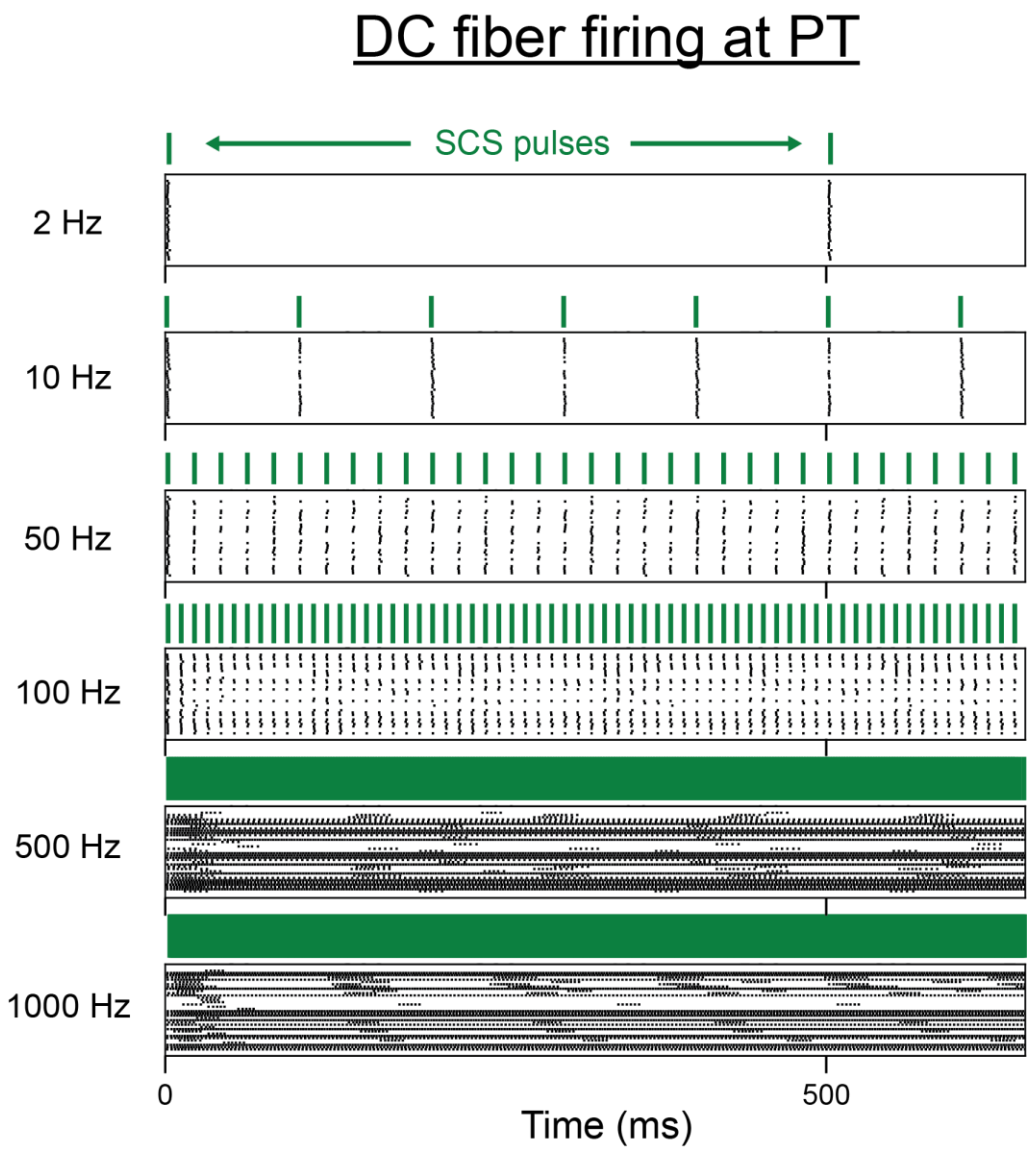

Supplementary Figure 4.2: Raster plot showing firing behavior of activated dorsal column (DC) axons at model perception threshold (PT). Note that the highest frequencies produce highly asynchronous and more rapid firing than lower frequencies. Note that at frequencies 10 – 100 Hz that the population firing rate is highly synchronized with the SCS pulses, but each individual fiber does not respond one-to-one with each pulse.

Chapter 5 - Conclusions

Chronic pain remains a major societal and public health burden and global cause of human suffering.[12] SCS is a promising therapy for patients with chronic pain that is refractory to conventional medical management. However, the clinical adoption of the various forms of modern SCS techniques have outpaced our scientific understanding of the neural effects and analgesic mechanisms of action of SCS systems. This dissertation used computational modeling to elucidate the neurophysiological effects of clinically relevant SCS.

5.1 Summary of major results

In Chapter 2, I characterized the neural recruitment patterns during conventional, burst, and 10-kHz SCS. I found that burst SCS always had the lowest activation thresholds, followed by conventional SCS, with 10-kHz SCS activation thresholds being notably higher. Importantly, I found that no SCS waveform preferentially activated local dorsal horn neurons, as their thresholds for activation were always considerably higher than for the myelinated Aβ fibers.

Additionally, I evaluated the effects of collateralization on activation thresholds for Aβ fibers. I found that including small-diameter collaterals produced considerable changes in activation thresholds, and that the magnitude of these effects depended on several factors. For instance, including several collaterals produced larger changes in threshold than a single collateral, and the spacing between collaterals also affected relative changes (with closer spacing producing larger changes in thresholds). Moreover, the effects were dependent on the ratio of diameters between the parent fiber and the collateral. Specifically, for a fixed collateral fiber diameter (2

μm), smaller diameter parent fibers tended to have smaller increases in threshold (or even decreases in threshold) compared to larger diameter parent fibers. Interestingly, the effects of collateralization were spatially-dependent on the position of the parent Aβ fibers within the dorsal columns, and collateralization tended to increase thresholds for medially-positioned fibers more than laterally-located axons. Importantly, fibers in the dorsal columns are not distributed randomly but are segregated medio-laterally based on somatotopy (and potentially fiber modality[166]). Thus, these results imply that different classes of fibers may be preferentially activated during SCS due to their location within the dorsal columns as well as collateralization properties.

Chapter 3 expands upon Chapter 2 to provide a more comprehensive analysis of the neural response to clinically relevant forms of SCS. Specifically, this project analyzed hypothesized subparesthetic mechanisms of action of novel SCS waveforms. I found that activation thresholds for C fibers were well above those for Aβ fibers, thus refuting the hypothesis that novel SCS waveforms may directly activate C fibers.[89] I also found that effects on spike timing in C fibers were negligible, thereby arguing against the hypothesis that novel SCS waveforms relieve pain through desynchronization of ongoing activity in these fibers.

When considering the effects of including stochastic ion channel properties in Aβ fiber models, I found that changes in activation threshold were negligible, but firing properties during suprathreshold SCS (i.e., the number and timing of spikes) varied. One important implication of this result is for future modeling studies of ECAPs during closed-loop SCS. ECAPs are generated by the synchronous firing of a population of axons. Previous studies have used deterministic axon models to estimate the neural recruitment from ECAP measurements.[127] However, including stochastic ion channel properties produced variation in the firing responses in otherwise identical

axons. Thus, deterministic models may underestimate the number of axons being activated, as their modeled responses are unrealistically synchronous.

Our analysis of local dorsal horn cells found that these neurons were preferentially depolarized in their axon terminals. Maximum axonal depolarizations were at least twice as large as in the somata and dendrites leading us to conclude that any subparesthetic modulation of local cells is likely to be presynaptic in nature.

Finally, in Chapter 4, I comprehensively evaluated the effects of pulse frequency (between 2 and 1000 Hz) on the neural response to SCS. Modeling results were compared with clinical perception, comfort, and discomfort thresholds for the same frequency range (with a fixed pulse width of 200 μs). I observed that at amplitudes just above activation threshold, DC axons did not respond in a one-to-one fashion with each stimulus pulse for frequencies of at least 10 Hz. Importantly, at frequencies ≥ 50 Hz, DC fibers fired asynchronously, and this effect was more pronounced as frequency increased.

Our clinical data showed that perception threshold was lower at high frequencies. One potential explanation for this observation is that high-frequency stimulation may induce synaptic temporal summation in the brainstem, thus lowering the threshold for perception. However, my dorsal column nucleus neuron model responded robustly to low-frequency synaptic inputs, firing in a one-to-one fashion up to at least 50 Hz with the maximum firing frequency plateauing at ~100 Hz. On the other hand, I found that clinical perception thresholds closely matched DC fiber activation thresholds, as higher stimulation frequencies reduced activation.

In the dorsal horn, I evaluated the effects of frequency on both the frequency-following properties in DC fiber collaterals as well as the output of the dorsal horn pain processing network. In the base model, collaterals were able to faithfully transmit spikes throughout their arbors at

frequencies up to 100 Hz, which is the upper range for conventional SCS. Above this frequency, branch point failure became increasingly common. However, frequency-following capabilities were highly sensitive to both sodium conductance and collateral morphological parameters (e.g., diameter). Very little is known about the electrophysiological and morphological parameters of these collaterals in humans, and future studies investigating these properties will be essential to interpreting these results and developing future modeling studies.

5.2 Future directions and closing remarks

The work described in this dissertation significantly contributes to our understanding of the neural effects of various clinically relevant forms of SCS. However, much remains to be learned about both the biophysical effects of SCS and best-practice implementation of SCS computer models as a scientific tool.

5.2.1 Identification of neural subpopulations underlying pain relief

In Chapter 2, I evaluated the neural recruitment profiles of conventional, burst, and 10-kHz SCS. Importantly, I found that these modalities followed the same general recruitment orders, although at different amplitudes. All waveforms activated large, myelinated Aβ fibers (rather than local interneurons and projection neurons), and activation thresholds decreased monotonically as fiber diameter increased. Thus, any activation of local dorsal horn neurons is likely to be trans-synaptic in nature.

This project systematically considered the effects of several important variables on activation thresholds in these Aβ fibers, including fiber diameter and spatial position, as well as a myriad of factors relating to collateralization properties (e.g., the number and spacing of collaterals). Future research should utilize these insights to investigate the role of activating

different specific fiber subpopulations on pain relief (and potentially paresthesia thresholds) during SCS. For instance, different physiological fiber subclasses differ in their number and spacing of collaterals,[139,166] which implies potential modality-specific activation of certain fiber populations during clinical SCS due to the effects of these variables on activation thresholds. Future work utilizing modern molecular biology techniques (e.g., optogenetics) will allow for direct testing of this notion and, more broadly, allow us to understand the specific contributions of the various neural subclasses to pain relief during SCS.

5.2.2 Understanding the neural basis of SCS-induced paresthesia

In modern SCS, there is a sharp dichotomy between systems that produce paresthesia and those that do not, and the lack of paresthesia is typically interpreted as signifying different neural effects and mechanisms of action compared to conventional SCS.[5] Despite the importance of understanding the basis of paresthesia, little is known about the specifics of its underlying neural basis. In Chapter 3, I evaluated potential mechanisms of action and biophysical effects of these subthreshold SCS modalities. However, interpretation of these results is complicated by the fact that it is currently impossible in a modeling to study to define a precise perception threshold for any individual SCS waveform, which precludes choosing a precise stimulation amplitude within the clinical subparesthetic range. Clearly, understanding the neural basis for paresthesia has clinical importance for developing subparesthetic systems as well as preclinical research implications (i.e., how to choose a subparesthetic amplitude in a rodent model that cannot report feeling the sensation).

In Chapter 4, I paired computational modeling with clinical data to understand the association between neural behavior and paresthesia thresholds. I found a close relationship between activation thresholds of DC fibers and clinical perception thresholds. Specifically, high-

frequency stimulation (i.e., stimulation at rates of at least 100 pulses per second) produced slightly reduced clinical perception thresholds compared to conventional 50-Hz SCS that closely resembled the frequency-dependent stimulation amplitudes necessary to activate 10% of fibers. Thus, these results suggest that paresthesia may involve the activation of a small subset of fibers, although future work will be necessary to determine the precise number (and the extent to which these fibers need to be synchronized, selective to a specific dermatome, etc.). The notion that activating a small subset of fibers match matches with clinical observations that ECAP thresholds are correlated with SCS perception thresholds, as well as the fact that perception thresholds can be above ECAP thresholds (implying DC fiber activation without paresthesia).[236] These results also offer a biophysical basis for determining stimulation amplitude relative to threshold in future computational modeling studies.

Future work expanding upon these insights will be invaluable to understand the neural correlates of paresthesia. Specifically, future work investigating spatial activation profiles will elucidate to what degree the activation needs to be coordinated within a specific region. For instance, it is known that DCN neurons receive surround inhibition,[249] as this could raise thresholds for paresthesia by activating fibers from adjacent dermatomes that exhibit mutual spatial inhibition.[202]

5.2.3 Development of a sensory fiber model

All projects described in this dissertation have included a model of DC fibers utilizing a form of the MRG model,[102] which is the gold standard for modeling extracellular stimulation in mammalian axons. However, this model was developed and parameterized as a motor nerve fiber, whereas the fibers of interest are sensory. Importantly, these two classes of fibers are known to be

biophysically distinct and differ in important features including strength-duration curve and their recovery cycles following excitation.[250]

In one impressive effort, Gaines and colleagues developed a sensory fiber model for extracellular stimulation, which showed impressive agreement with experimental data including conduction velocity and strength-duration properties.[248] Unfortunately, one key validation metric of these sensory models, the afterpotential, was inappropriately validated by comparison with recordings made from cell somata in the DRG.[248,251] Future development and validation of a high quality sensory nerve fiber model will be of vital importance to understanding the effects of SCS on DC fibers to the highest degree of accuracy.

5.2.4 Final conclusions

There is an imperative clinical need to better understand the neurophysiological effects of SCS to improve clinical outcomes and design systems targeted to treat an individual patient's specific pathophysiology. Computational modeling is well suited to investigate this knowledge gap, as it can directly probe the effects of stimulation at the human scale, bypassing technical concerns due to differences in the electric field distributions in preclinical models. The work presented in this dissertation greatly enhances our understanding of both the direct neural recruitment during various clinically relevant SCS waveforms as well as higher order effects such as synaptic transmission in the brainstem, suprathreshold firing rates, and frequency-following properties within the DC fiber collaterals.

An essential next step will be to utilize these insights, and the developed computational framework, to prospectively develop stimulation strategies rather than retrospectively investigate existing modalities. Initial steps have been taken in this direction using model-based approaches to facilitate clinical programming. One potential avenue of research is the use of patient-specific

modeling to target neural populations at a subjective-specific level, which is supported by successful initial trials utilizing this approach in deep brain stimulation.

Ultimately, future advancement in our scientific understanding SCS will be a collaborative endeavor that combines the expertise of engineers, basic scientists, and clinicians. The results presented in this dissertation provide a starting point to design future preclinical and human subject experiments as well as interpret clinical observations of current SCS systems.

Bibliography

1. Sdrulla, A. D., Guan, Y. & Raja, S. N. Spinal Cord Stimulation: Clinical Efficacy and Potential Mechanisms. *Pain Practice* **18**, 1048–1067 (2018).
2. Oakley, J. C. & Prager, J. P. *Spinal cord stimulation: Mechanisms of action*. *Spine* vol. 27 (Elsevier Ltd, 2002).
3. Shealy, C. N., Mortimer, J. T. & Reswick, J. B. Electrical inhibition of pain by stimulation of the dorsal columns: preliminary clinical report. *Anesth Analg* **46**, 489–491 (1967).
4. Chow, C. & Rosenquist, R. Trends in spinal cord stimulation utilization: change, growth and implications for the future. *Reg Anesth Pain Med* **48**, 296–301 (2023).
5. Caylor, J. *et al.* Spinal cord stimulation in chronic pain: evidence and theory for mechanisms of action. *Bioelectron Med* **5**, 1–41 (2019).
6. Titus, N. D., Gilbert, J. E. & Grill, W. M. Biophysics and Mechanisms of Spinal Cord Stimulation for Chronic Pain. in *Handbook of Neuroengineering* 1–45 (Springer Singapore, 2021). doi:10.1007/978-981-15-2848-4_99-2.
7. Raja, S. N. *et al.* The revised International Association for the Study of Pain definition of pain: concepts, challenges, and compromises. *Pain* **161**, 1976–1982 (2020).
8. Woolf, C. J. What is this thing called pain? *Journal of Clinical Investigation* **120**, 3742–3744 (2010).
9. Goldberg, Y. P. *et al.* Loss-of-function mutations in the Nav1.7 gene underlie congenital indifference to pain in multiple human populations. *Clin Genet* **71**, 311–319 (2007).

10. Kuner, R. & Flor, H. Structural plasticity and reorganisation in chronic pain. *Nat Rev Neurosci* **18**, 20–30 (2016).

11. Treede, R. D. *et al.* A classification of chronic pain for ICD-11. *Pain* **156**, 1003–1007 (2015).

12. Cohen, S. P., Vase, L. & Hooten, W. M. Chronic pain: an update on burden, best practices, and new advances. *The Lancet* **397**, 2082–2097 (2021).

13. Dahlhamer, J. *et al.* Prevalence of chronic pain and high-impact chronic pain among adults—United States, 2016. *Morbidity and Mortality Weekly Report* **67**, 1001–1006 (2018).

14. Gaskin, D. J. & Richard, P. The economic costs of pain in the United States. *Journal of Pain* **13**, 715–724 (2012).

15. Vellucci, R. Heterogeneity of Chronic Pain. *Clin Drug Investig* **32**, 3–10 (2012).

16. Gatchel, R. J., Peng, Y. B., Peters, M. L., Fuchs, P. N. & Turk, D. C. The Biopsychosocial Approach to Chronic Pain: Scientific Advances and Future Directions. *Psychol Bull* **133**, 581–624 (2007).

17. Turk, D. C., Wilson, H. D. & Cahana, A. Treatment of chronic non-cancer pain. *The Lancet* **377**, 2226–2235 (2011).

18. Sarzi-Puttini, P. *et al.* The Appropriate Treatment of Chronic Pain. *Clin Drug Investig* **32**, 21–33 (2012).

19. Hylands-White, N., Duarte, R. V. & Raphael, J. H. An overview of treatment approaches for chronic pain management. *Rheumatol Int* **37**, 29–42 (2017).

20. Alles, S. R. A. & Smith, P. A. Etiology and pharmacology of neuropathic pain. *Pharmacol Rev* **70**, 315–347 (2018).

21. Yekkirala, A. S., Roberson, D. P., Bean, B. P. & Woolf, C. J. Breaking barriers to novel analgesic drug development. *Nat Rev Drug Discov* **16**, 545–564 (2017).

22. Finnerup, N. B. *et al.* Pharmacotherapy for neuropathic pain in adults: A systematic review and meta-analysis. *Lancet Neurol* **14**, 162–173 (2015).

23. Chou, R. *et al.* The effectiveness and risks of long-term opioid therapy for chronic pain: A systematic review for a national institutes of health pathways to prevention workshop. *Ann Intern Med* **162**, 276–286 (2015).

24. Nuckols, T. K. *et al.* Opioid Prescribing: A Systematic Review and Critical Appraisal of Guidelines for Chronic Pain. *Ann Intern Med* **160**, 38–47 (2014).

25. Volkow, N. D. & McLellan, A. T. Opioid Abuse in Chronic Pain — Misconceptions and Mitigation Strategies. *New England Journal of Medicine* **374**, 1253–1263 (2016).

26. Breivik, H., Collett, B., Ventafridda, V., Cohen, R. & Gallacher, D. Survey of chronic pain in Europe: Prevalence, impact on daily life, and treatment. *European Journal of Pain* **10**, 287 (2006).

27. Ussai, S. *et al.* Impact of potential inappropriate NSAIDs use in chronic pain. *Drug Des Devel Ther* **9**, 2073–2077 (2015).

28. Edwards, R. R. *et al.* Optimizing and Accelerating the Development of Precision Pain Treatments for Chronic Pain: IMMPACT Review and Recommendations. *Journal of Pain* **24**, 204–225 (2023).

29. Aronoff, Gerald. M. Chronic pain and the disability epidemic. *Clin J Pain* **7**, 330–338 (1991).

30. Tunks, E. R., Crook, J. & Weir, R. Epidemiology of Chronic Pain With Psychological Comorbidity: Prevalence, Risk, Course, and Prognosis. *The Canadian Journal of Psychiatry* **53**, 224–234 (2008).

31. Woolf, C. J. & Ma, Q. Nociceptors-Noxious Stimulus Detectors. *Neuron* **55**, 353–364 (2007).

32. Abraira, V. E. & Ginty, D. D. The sensory neurons of touch. *Neuron* **79**, 618–639 (2013).

33. Djouhri, L. & Lawson, S. N. Aβ-fiber nociceptive primary afferent neurons: A review of incidence and properties in relation to other afferent A-fiber neurons in mammals. in *Brain Research Reviews* vol. 46 131–145 (2004).

34. Basbaum, A. I., Bautista, D. M., Scherrer, G. & Julius, D. Cellular and Molecular Mechanisms of Pain. *Cell* **139**, 267–284 (2009).

35. Todd, A. J. Neuronal circuitry for pain processing in the dorsal horn. *Nat Rev Neurosci* **11**, 823–836 (2010).

36. Rexed, B. The cytoarchitectonic organization of the spinal cord in the cat. *Journal of Comparative Neurology* **96**, 415–495 (1952).

37. Todd, A. J. Identifying functional populations among the interneurons in laminae I-III of the spinal dorsal horn. *Mol Pain* **13**, (2017).

38. Peirs, C., Dallel, R. & Todd, A. J. Recent advances in our understanding of the organization of dorsal horn neuron populations and their contribution to cutaneous mechanical allodynia. *J Neural Transm* **127**, 505–525 (2020).

39. Yasaka, T., Tiong, S. Y. X., Hughes, D. I., Riddell, J. S. & Todd, A. J. Populations of inhibitory and excitatory interneurons in lamina II of the adult rat spinal dorsal horn

revealed by a combined electrophysiological and anatomical approach. *Pain* **151**, 475–488 (2010).

40. Prescott, S. A. & De Koninck, Y. Four cell types with distinctive membrane properties and morphologies in lamina I of the spinal dorsal horn of the adult rat. *Journal of Physiology* **539**, 817–836 (2002).

41. Häring, M. *et al.* Neuronal atlas of the dorsal horn defines its architecture and links sensory input to transcriptional cell types. *Nat Neurosci* **21**, 869–880 (2018).

42. Wercberger, R. & Basbaum, A. I. Spinal cord projection neurons: a superficial, and also deep analysis. *Curr Opin Physiol* **11**, 109–115 (2019).

43. Willis, W. D., Zhang, X., Honda, C. N. & Giesler, G. J. Projections from the marginal zone and deep dorsal horn to the ventrobasal nuclei of the primate thalamus. *Pain* **92**, 267–276 (2001).

44. Coull, J. A. M. *et al.* Trans-synaptic shift in anion gradient in spinal lamina I neurons as a mechanism of neuropathic pain. *Nature* **424**, 935–938 (2003).

45. Prescott, S. A. Synaptic inhibition and disinhibition in the spinal dorsal horn. *Prog Mol Biol Transl Sci* **131**, 359–383 (2015).

46. Bardoni, R. *et al.* Pre- and postsynaptic inhibitory control in the spinal cord dorsal horn. *Ann N Y Acad Sci* **1279**, 90–96 (2013).

47. Van Den Pol, A. N., Obrietan, K. & Chen, G. Excitatory Actions of GABA after Neuronal Trauma. *The Journal of Neuroscience* **16**, 4283–4292 (1996).

48. Lempka, S. F. & Patil, P. G. Innovations in spinal cord stimulation for pain. *Curr Opin Biomed Eng* **8**, 51–60 (2018).

49. Melzack, R. & Wall, P. Pain Mechanisms: A New Theory: A gate control system modulates sensory input from the skin before it evokes pain perception and response. *Science* **150**, 971–979 (1965).

50. Millan, M. J. Descending control of pain. *Prog Neurobiol* **66**, 355–474 (2002).

51. Mendell, L. M. Constructing and deconstructing the gate theory of pain. *Pain* **155**, 210–216 (2014).

52. Zhang, T. C. *et al.* Spinal sensory projection neuron responses to spinal cord stimulation are mediated by circuits beyond gate control. *J Neurophysiol* **114**, 284–300 (2015).

53. Duan, B. *et al.* Identification of spinal circuits transmitting and gating mechanical pain. *Cell* **159**, 1417–1432 (2014).

54. Sdrulla, A. D. *et al.* Electrical stimulation of low-threshold afferent fibers induces a prolonged synaptic depression in lamina II dorsal horn neurons to high-threshold afferent inputs in mice. *Pain* **156**, 1008–1017 (2015).

55. Guan, Y. *et al.* Spinal cord stimulation-induced analgesia: electrical stimulation of dorsal column and dorsal roots attenuates dorsal horn neuronal excitability in neuropathic rats. *Anesthesiology* **113**, 1392–1405 (2010).

56. Moffitt, M. A., Lee, D. C. & Bradley, K. Spinal Cord Stimulation: Engineering Approaches to Clinical and Physiological Challenges. in *Implantable Neural Prostheses 1: devices and applications* 155–194 (2009). doi:10.1007/978-0-387-77261-5_5.

57. Nashold, B., Somjen, G. & Friedman, H. Paresthesias and EEG Potentials Evoked by Stimulation of the Dorsal Funiculi in Man. *Exp Neurol* **36**, 273–287 (1972).

58. North, R. B., Ewend, M. G., Lawton, M. T. & Piantadosi, S. Spinal cord stimulation for chronic, intractable pain: Superiority of ‘multi-channel’ devices. *Pain* **44**, 119–130 (1991).

59. Barchini, J. *et al.* Spinal segmental and supraspinal mechanisms underlying the pain-relieving effects of spinal cord stimulation: An experimental study in a rat model of neuropathy. *Neuroscience* **215**, 196–208 (2012).

60. Baliki, M., Jabbur, S. J. & Saadé, N. E. Attenuation of neuropathic pain by segmental and supraspinal activation of the dorsal column system in awake rats. *Neuroscience* **112**, 541–553 (2002).

61. Saadé, N. E., Tabet, M. S., Banna I, N. R., Atweh, S. F. & Jabbur, S. J. Inhibition of nociceptive evoked activity in spinal neurons through a dorsal column-brainstem-spinal loop. *Brain Res* **339**, 115–118 (1985).

62. Saadé, N. E., Atweh, S. F., Tabet, M. S. & Jabbur, S. J. Inhibition of nociceptive withdrawal flexion reflexes through a dorsal column-brainstem-spinal loop. *Brain Res* **335**, 306–308 (1985).

63. North, R. B. *et al.* Spinal Cord Stimulator Adjustment to Maximize Implanted Battery Longevity: A Randomized, Controlled Trial Using a Computerized, Patient-Interactive Programmer. *Neuromodulation* **7**, 13–25 (2004).

64. North, R. B., Kidd, D. H., Zahurak, M., James, C. S. & Long, D. M. Spinal cord stimulation for chronic, intractable pain: experience over two decades. *Neurosurgery* **32**, 384–395 (1993).

65. Oakley, J. C. Spinal cord stimulation in axial low back pain: Solving the dilemma. *Pain Medicine* **7**, S58–S63 (2006).

66. Barolat, G., Zeme, S. & Ketcik, B. Mapping of sensory responses to epidural stimulation of the intraspinal neural structures in man. *J. Neurosurg* **78**, 233–239 (1993).

67. Heijmans, L. & Joosten, E. A. Mechanisms and mode of action of spinal cord stimulation in chronic neuropathic pain. *Postgrad Med* **132**, 17–21 (2020).

68. Ross, E. & Abejõn, D. Improving patient experience with spinal cord stimulation: Implications of position-related changes in neurostimulation. *Neuromodulation* **17**, 36–41 (2014).

69. Fishman, M. *et al.* Twelve-Month results from multicenter, open-label, randomized controlled clinical trial comparing differential target multiplexed spinal cord stimulation and traditional spinal cord stimulation in subjects with chronic intractable back pain and leg pain. *Pain Practice* **21**, 912–923 (2021).

70. Jones, M. G. *et al.* Neuromodulation using ultra low frequency current waveform reversibly blocks axonal conduction and chronic pain. *Sci Transl Med* **13**, eabg9890 (2021).

71. De Ridder, D., Vanneste, S., Plazier, M., Van Der Loo, E. & Menovsky, T. Burst spinal cord stimulation: Toward paresthesia-free pain suppression. *Neurosurgery* **66**, 986–990 (2010).

72. Kapural, L. *et al.* Novel 10-kHz High-frequency Therapy (HF10 Therapy) Is Superior to Traditional Low-frequency Spinal Cord Stimulation for the Treatment of Chronic Back and Leg Pain. *Anesthesiology* **123**, 851–860 (2015).

73. Mekhail, N. *et al.* Long-term safety and efficacy of closed-loop spinal cord stimulation to treat chronic back and leg pain (Evoke): a double-blind , randomised , controlled trial. **4422**, 1–12 (2019).

74. North, J. M., Hong, K. S. J. & Cho, P. Y. Clinical Outcomes of 1 kHz Subperception Spinal Cord Stimulation in Implanted Patients With Failed Paresthesia-Based Stimulation:

Results of a Prospective Randomized Controlled Trial. *Neuromodulation* **19**, 731–737 (2016).

75. Schechter, R. *et al.* Conventional and kilohertz-frequency spinal cord stimulation produces intensity- and frequency-dependent inhibition of mechanical hypersensitivity in a rat model of neuropathic pain. *Anesthesiology* **119**, 422–432 (2013).

76. Li, S., Farber, J. P., Linderoth, B., Chen, J. & Foreman, R. D. Spinal Cord Stimulation With "Conventional Clinical" and Higher Frequencies on Activity and Responses of Spinal Neurons to Noxious Stimuli: An Animal Study. *Neuromodulation* **21**, 440–447 (2018).

77. Kriek, N., Groeneweg, J. G., Stronks, D. L., de Ridder, D. & Huygen, F. J. P. M. Preferred frequencies and waveforms for spinal cord stimulation in patients with complex regional pain syndrome: A multicentre, double-blind, randomized and placebo-controlled crossover trial. *European Journal of Pain* **21**, 507–519 (2017).

78. Thomson, S. J. *et al.* Effects of Rate on Analgesia in Kilohertz Frequency Spinal Cord Stimulation: Results of the PROCO Randomized Controlled Trial. *Neuromodulation* **21**, 67–76 (2018).

79. Linderoth, B. & Foreman, R. D. Conventional and Novel Spinal Stimulation Algorithms: Hypothetical Mechanisms of Action and Comments on Outcomes. *Neuromodulation* **20**, 525–533 (2017).

80. Chakravarthy, K., Richter, H., Christo, P. J., Williams, K. & Guan, Y. Spinal Cord Stimulation for Treating Chronic Pain: Reviewing Preclinical and Clinical Data on Paresthesia-Free High-Frequency Therapy. *Neuromodulation* **21**, 10–18 (2018).

81. De Carolis, G. *et al.* Paresthesia-independence: An assessment of technical factors related to 10 kHz paresthesia-free spinal cord stimulation. *Pain Physician* **20**, 331–341 (2017).

82. Crosby, N. D., Janik, J. J. & Grill, W. M. Modulation of activity and conduction in single dorsal column axons by kilohertz-frequency spinal cord stimulation. *J Neurophysiol* **117**, 136–147 (2017).

83. Lempka, S. F., McIntyre, C. C., Kilgore, K. L. & Machado, A. G. Computational Analysis of Kilohertz Frequency Spinal Cord Stimulation for Chronic Pain Management. *Anesthesiology* **122**, 1362–1376 (2015).

84. Lee, K. Y. *et al.* Low-intensity, Kilohertz Frequency Spinal Cord Stimulation Differently Affects Excitatory and Inhibitory Neurons in the Rodent Superficial Dorsal Horn. *Neuroscience* **428**, 132–139 (2020).

85. Finch, P., Price, L. & Drummond, P. High-Frequency (10 kHz) Electrical Stimulation of Peripheral Nerves for Treating Chronic Pain: A Double-Blind Trial of Presence vs Absence of Stimulation. *Neuromodulation* **22**, 529–536 (2019).

86. Deer, T. *et al.* Success Using Neuromodulation With BURST (SUNBURST) Study: Results From a Prospective, Randomized Controlled Trial Using a Novel Burst Waveform. *Neuromodulation* **21**, 56–66 (2018).

87. Crosby, N. D. *et al.* Burst and tonic spinal cord stimulation differentially activate gabaergic mechanisms to attenuate pain in a rat model of cervical radiculopathy. *IEEE Trans Biomed Eng* **62**, 1604–1613 (2015).

88. Meuwissen, K. P. V., de Vries, L. E., Gu, J. W., Zhang, T. C. & Joosten, E. A. J. Burst and Tonic Spinal Cord Stimulation Both Activate Spinal GABAergic Mechanisms to

Attenuate Pain in a Rat Model of Chronic Neuropathic Pain. *Pain Practice* **20**, 75–87 (2020).

89. Ahmed, S., Yearwood, T., De Ridder, D. & Vanneste, S. Burst and high frequency stimulation: underlying mechanism of action. *Expert Rev Med Devices* **15**, 61–70 (2018).

90. Yearwood, T. *et al.* Comparison of Neural Activity in Chronic Pain Patients During Tonic and Burst Spinal Cord Stimulation Using Fluorodeoxyglucose Positron Emission Tomography. *Neuromodulation* **2019**, (2019).

91. Meuwissen, K. P. V. *et al.* Active Recharge Burst and Tonic Spinal Cord Stimulation Engage Different Supraspinal Mechanisms: A Functional Magnetic Resonance Imaging Study in Peripherally Injured Chronic Neuropathic Rats. *Pain Practice* **20**, 510–521 (2020).

92. Quindlen-Hotek, J. C. *et al.* Changes in Neuronal Activity in the Anterior Cingulate Cortex and Primary Somatosensory Cortex With Nonlinear Burst and Tonic Spinal Cord Stimulation. *Neuromodulation* **23**, 594–604 (2020).

93. Saber, M. *et al.* Tonic, Burst, and Burst-Cycle Spinal Cord Stimulation Lead to Differential Brain Activation Patterns as Detected by Functional Magnetic Resonance Imaging. *Neuromodulation* **25**, 53–63 (2022).

94. De Ridder, D. & Vanneste, S. Burst and tonic spinal cord stimulation: Different and common brain mechanisms. *Neuromodulation* **19**, 47–59 (2016).

95. Sankarasubramanian, V. *et al.* Objective Measures to Characterize the Physiological Effects of Spinal Cord Stimulation in Neuropathic Pain: A Literature Review. *Neuromodulation* **22**, 127–148 (2019).

96. Linderoth, B. & Foreman, R. D. Mechanisms of spinal cord stimulation in painful syndromes: Role of animal models. *Pain Medicine* **7**, 14–26 (2006).

97. Formento, E. *et al.* Electrical spinal cord stimulation must preserve proprioception to enable locomotion in humans with spinal cord injury. *Nat Neurosci* **21**, 1728–1741 (2018).

98. Holsheimer, J. Computer modelling of spinal cord stimulation and its contribution to therapeutic efficacy. *Spinal Cord* **36**, 531–540 (1998).

99. Liang, L. *et al.* A systematic review of computational models for the design of spinal cord stimulation therapies: from neural circuits to patient-specific simulations. *J Physiol* (2022) doi:10.1113/JP282884#support-information-section.

100. Khadka, N. *et al.* Realistic anatomically detailed open-source spinal cord stimulation (RADO-SCS) model. *J Neural Eng* **17**, (2020).

101. Gunalan, K., Howell, B. & McIntyre, C. C. Quantifying axonal responses in patient-specific models of subthalamic deep brain stimulation. *Neuroimage* **172**, 263–277 (2018).

102. McIntyre, C. C., Richardson, A. G. & Grill, W. M. Modeling the excitability of mammalian nerve fibers: Influence of afterpotentials on the recovery cycle. *J Neurophysiol* **87**, 995–1006 (2002).

103. Zander, H. J., Graham, R. D., Anaya, C. J. & Lempka, S. F. Anatomical and technical factors affecting the neural response to epidural spinal cord stimulation. *J Neural Eng* **17**, (2020).

104. Plonsey, R. & Heppner, D. B. Considerations of quasi-stationarity in electrophysiological systems. *Bull Math Biophys* **29**, 657–661 (1967).

105. Lempka, S. F. *et al.* Patient-Specific Analysis of Neural Activation During Spinal Cord Stimulation for Pain. *Neuromodulation* **23**, 572–581 (2020).

106. Hodgkin, A. L. & Huxley, A. F. A quantitative description of membrane current and its application to conduction and excitation in nerve. *J Physiol* **117**, 500–544 (1952).

107. Sterratt, D., Graham, B., Gillies, A. & Willshaw, D. *Principles of computational modelling in neuroscience*. *Principles of Computational Modelling in Neuroscience* (2011). doi:10.1017/CBO9780511975899.

108. Hines, M. L. & Carnevale, N. T. The NEURON Simulation Environment. *Neural Comput* **9**, 1179–1209 (1997).

109. Veizi, E. *et al.* Spinal Cord Stimulation (SCS) with Anatomically Guided (3D) Neural Targeting Shows Superior Chronic Axial Low Back Pain Relief Compared to Traditional SCS-LUMINA Study. *Pain Medicine* **18**, 1534–1548 (2017).

110. Rogers, E. R., Zander, H. J. & Lempka, S. F. Neural Recruitment During Conventional, Burst, and 10-kHz Spinal Cord Stimulation for Pain. *Journal of Pain* **23**, 434–449 (2022).

111. Kumar, K. & Rizvi, S. Cost-effectiveness of spinal cord stimulation therapy in management of chronic pain. *Pain Medicine* **14**, 1631–1649 (2013).

112. Taylor, R. S., Desai, M. J., Rigoard, P. & Taylor, R. J. Predictors of pain relief following spinal cord stimulation in chronic back and leg pain and failed back surgery syndrome: A systematic review and meta-regression analysis. *Pain Practice* **14**, 489–505 (2013).

113. Zhang, T. C., Janik, J. J. & Grill, W. M. Mechanisms and models of spinal cord stimulation for the treatment of neuropathic pain. *Brain Res* **1569**, 19–31 (2014).

114. VanBuyten, J. P., Al-Kaisy, A., Smet, I., Palmisani, S. & Smith, T. High-frequency spinal cord stimulation for the treatment of chronic back pain patients: Results of a prospective multicenter European clinical study. *Neuromodulation* **16**, 59–65 (2013).

115. Linderoth, B. & Foreman, R. D. Conventional and Novel Spinal Stimulation Algorithms: Hypothetical Mechanisms of Action and Comments on Outcomes. *Neuromodulation* **20**, 525–533 (2017).

116. Jensen, M. P. & Brownstone, R. M. Mechanisms of spinal cord stimulation for the treatment of pain: Still in the dark after 50 years. *European Journal of Pain* **23**, 652–659 (2019).

117. Struijk, J. J., Holsheimer, J. & Boom, H. B. K. Excitation of dorsal root fibers in spinal cord stimulation: A theoretical study. *IEEE Trans Biomed Eng* **40**, 632–639 (1993).

118. Struijk, J. J., Holsheimer, J., van der Heide, G. G. & Boom, H. B. K. Recruitment of dorsal column fibers in spinal cord stimulation: Influence of collateral branching. *IEEE Trans Biomed Eng* **39**, 903–912 (1992).

119. Holsheimer, J. Which neuronal elements are activated directly by spinal cord stimulation. *Neuromodulation* **5**, 25–31 (2002).

120. Coburn, B. A theoretical study of epidural electrical stimulation of the spinal cord—part II: Effects on long myelinated fibers. *IEEE Trans Biomed Eng* **11**, 978–986 (1985).

121. Coburn, B. & Sin, W. K. A theoretical study of epidural electrical stimulation of the spinal cord—part I: Finite element analysis of stimulus fields. *IEEE Trans Biomed Eng* **11**, 971–977 (1985).

122. Khadka, N. *et al.* Realistic anatomically detailed open-source spinal cord stimulation (RADO-SCS) model. *J Neural Eng* **17**, 026033 (2020).

123. Capogrosso, M. & Lempka, S. F. A computational outlook on neurostimulation. *Bioelectron Med* **6**, 1–7 (2020).

124. Chakravarthy, K., Malayil, R., Kirketeig, T. & Deer, T. Burst spinal cord stimulation: A systematic review and pooled analysis of real-world evidence and outcomes data. *Pain Medicine* **20**, S47–S57 (2019).

125. Lempka, S. F., Howell, B., Gunalan, K., Machado, A. G. & McIntyre, C. C. Characterization of the stimulus waveforms generated by implantable pulse generators for deep brain stimulation. *Clinical Neurophysiology* **129**, 731–742 (2018).

126. Hines, M. L. & Carnevale, N. T. NEURON: A tool for neuroscientists. *Neuroscientist* **7**, 123–135 (2001).

127. Anaya, C. J., Zander, H. J., Graham, R. D., Sankarasubramanian, V. & Lempka, S. F. Evoked Potentials Recorded From the Spinal Cord During Neurostimulation for Pain: A Computational Modeling Study. *Neuromodulation* **23**, 64–73 (2020).

128. Geddes, L. A. & Baker, L. E. The specific resistance of biological material-A compendium of data for the biomedical engineer and physiologist. *Med Biol Eng* **5**, 271–293 (1967).

129. Grill, W. M. & Thomas Mortimer, J. Electrical properties of implant encapsulation tissue. *Ann Biomed Eng* **22**, 23–33 (1994).

130. Gabriel, S., Lau, R. W. & Gabriel, C. The dielectric properties of biological tissues: II. Measurements in the frequency range 10 Hz to 20 GHz. *Phys Med Biol* **41**, 2251–2269 (1996).

131. Howell, B., Lad, S. P. & Grill, W. M. Evaluation of intradural stimulation efficiency and selectivity in a computational model of spinal cord stimulation. *PLoS One* **10**, (2015).

132. Howell, B. & McIntyre, C. C. Analyzing the tradeoff between electrical complexity and accuracy in patient-specific computational models of deep brain stimulation. *J Neural Eng* **13**, 036023 (2016).

133. Kameyama, T., Hashizume, Y. & Sobue, G. Morphologic features of the normal human cadaveric spinal cord. *Spine (Phila Pa 1976)* **21**, 1285–1290 (1996).

134. Bozkurt, M. *et al.* Microsurgical anatomy of the dorsal thoracic rootlets and dorsal root entry zones. *Acta Neurochir (Wien)* **154**, 1235–1239 (2012).

135. Holsheimer, J., Den Boer, J. A., Struijk, J. J. & Rozeboom, A. R. MR assessment of the normal position of the spinal cord in the spinal canal. *American Journal of Neuroradiology* **15**, 951–959 (1994).

136. Lee, D., Hershey, B., Bradley, K. & Yearwood, T. Predicted effects of pulse width programming in spinal cord stimulation: A mathematical modeling study. *Med Biol Eng Comput* **49**, 765–774 (2011).

137. Tschirhart, C. E., Finkelstein, J. A. & Whyne, C. M. Biomechanics of vertebral level, geometry, and transcortical tumors in the metastatic spine. *J Biomech* **40**, 46–54 (2007).

138. Peterson, E. J., Izad, O. & Tyler, D. J. Predicting myelinated axon activation using spatial characteristics of the extracellular field. *J Neural Eng* **8**, (2011).

139. Brown, A. G. *Organization in the Spinal Cord: The Anatomy and Physiology of Identified Neurones*. (Springer-Verlag, 1981).

140. Wesselink, W. A., Holsheimer, J. & Boom, H. B. K. A model of the electrical behaviour of myelinated sensory nerve fibres based on human data. *Med Biol Eng Comput* **37**, 228–235 (1999).

141. Danner, S. M., Hofstoetter, U. S., Ladenbauer, J., Rattay, F. & Minassian, K. Can the human lumbar posterior columns be stimulated by transcutaneous spinal cord stimulation? A modeling study. *Artif Organs* **35**, 257–262 (2011).

142. Brown, A. G., Fyffe, R. E. W. & Noble, R. Projections from Pacinian corpuscles and rapidly adapting mechanoreceptors of glabrous skin to the cat's spinal cord. *J Physiology* **307**, 385–400 (1980).

143. Brown, A. G., Rose, P. K. & Snow, P. J. Morphology and Organization of Axon Collaterals from Afferent Fibres of Slowly Adapting Type I Units in Cat Spinal Cord. *J Physiology* **277**, 15–27 (1978).

144. Brown, A. G., Fyffe, R. E. W., Rose, P. K. & Snow, P. J. Morphology and Organization from Axons of Type II Slowly Adapting Units in the Cat. *J Physiology* **316**, 469–480 (1981).

145. Radman, T., Ramos, R. L., Brumberg, J. C. & Bikson, M. Role of cortical cell type and morphology in sub- and suprathreshold uniform electric field stimulation. *Brain Stimul* **2**, 215–228 (2009).

146. Ranck Jr, J. B. Which elements are excited in electrical stimulation of mammalian central nervous system: A review. *Brain Res* **98**, 417–440 (1975).

147. Luz, L. L., Szucs, P., Pinho, R. & Safronov, B. V. Monosynaptic excitatory inputs to spinal lamina I anterolateral-tract-projecting neurons from neighbouring lamina I neurons. *Journal of Physiology* **588**, 4489–4505 (2010).

148. Ascoli, G. A., Donohue, D. E. & Halavi, M. NeuroMorpho.Org: A central resource for neuronal morphologies. *Journal of Neuroscience* **27**, 9247–9251 (2007).

149. Aberra, A. S., Peterchev, A. V. & Grill, W. M. Biophysically realistic neuron models for simulation of cortical stimulation. *J Neural Eng* **15**, (2018).

150. Hursh, J. B. Conduction velocity and diameter of nerve fibers. *American Journal of Physiology* **127**, 131–139 (1939).

151. Hess, A. & Young, J. Z. Correlation of internodal length and fibre diameter in the central nervous system. *Nature* **164**, 490–491 (1949).

152. Chomiak, T. & Hu, B. What is the optimal value of the g-ratio for myelinated fibers in the rat CNS? A theoretical approach. *PLoS One* **4**, e7754 (2009).

153. Eyal, G., Mansvelder, H. D., de Kock, C. P. J. & Segev, I. Dendrites impact the encoding capabilities of the axon. *Journal of Neuroscience* **34**, 8063–8071 (2014).

154. Melnick, I. V., Santos, S. F. A., Szokol, K., Szûcs, P. & Safronov, B. V. Ionic Basis of Tonic Firing in Spinal Substantia Gelatinosa Neurons of Rat. *J Neurophysiol* **91**, 646–655 (2004).

155. Zhang, T. C., Janik, J. J. & Grill, W. M. Modeling effects of spinal cord stimulation on wide-dynamic range dorsal horn neurons: Influence of stimulation frequency and GABAergic inhibition. *J Neurophysiol* **112**, 552–567 (2014).

156. Gentet, L. J., Stuart, G. J. & Clements, J. D. Direct measurement of specific membrane capacitance in neurons. *Biophys J* **79**, 314–320 (2000).

157. Wolff, M., Vogel, W. & Safronov, B. V. Uneven distribution of K+ channels in soma, axon and dendrites of rat spinal neurones: Functional role of the soma in generation of action potentials. *Journal of Physiology* **509**, 767–776 (1998).

158. Ruscheweyh, R. & Sandkühler, J. Lamina-specific membrane and discharge properties of rat spinal dorsal horn neurones in vitro. *Journal of Physiology* **541**, 231–244 (2002).

159. McIntyre, C. C. & Grill, W. M. Selective microstimulation of central nervous system neurons. *Ann Biomed Eng* **28**, 219–233 (2000).

160. He, J., Barolat, G., Holsheimer, J. & Struijk, J. J. Perception threshold and electrode position for spinal cord stimulation. *Pain* **59**, 55–63 (1994).

161. Song, Z., Viisanen, H., Meyerson, B. A., Pertovaara, A. & Linderoth, B. Efficacy of kilohertz-frequency and conventional spinal cord stimulation in rat models of different pain conditions. *Neuromodulation* **17**, 226–234 (2014).

162. Tang, R. *et al.* Comparison of burst and tonic spinal cord stimulation on spinal neural processing in an animal model. *Neuromodulation* **17**, 143–151 (2014).

163. Macefield, G., Gandevia, S. C. & Burke, D. Perceptual responses to microstimulation of single afferents innervating joints, muscles and skin of the human hand. *Journal of Physiology* **429**, 113–129 (1990).

164. Reddy, C. G. *et al.* Ovine model of neuropathic pain for assessing mechanisms of spinal cord stimulation therapy via dorsal horn recordings, von Frey filaments, and gait analysis. *J Pain Res* **11**, 1147–1162 (2018).

165. Levy, R. M. Anatomic considerations for spinal cord stimulation. *Neuromodulation* **17**, 2–11 (2014).

166. Niu, J. *et al.* Modality-based organization of ascending somatosensory axons in the direct dorsal column pathway. *Journal of Neuroscience* **33**, 17691–17709 (2013).

167. Rattay, F. Analysis of models for external stimulation of axons. *IEEE Trans Biomed Eng* **10**, 974–977 (1986).

168. Nagarajan, S. S., Durand, D. M. & Warman, E. N. Effects of induced electric fields on finite neuronal structures: A simulation study. *IEEE Trans Biomed Eng* **40**, 1175–1188 (1993).

169. Basser, P. J. & Roth, B. J. New currents in electrical stimulation of excitable tissues. *Annu Rev Biomed Eng* **2**, 377–397 (2000).

170. Bower, K. L. & McIntyre, C. C. Deep brain stimulation of terminating axons. *Brain Stimul* **13**, 1863–1870 (2020).

171. Holsheimer, J., Struijk, J. J. & Tas, N. R. Effects of electrode geometry and combination on nerve fibre selectivity in spinal cord stimulation. *Med Biol Eng Comput* **33**, 676–682 (1995).

172. Hosobuchi, Y., Adams, J. E. & Weinstein, P. R. Preliminary percutaneous dorsal column stimulation prior to permanent implantation. *J Neurosurg* **37**, 242–245 (1972).

173. Mekhail, N. *et al.* Long-term safety and efficacy of closed-loop spinal cord stimulation to treat chronic back and leg pain (Evoke): A double-blind, randomised, controlled trial. *Lancet Neurol* **19**, 123–134 (2020).

174. Miller, J. P. *et al.* Parameters of Spinal Cord Stimulation and Their Role in Electrical Charge Delivery: A Review. *Neuromodulation* **19**, 373–384 (2016).

175. Reato, D., Rahman, A., Bikson, M. & Parra, L. C. Effects of weak transcranial alternating current stimulation on brain activity-a review of known mechanisms from animal studies. *Front Hum Neurosci* **7**, 687 (2013).

176. Jackson, M. P. *et al.* Animal models of transcranial direct current stimulation: Methods and mechanisms. *Clinical Neurophysiology* **127**, 3425–3454 (2016).

177. Chakraborty, D., Truong, D. Q., Bikson, M. & Kaphzan, H. Neuromodulation of axon terminals. *Cerebral Cortex* **28**, 2786–2794 (2018).

178. Simopoulos, T., Aner, M., Sharma, S., Ghosh, P. & Gill, J. S. Explantation of Percutaneous Spinal Cord Stimulator Devices: A Retrospective Descriptive Analysis of a Single-Center 15-Year Experience. *Pain Medicine* **20**, 1355–1361 (2019).

179. Amirdelfan, K. *et al.* Long-term quality of life improvement for chronic intractable back and leg pain patients using spinal cord stimulation: 12-month results from the SENZA-RCT. *Quality of Life Research* **27**, 2035–2044 (2018).

180. Cameron, T. & Alo, K. M. Effects of posture on stimulation parameters in spinal cord stimulation. *Neuromodulation: Technology at the Neural Interface* **1**, 177–183 (1998).

181. Peeters, J. B. & Raftopoulos, C. Tonic, Burst, High-Density, and 10-kHz High-Frequency Spinal Cord Stimulation: Efficiency and Patients' Preferences in a Failed Back Surgery Syndrome Predominant Population. Review of Literature. *World Neurosurg* **144**, e331–e340 (2020).

182. Kuo, S. W., Zhang, T., Esteller, R. & Grill, W. M. In Vivo Measurements Reveal that Both Low- and High-frequency Spinal Cord Stimulation Heterogeneously Modulate Superficial Dorsal Horn Neurons. *Neuroscience* **520**, 119–131 (2023).

183. Schnapp, W. D. & J-R Delcroix, G. Randomized Trial Improved Sensation Resulting From Spinal Cord Stimulation for the Treatment of Painful Diabetic Neuropathy: The Possible Role of Stochastic Resonance. *Pain Physician* **25**, E1399–E1403 (2022).

184. Bossetti, C. A., Birdno, M. J. & Grill, W. M. Analysis of the quasi-static approximation for calculating potentials generated by neural stimulation. *J Neural Eng* **5**, 44–53 (2008).

185. Graham, R. D., Bruns, T. M., Duan, B. & Lempka, S. F. Dorsal root ganglion stimulation for chronic pain modulates Aβ-fiber activity but not C-fiber activity: A computational modeling study. *Clinical Neurophysiology* **130**, 941–951 (2019).

186. Formento, E. *et al.* Electrical spinal cord stimulation must preserve proprioception to enable locomotion in humans with spinal cord injury. *Nat Neurosci* **21**, 1728–1741 (2018).

187. Vallbo, A. B. & Al-Falahe, N. A. Human muscle spindle response in a motor learning task. *Journal of Physiology* **421**, 553–568 (1990).

188. Ackerley, R. & Holmes Watkins, R. Microneurography as a tool to study the function of individual C-fiber afferents in humans: responses from nociceptors, thermoreceptors, and mechanoreceptors. *J Neurophysiol* **120**, 2834–2846 (2018).

189. Victor, J. D. & Purpura, K. P. Nature and Precision of Temporal Coding in Visual Cortex: A Metric-Space Analysis. *J Neurophysiol* **76**, 1310–1326 (1996).

190. Sigworth, F. J. The variance of sodium current fluctuations at the node of Ranvier. *J Physiol* **307**, 97–129 (1980).

191. Faisal, A. A., White, J. A. & Laughlin, S. B. Ion-channel noise places limits on the miniaturization of the brain's wiring. *Current Biology* **15**, 1143–1149 (2005).

192. Rubinstein, J. T., Wilson, B. S., Finley, C. C. & Abbas, P. J. Pseudospontaneous activity: stochastic independence of auditory nerve fibers with electrical stimulation. *Hear Res* **127**, 108–118 (1999).

193. Orio, P. & Soudry, D. Simple, fast and accurate implementation of the diffusion approximation algorithm for stochastic ion channels with multiple states. *PLoS One* **7**, (2012).

194. Mirzakhalili, E., Barra, B., Capogrosso, M. & Lempka, S. F. Biophysics of Temporal Interference Stimulation. *Cell Syst* 1–16 (2020) doi:10.1016/j.cels.2020.10.004.

195. McIntyre, C. C., Richardson, A. G. & Grill, W. M. Modeling the excitability of mammalian nerve fibers: Influence of afterpotentials on the recovery cycle. *J Neurophysiol* **87**, 995–1006 (2002).

196. Szucs, P. *et al.* Axon diversity of lamina I local-circuit neurons in the lumbar spinal cord. *Journal of Comparative Neurology* **521**, 2719–2741 (2013).

197. Antal, Z., Luz, L. L., Safronov, B. V., Antal, M. & Szücs, P. Neurons in the lateral part of the lumbar spinal cord show distinct novel axon trajectories and are excited by short propriospinal ascending inputs. *Brain Struct Funct* **221**, 2343–2360 (2016).

198. Stoney, S. D., Thompson, W. D. & Asanuma, H. Excitation of pyramidal tract cells by intracortical microstimulation: Effective extent of stimulating current. *J Neurophysiol* **31**, 659–669 (1968).

199. Feirabend, H. K. P., Choufoer, H., Ploeger, S., Holsheimer, J. & Van Gool, J. D. Morphometry of human superficial dorsal and dorsolateral column fibres: significance to spinal cord stimulation. *Brain* **125**, 1137–1149 (2002).

200. Sagalajev, B. *et al.* Paresthesia during spinal cord stimulation depends on synchrony of dorsal column axon activation. *bioRxiv* (2023) doi:10.1101/2023.01.10.523167.

201. Jefferys, J. G. R. Nonsynaptic Modulation of Neuronal Activity in the Brain: Electric Currents and Extracellular Ions. *Physiol Rev* **75**, 689–723 (1995).

202. Gilbert, J. E., Titus, N., Zhang, T., Esteller, R. & Grill, W. M. Surround Inhibition Mediates Pain Relief by Low Amplitude Spinal Cord Stimulation: Modeling and Measurement. *eNeuro* **9**, (2022).

203. Olausson, H. *et al.* Unmyelinated tactile afferents signal touch and project to insular cortex. *Nat Neurosci* **5**, 900–904 (2002).

204. Arlotti, M., Rahman, A., Minhas, P. & Bikson, M. Axon terminal polarization induced by weak uniform DC electric fields: A modeling study. in *Proceedings of the Annual International Conference of the IEEE Engineering in Medicine and Biology Society, EMBS* 4575–4578 (2012). doi:10.1109/EMBC.2012.6346985.

205. Tiede, J. *et al.* Novel spinal cord stimulation parameters in patients with predominant back pain. *Neuromodulation* **16**, 370–375 (2013).

206. Metzger, C. S. *et al.* A novel fast-acting sub-perception spinal cord stimulation therapy enables rapid onset of analgesia in patients with chronic pain. *Expert Rev Med Devices* **18**, 299–306 (2021).

207. De Groote, S. *et al.* Functional magnetic resonance imaging: Cerebral function alterations in subthreshold and suprathreshold spinal cord stimulation. *J Pain Res* **11**, 2517–2526 (2018).

208. Sato, K. L., King, E. W., Johanek, L. M. & Sluka, K. A. Spinal cord stimulation reduces hypersensitivity through activation of opioid receptors in a frequency-dependent manner. *European Journal of Pain* **17**, 551–561 (2013).

209. Gmel, G. E. *et al.* The Effect of Spinal Cord Stimulation Frequency on the Neural Response and Perceived Sensation in Patients With Chronic Pain. *Front Neurosci* **15**, (2021).

210. Abejón, D., Rueda, P. & Vallejo, R. Threshold Evolution as an Analysis of the Different Pulse Frequencies in Rechargeable Systems for Spinal Cord Stimulation. *Neuromodulation* **19**, 276–282 (2016).

211. Hari, K. *et al.* GABA facilitates spike propagation through branch points of sensory axons in the spinal cord. *Nat Neurosci* **25**, 1288–1299 (2022).

212. Sagalajev, B. *et al.* Paresthesia during spinal cord stimulation depends on synchrony of dorsal column axon activation. *bioRxiv* (2023) doi:10.1101/2023.01.10.523167.

213. Thomson, A. M. Molecular frequency filters at central synapses. *Prog Neurobiol* **62**, 159–196 (2000).

214. Johnson, M. D. & McIntyre, C. C. Quantifying the neural elements activated and inhibited by globus pallidus deep brain stimulation. *J Neurophysiol* **100**, 2549–2563 (2008).

215. Bengtsson, F., Brasselet, R., Johansson, R. S., Arleo, A. & Jörntell, H. Integration of Sensory Quanta in Cuneate Nucleus Neurons In Vivo. *PLoS One* **8**, (2013).

216. Nuñez, A. & Buño, W. In vitro electrophysiological properties of rat dorsal column nuclei neurons. *European Journal of Neuroscience* **11**, 1865–1876 (1999).

217. Tsodyks, M. v & Markram, H. The neural code between neocortical pyramidal neurons depends on neurotransmitter release probability. *Proceedings of the national academy of sciences* **94**, 719–723 (1997).

218. Farokhniaee, A. A. & McIntyre, C. C. Theoretical principles of deep brain stimulation induced synaptic suppression. *Brain Stimul* **12**, 1402–1409 (2019).

219. Turecek, J., Lehnert, B. P. & Ginty, D. D. The encoding of touch by somatotopically aligned dorsal column subdivisions. *Nature* **612**, 310–315 (2022).

220. Vickery, R. M., Gynther, B. D. & Rowe, M. J. Synaptic transmission between single slowly adapting type I fibres and their cuneate target neurones in cat. *J Physiol* **474**, 379–392 (1994).

221. Ferrington, D. G., Rowe, M. J. & Tarvin, R. P. Actions of single sensory fibres on cat dorsal column nuclei neurones: vibratory signalling in a one-to-one linkage. *J Physiol* **386**, 293–309 (1987).

222. Gynther -R M Vickery, B. D., Rowe, M. J., Gynther, B. D. & Vickery M J Rowe, R. M. *Transmission characteristics for the 1:1 linkage between slowly adapting type II fibers and their cuneate target neurons in cat*. *Exp Brain Res* vol. 105 (1995).

223. Rowe, M. J. Synaptic transmission between single tactile and kinaesthetic sensory nerve fibers and their central target neurones. *Behavioural brain research* **135**, 197–212 (2002).

224. Brown, A.G.; Fyffe, R.E.W.; Noble, R. Projections from Pacinian corpuscles and rapidly adapting mechanoreceptors of glabrous skin to the cat's spinal cord. *J Physiology* 385–400 (1980).

225. Grill, W. M., Cantrell, M. B. & Robertson, M. S. Antidromic propagation of action potentials in branched axons: Implications for the mechanisms of action of deep brain stimulation. *J Comput Neurosci* **24**, 81–93 (2008).

226. Iles, J. F. Central terminations of muscle afferents on motoneurones in the cat spinal cord. *J Physiol* **262**, 91–117 (1976).

227. Ishizuka, N., Mannen, H., Hongo, T. & Sasaki, S. Trajectory of group Ia afferent fibers stained with horseradish peroxidase in the lumbosacral spinal cord of the cat: Three dimensional reconstructions from serial sections. *Journal of Comparative Neurology* **186**, 189–211 (1979).

228. Parker, J. L., Karantonis, D. M., Single, P. S., Obradovic, M. & Cousins, M. J. Compound action potentials recorded in the human spinal cord during neurostimulation for pain relief. *Pain* **153**, 593–601 (2012).

229. McIntyre, C. C., Grill, W. M., Sherman, D. L. & Thakor, N. v. Cellular Effects of Deep Brain Stimulation: Model-Based Analysis of Activation and Inhibition. *J Neurophysiol* **91**, 1457–1469 (2004).

230. Miocinovic, S. *et al.* Computational analysis of subthalamic nucleus and lenticular fasciculus activation during therapeutic deep brain stimulation. *J Neurophysiol* **96**, 1569–1580 (2006).

231. Parker, J., Karantonis, D. & Single, P. Hypothesis for the mechanism of action of ECAP-controlled closed-loop systems for spinal cord stimulation. *Healthc Technol Lett* **7**, 76–80 (2020).

232. Simone, D. A. *et al.* Neurogenic Hyperalgesia: Central Neural Correlates in Responses of Spinothalamic Tract Neurons. *J Neurophysiol* **66**, 228–246 (1991).

233. DeVos, C. C., Bom, M. J., Vanneste, S., Lenders, M. W. P. M. & de Ridder, D. Burst spinal cord stimulation evaluated in patients with failed back surgery syndrome and painful diabetic neuropathy. *Neuromodulation* **17**, 152–159 (2014).

234. Mekhail, N. *et al.* Long-term safety and efficacy of closed-loop spinal cord stimulation to treat chronic back and leg pain (Evoke): a double-blind, randomised, controlled trial. *Lancet Neurol* **19**, 123–134 (2020).

235. Mekhail, N. *et al.* Durability of Clinical and Quality-of-Life Outcomes of Closed-Loop Spinal Cord Stimulation for Chronic Back and Leg Pain: A Secondary Analysis of the Evoke Randomized Clinical Trial. *JAMA Neurol* **79**, 251–260 (2022).

236. Pilitsis, J. G. *et al.* The Evoked Compound Action Potential as a Predictor for Perception in Chronic Pain Patients: Tools for Automatic Spinal Cord Stimulator Programming and Control. *Front Neurosci* **15**, (2021).

237. Ochoa, J. & Torebjörk, E. Sensations evoked by intraneural microstimulation of single mechanoreceptor units innervating the human hand. *J Physiol* **342**, 633–654 (1983).

238. Graczyk, E. L. *et al.* The neural basis of perceived intensity in natural and artificial touch. *Sci Transl Med* **8**, (2016).

239. Ng, K. K. W., Tee, X., Vickery, R. M. & Birznieks, I. The Relationship Between Tactile Intensity Perception and Afferent Spike Count is Moderated by a Function of Frequency. *IEEE Trans Haptics* **15**, 14–19 (2022).

240. Marcus, P. L. & Fuglevand, A. J. Perception of electrical and mechanical stimulation of the skin: implications for electrotactile feedback. *J Neural Eng* **6**, 66008 (2009).

241. Jelinek, H. F. & McIntyre, R. Electric pulse frequency and magnitude of perceived sensation during electrocutaneous forearm stimulation. *Arch Phys Med Rehabil* **91**, 1378–1382 (2010).

242. Graczyk, E. L., Christie, B. P., He, Q., Tyler, D. J. & Bensmaia, S. J. Frequency Shapes the Quality of Tactile Percepts Evoked through Electrical Stimulation of the Nerves. *Journal of Neuroscience* **42**, 2052–2064 (2022).

243. Nicol, M. J. & Walmsley, B. A serial section electron microscope study of an identified la afferent collateral in the cat spinal cord. *Journal of Comparative Neurology* **314**, 257–277 (1991).

244. Deschênes, M. & Landry, P. Axonal branch diameter and spacing of nodes in the terminal arborization of identified thalamic and cortical neurons. *Brain Res* **191**, 538–544 (1980).

245. Saito, K. Branchings at the central node of Ranvier, observed in the anterior horn and Clarke's nucleus of the cat. An electron microscopic study. *Neuroscience* **4**, 391–399 (1979).

246. Sweet, J., Badjatiya, A., Tan, D. & Miller, J. Paresthesia-Free High-Density Spinal Cord Stimulation for Postlaminectomy Syndrome in a Prescreened Population: A Prospective Case Series. *Neuromodulation* **19**, 260–267 (2016).

247. Solanes, C. *et al.* 3D patient-specific spinal cord computational model for SCS management: potential clinical applications. *J Neural Eng* **18**, (2021).

248. Gaines, J. L., Finn, K. E., Slopsema, J. P., Heyboer, L. A. & Polasek, K. H. A model of motor and sensory axon activation in the median nerve using surface electrical stimulation. *J Comput Neurosci* **45**, 29–43 (2018).

249. Canedo, A. & Aguilar, J. Spatial and cortical influences exerted on cuneothalamic and thalamocortical neurons of the cat. *European Journal of Neuroscience* **12**, 2515–2533 (2000).

250. Kiernan, M. C., Mogyoros, I., Burke, D. & Kiernan, M. Differences in the recovery of excitability in sensory and motor axons of human median nerve. *Brain* **119**, 1099–1105 (1996).

251. Stebbing, M. J. *et al.* Changes in the action potential in sensory neurones after peripheral axotomy in vivo. *Neuroreport* **10**, 201–206 (1999).